EPA-R2-73-219

June 1973

Environmental Protection Technology Series

Feasibility Study of In-Situ Source Monitoring of Particulate Composition by Raman or Fluorescence Scatter

Office of Research and Monitoring
U.S. Environmental Protection Agency
Washington, D.C. 20460

EPA-R2-73-219

Feasibility Study of In-Situ Source Monitoring of Particulate Composition by Raman or Fluorescence Scatter

by

M. L. Wright

Stanford Research Institute
333 Ravenswood Avenue
Menlo Park, California 94025

Contract No. 68-02-0594
Program Element No. 1A1010

EPA Project Officer: John S. Nader

Chemistry and Physics Laboratory
National Environmental Research Center
Research Triangle Park, North Carolina 27711

Prepared for

OFFICE OF RESEARCH AND MONITORING
U.S. ENVIRONMENTAL PROTECTION AGENCY
WASHINGTON, D.C. 20460

June 1973

This report has been reviewed by the Environmental Protection Agency and approved for publication. Approval does not signify that the contents necessarily reflect the views and policies of the Agency, nor does mention of trade names or commercial products constitute endorsement or recommendation for use.

ABSTRACT

The purpose of this project was to assess the feasibility of in-stack monitoring of an air-suspended particulate stream by fluorescence or Raman optical interactions. The study explored the feasibility of two approaches: quantitatively monitoring a prescribed constituent, and monitoring the relative concentrations of several constituents simultaneously. Fluorescence-monitoring systems were found suitable for the second.

The method of approach was to assess the magnitude of the Raman and fluorescence interaction, and then calculate the detectability of that material for a typical in-stack system. Thirty-four materials were investigated on the project; thirteen materials had significant fluorescent responses and twenty-two materials had measurable Raman responses. When these responses were used to calculate in-stack detectability, all thirteen materials could be detected by fluorescence systems (although few could be uniquely identified), and fifteen of the twenty-two Raman-active materials could be detected by a Raman system.

The use of a laboratory Raman instrument to analyze conventionally sampled particulates was considered. The primary advantage of this instrument appears to be the capability for measuring ions--for example, sulfate.

Finally, a few crude experiments were made to detect the fluorescent response of a particulate material suspended in a liquid (rather than air). These measurements showed substantial interference from fluorescence by the liquid medium; nevertheless, a component of the particulate

fluorescence was detectable. This experimental result partially verifies the calculated feasibility of detection by fluorescence.

It is concluded that both fluorescence and Raman in-stack monitoring systems can yield useful information about the quantity and composition of a particulate stream. Recommendations are made for additional efforts toward achieving an operational in-stack monitoring system.

CONTENTS

ABSTRACT iii

LIST OF ILLUSTRATIONS vii

LIST OF TABLES ix

I INTRODUCTION 1

II MATERIALS 3

III FLUORESCENT RESPONSE MEASUREMENTS 7

A. General 7

B. Measurement Results and Discussion 11

IV RAMAN RESPONSE MEASUREMENTS 21

A. General 21

B. Measurement Results and Discussion 27

V IN-STACK MONITORING SYSTEMS 41

A. General 41

B. Fluorescence-Monitoring Systems 42

C. Raman Monitoring Systems 48

1. General 48
2. Spectrometer-Type System 48
3. Filter-Type System 59
4. Performance Summary for Raman Systems 65

VI LABORATORY MEASUREMENT CAPABILITIES 71

A. General 71

B. Measurable Material Properties 71

C. Instrumental Considerations 72

VII AEROSOL MEASUREMENTS 75

VIII CONCLUSIONS 77

IX RECOMMENDATIONS 79

Appendix A MEASURED FLUORESCENT RESPONSE SPECTRA 81

Appendix B MEASURED RAMAN SPECTRA 91

REFERENCES 110

ILLUSTRATIONS

1	Schematic Diagram of a Fluorescence Measuring Instrument .	8
2	Optical Attenuation of Air	12
3	Typical Fluorescence Measurement Curve (for $CaSO_4$)	13
4	Fluorescence Response Shift with Varying Excitation Wavelength--for Phosphate Rock Feed Material	15
5	Fluorescence Response Shift with a Single Constituent (for CaF_2)	16
6	Minimal Fluorescence Response Shift--for Super Phosphate Storage Product	17
7	Excitation and Fluorescence Response Wavelengths	19
8	Schematic Diagram of Raman Measurement Instrument	22
9	Raman Response Curve for $(NH_4)_2SO_4$	28
10	Raman Response Curve for $CaSO_4$	29
11	Wavenumber Shift-to-Wavelength Shift Conversion Chart . . .	30
12	Raman Spectral Response Summary	36
A-1	Relative Response for Baird-Atomic Spectrofluorimeter Source and Detector	83
A-2	Fluorescent Response of AlF_3	84
A-3	Fluorescent Response of $CuSO_4$	84
A-4	Fluorescent Response of Cryolite	85
A-5	Fluorescent Response of $Al_2(SO_4)_3$	85
A-6	Fluorescent Response of EPA Raw Alumina	86
A-7	Fluorescent Response of $HgSO_4$	86
A-8	Fluorescent Response of EPA Zinc Smelter Feed Material . .	87
A-9	Fluorescent Response of EPA Coal--Source, NBS	87
A-10	Fluorescent Response of EPA Phosphate Rock Feed Material .	88
A-11	Fluorescent Response of EPA copper Smelter Feed Material .	88
A-12	Fluorescent Response of EPA Fly Ash	89

A-13 Fluorescent Response of EPA Lead Smelter Feed Material . 89

A-14 Fluorescent Response of Particulate AlF_3 in Water 90

B-1 Raman Response of $HgSO_4$ 92

B-2 Raman Response of $PbSO_4$ 93

B-3 Raman Response of $CdSO_4$ 94

B-4 Raman Response of $Al_2(SO_4)_3$ 95

B-5 Raman Response of $Al_2(SO_4)_3$ (6471 Å) 96

B-6 Raman Response of $HgCl_2$ 97

B-7 Raman Response of $CdCl_2$ 98

B-8 Raman Response of $CuCl_2$ 99

B-9 Raman Response of PbO 100

B-10 Raman Response of CdS 101

B-11 Raman Response of CaF_2 102

B-12 Raman Response of AlF_3 103

B-13 Raman Response of EPA Phosphate Rock Feed Material . . . 104

B-14 Raman Response of EPA Zinc Smelter Feed Material 105

B-15 Raman Response of EPA Triple Super-Phosphate Storage Product (6471 Å) 106

B-16 Raman Response of EPA Coal--Source, NBS (6471 Å) 107

B-17 Raman Response of EPA Coal--Source, NBS 108

B-18 Raman Response of Napthalene 109

TABLES

1 Materials Analyzed for Optical-Monitoring Potential 5

2 Relative Fluorescence Intensities 14

3 Relative Raman Response Intensities 31

4 Comparison of Various Measurements of the Raman Cross Section of Benzene (992 cm^{-1} Line) 39

5 Fluorescent-Reference-Material Measurement 44

6 Relative Raman Cross Sections for Gases 56

7 Raman In-Stack Monitoring-Instrument Performance Summary . . 66

8 Raman Shifts of Molecular Ions 73

I INTRODUCTION

Analytical techniques currently used for determining the composition of aerosols require some type of sampling. This sampling procedure may change the characteristics of the aerosol in such a way that the measured sample properties are not representative of the aerosol properties in the stack. An in-situ technique, particularly one utilizing optical methods, would avoid disturbing the aerosol in the stack and would give an indication of the true characteristics of the aerosol in the stack.

The two most promising optical-material interactions are the well-known Raman and fluorescence scattering properties of materials. Raman scattering from materials is often proposed as a method of analysis because of the relatively narrow and distinct Raman peaks obtained in the spectra of many materials. However, this specificity advantage is offset by the weak nature of the Raman interaction. In many cases too few photons are scattered to permit measurements to be made using Raman scatter. Fluorescence, on the other hand, offers a much stronger optical interaction than the Raman scatter. This advantage is partially offset by the broad nature of the spectral excitation and response characteristics of most fluorescent materials, particularly in the solid state. Discrimination between several materials is much more difficult with fluorescence than it is with Raman scatter, due to the broad, diffuse nature of these fluorescence spectral responses. Thus, both effects present some difficulties, which in some cases will prevent realistic field measurements.

This project was concerned with the analysis of the feasibility of in-situ stack monitoring using either Raman or fluorescence scattering properties. The analysis considered monitoring from two points of view: (1) the feasibility of quantitatively monitoring a prescribed molecular constituent, and (2) the feasibility of qualitatively monitoring the relative concentrations of several molecular constituents simultaneously. The relatively strong but nonspecific nature of the fluorescent response makes it suitable for quantitatively monitoring a prescribed molecular constituent. Qualitative monitoring of several constituents is best accomplished through use of the Raman effect. Both methods were found to be feasible for several materials.

The general approach taken in this project was, first, to determine by experimental measurements whether a specific material had a significant Raman or fluorescence response. If a significant response was found, an estimate of the detectability of that material was made for typical monitoring system configurations.

The key to the successful application of either monitoring approach is the existence of a sufficiently large optical interaction. It should be noted that not all materials possess a significant Raman or Fluorescent response characteristic. This is particularly true for glassy materials such as fly ash. This material was of particular interest to both EPA and SRI; however, measurements of the fluorescent and Raman spectra of fly ash were made, and no Raman or fluorescent response was found for any of the fly-ash samples. Thus, fly ash appears to be a distinctly unpromising material for in-stack analysis by Raman or in-situ fluorescence techniques. Other materials were found to be much more promising and are discussed in later sections of the report.

II MATERIALS

The contract specifies that ten materials would be selected jointly by SRI and EPA personnel for optical characterization. The procedure finally adopted was for EPA to specify broad guidelines detailing the rationale for particulate monitoring and indicating specific industrial processes whose pollutants were believed to be of greatest concern at the present time. Within these guidelines, SRI was directed to select the specific materials that would be examined. The materials selected were primarily simple chemical compounds that were easily prepared for optical analysis; thus it was possible to examine more than the ten materials specified in the contract, and a total of 34 materials were examined. This total does not include 14 samples of stack emission products that were obtained well after the technical work stopped and thus were not completely evaluated. The latter samples were supplied through the courtesy of Dr. Milton Feldstein of the Bay Area Air Pollution Control District (BAAPCD).

The EPA guideline stated that the particulates of primary interest in this project should be those with chemical-related health effects, and that other particulate material should be of only secondary interest. The materials of interest were grouped into several categories, again by EPA direction. These groupings are (1) fly ash from coal-burning power plants; (2) calcium and ammonium sulphates from heating sources; (3) lead, copper, cadmium, and mercury compounds from smelters, incinerators, alloy plants, and steel mills; (4) fluorides from aluminum reduction plants or phosphorous plants; (5) other particulates of general interest, including sulphates, chlorides, oxides, and sulphides of

lead, cadmium, zinc, mercury, copper, nickel, chromium, vanadium, arsenic, and beryllium; and (6) a representative organic material.

The specific materials that were examined on this project are listed in Table 1.

The organic material originally selected was the particulate emission from an asphalt batch plant. Difficulty in obtaining such a sample resulted in the substitution of the NBS coal sample for the originally chosen asphalt batch plant sample. Both of these materials probably contain a complex mixture of many organic compounds, and the Raman and fluorescence measurements were not expected to yield constituent data on either material. Time and funds did not permit the examination of simpler organic pollutant materials on this project, although they offer significant potential for either Raman or fluorescence monitoring.

Table 1

MATERIALS ANALYZED FOR OPTICAL-MONITORING POTENTIAL

Materials supplied by SRI
Calcium fluoride (CaF_2)
Mercury sulfate ($HgSO_4$)
Aluminum fluoride (AlF_3)
Aluminum sulfate [$Al_2(SO_4)_3 \cdot 18H_2O$]
Cupric sulfate ($CuSO_4 \cdot 5H_2O$)
Calcium sulfate ($CaSO_4 \cdot 2H_2O$)
Cryolite (Na_3AlF_6)
Water (H_2O)
Cupric chloride ($CuCl_2 \cdot 2H_2O$)
Lead chloride ($PbCl_2$)
Mercuric oxide (HgO)
Cupric oxide (CuO)
Cuprous oxide (Cu_2O)
Mercuric sulfide (HgS)
Sulfuric acid (H_2SO_4)
Lead sulfate ($PbSO_4$)
Lead sulfide (PbS)
Lead oxide, mono (PbO)
Cadmium sulfate ($3CdSO_4 \cdot 8H_2O$)
Cadmium oxide (CdO)
Aluminum oxide (alumina) (Al_2O_3)
Ammonium sulfate [$(NH_4)_2SO_4$]
Fly ash (4 samples)
Materials supplied by EPA
Triple superphosphate storage product
Phosphate rock feed material
Raw alumina
Coal (source, NBS)
Zinc smelter feed material
Copper smelter feed material
Lead smelter feed material
Fly ash

III FLUORESCENCE RESPONSE MEASUREMENTS

A. General

The two main requirements of the fluorescence measurement program were, first, to be able to detect fluorescent response amplitudes down to a level comparable to that of the Raman response peak of water, and, second, to detect fluorescent responses over the entire wavelength range of 200 to 700 nm. These requirements led to the selection of two separate fluorescence measurement systems for complete wavelength coverage. One of these instruments was modified to obtain a substantial improvement in performance and was also calibrated to provide more quantitative information for comparison of the response levels of various materials.

The spectrofluorimeter on which the majority of the sample measurements were made was a Fluorispec, Model SF-1, made by Baird Atomic, Inc. This instrument covers the wavelength range 220 to 700 nm. It was chosen primarily because it utilizes double monochrometers for both the source and detector, thus giving superior scattered-light rejection for fluorescence measurements. A diagram of this instrument system is shown in Fig. 1. Most routine laboratory fluorescence measurements are made on transparent or semitransparent solutions in which the scattering of the source (or exciting) light is relatively low. Solid samples were used on this project, many of which are white powders reflecting large amounts of source light scattered to the detector. Thus, it is particularly important, when measuring either solid samples or aerosols, to achieve a high degree of scattered-light rejection.

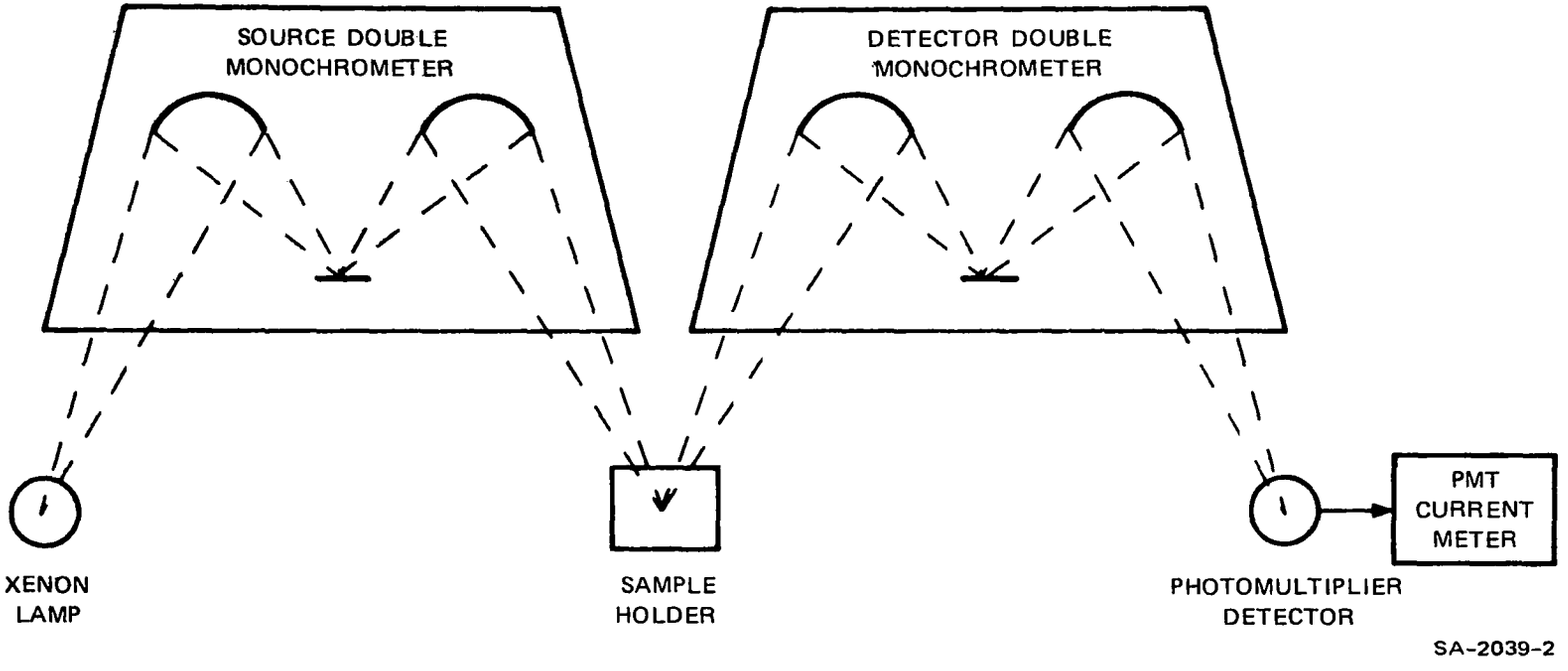

FIGURE 1 SCHEMATIC DIAGRAM OF A FLUORESCENCE MEASURING INSTRUMENT

Several modifications of this instrument were made to improve the sensitivity, accuracy, and repeatability of the fluorescence measurements. First, the exciter lamp in the source unit was replaced in order to improve the ultraviolet-light output. This new lamp increased the UV light output by a factor of approximately five. The UV output of these lamps degrades faster than does the visible performance, however, so this degree of improvement was not maintained over the entire measurement program. Second, a large portion of the original instrument electronics was bypassed in order to increase the stability and repeatability of the measurements and to lower the effective noise level below that provided by the original instrument. These instrument modifications included replacement of the photomultiplier power supply with a well regulated Power Designs commercial power supply, and the direct monitoring of the photomultiplier current by a sensitive Hewlett-Packard 425A current meter. Some portions of the passive photomultiplier circuitry have been retained as in the original instrument, but all of the active portions of the photomultiplier circuitry have been replaced. In addition, the original 1P21 has been replaced by a 1P28 photomultiplier to further improve the UV performance of the instrument. The effect of these modifications has been monitored by observing the Raman peak of water and has resulted in a clearly enhanced signal-to-noise ratio (SNR) for the Raman response. In addition, the amplitude response was stabilized and is available as an absolute current level that can in turn be related to an absolute light level at the detector. These modifications allow a quantitative comparison of response levels to be made over the full dynamic range of the photomultiplier.

Both the source and the detector portions of the Baird-Atomic spectrofluorimeter were calibrated in order to allow accurate amplitude correction to be made on the measured fluorescent responses. These

relative-amplitude calibrations can be partially converted to absolute calibrations through the use of materials with known quantum yields.[1,2*] This type of absolute calibration is still of limited utility in the present program, however, because such measurements are ordinarily done in liquid samples with more easily defined geometries. The use of solid samples, as in the present program, does not offer the possibility of easily controlled geometries; this factor will contribute substantially to errors in determining absolute cross sections for the materials, even though the system has been calibrated with materials of known quantum yields.

The second measurement system consists of an Aminco-Bowman Spectrophotofluorimeter. This machine covers the wavelength range 200 to 800 nm, although it was utilized only for measurements in the source range 200 to 220 nm because of the superior performance of the Baird-Atomic instrument at other wavelengths. Modifications of this machine were also planned. However, the scattered-light response of this single-monochromator instrument was so large that the only modification made was a replacement of the photomultiplier tube to enhance the UV performance of the instrument. The performance of this instrument, even with this scattered-light limitation, was still judged adequate to determine the presence of any responses that would be useful for identification in in-stack measurement systems.

No measurements were made at wavelengths shorter than 200 nm because of the abrupt increase in the attenuation of air at these shorter wavelengths. This attenuation will affect both the measurements and the operation of the final system. The attenuation curve for "standard

*References are listed at the end of the report.

atmosphere" air is shown in Fig. 2. For special applications, operation is possible in the "notches" of the rising curve, but in general 200 nm is considered to be the transmission limit.

The procedure used for the measurement of each material involved a manual scan of wavelengths to locate the positions of any significant fluorescent responses. When definite response-peak locations could be determined manually, only those regions of greatest significance (i.e., peaks within a factor of 10 of the largest peak) were run quantitatively on the system. Materials without an easily discerned maximum response level were examined at a variety of wavelengths for low-level fluorescence responses. A typical example of an actual response run is shown in Fig. 3 for calcium sulfate ($CaSo_4$). This figure shows the two types of response curves often used to characterize fluorescent materials. The curve on the left side of the figure shows the response of the material to a varying source (or excitation) wavelength with the detector fixed in wavelength at the maximum fluorescent response position (440 nm in this example). The sharp rise at the long-wavelength end of the excitation curve is caused by the response to scattered source light as the source and detector wavelengths become close together. The right-hand curve shows the response of the material for a varying detector wavelength with the excitation wavelength at the peak of the excitation response curve (369 nm in this example). This pair of curves for each material indicates the maximum amplitude response that would be available for optimum source and detector wavelengths.

B. Measurement Results and Discussion

The results of the measurements made on the Baird-Atomic system are shown in Table 2. This table shows the wavelength location of the excitation and fluorescent peaks and indicates the normalized relative amplitude of the fluorescence peak for each material. The response level

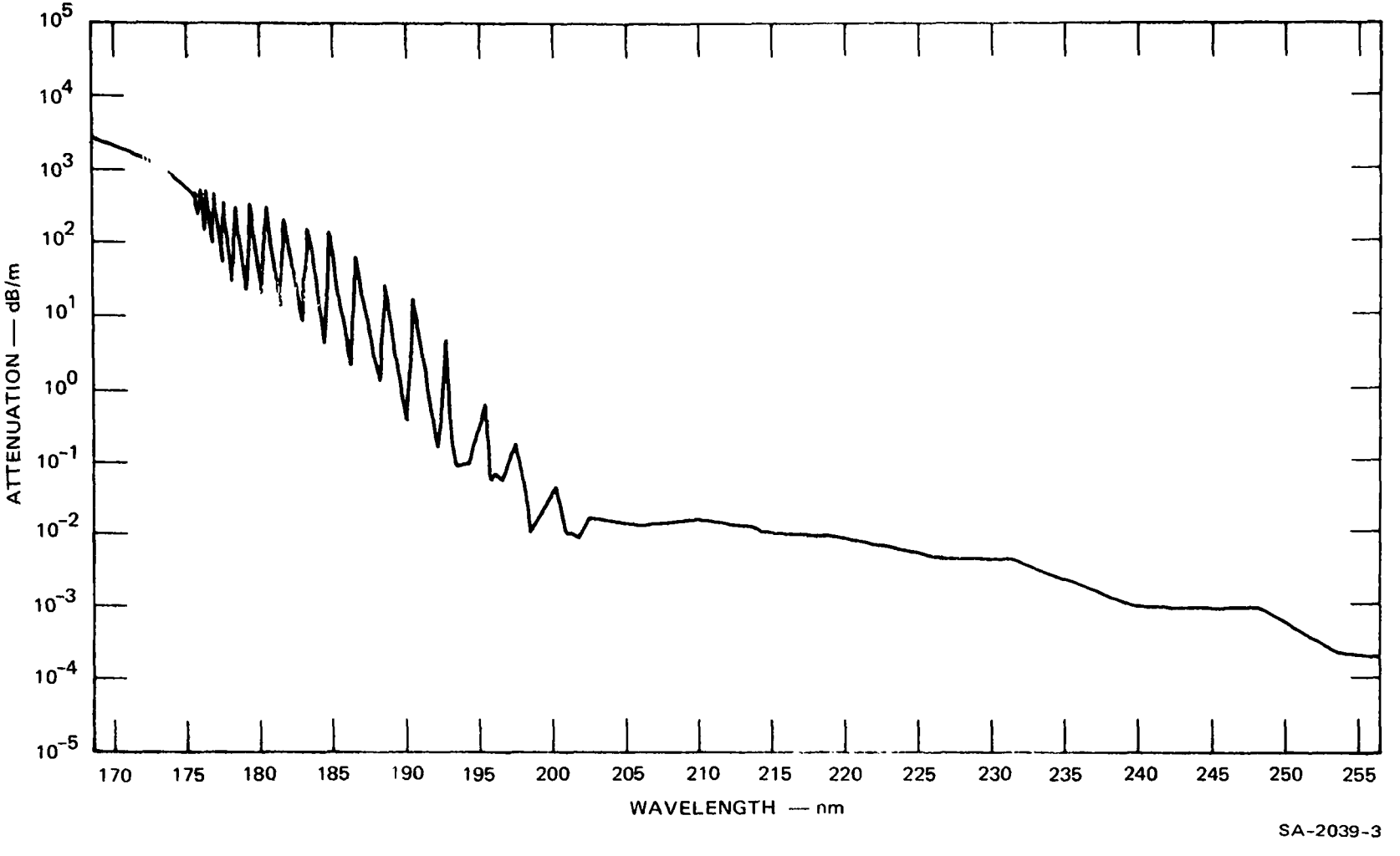

FIGURE 2 OPTICAL ATTENUATION OF AIR

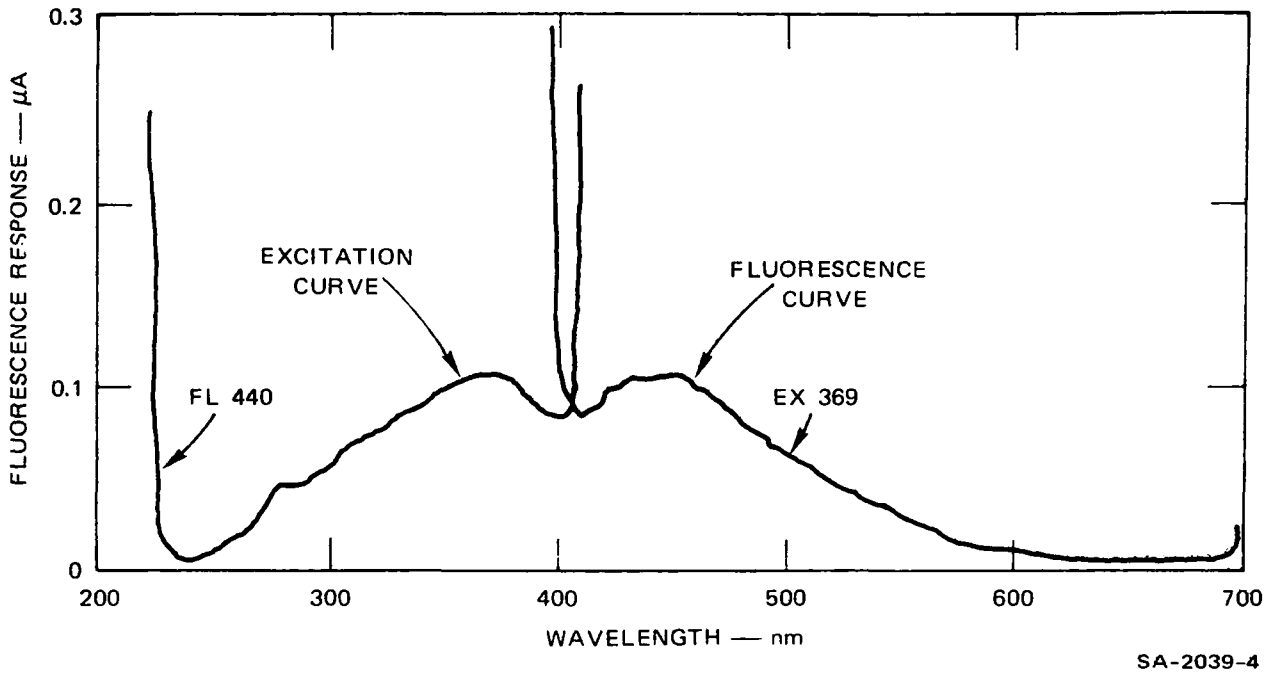

FIGURE 3 TYPICAL FLUORESCENCE MEASUREMENT CURVE (for $CaSO_4$)

for the Raman peak of water is included also to indicate the relative fluorescence strengths compared to a typical Raman response. Note, however, that the Raman response is for a liquid sample in which the geometry is significantly different than that present for the rest of the samples, which are solids. The last column in Table 2 gives the photon count for the stack monitoring instrument. These values will be discussed fully in Section V-B of the report and are included here to minimize the number of tables in the report.

The materials shown in Table 2 were also checked on the Aminco-Bowman system at wavelengths down to 200 nm. Only four materials were found to have a significant fluorescence at these short wavelengths that was not revealed by the Baird-Atomic instrument. These are:

Material	Fluorescence Wavelength (nm)
$HgSO_4$	500
$HgCl_2$	390/490 (2 peaks)
CdO	510
CdS	550

Table 2

RELATIVE FLUORESCENCE INTENSITIES

Material	Peak Wavelength (nm)		Normalized Peak Signal Level (μA)	Peak Photon Count (photons/s)
	Excitation	Fluorescence		
CaF_2	372	452	8.23	2.96×10^6
EPA phosphate rock feed sample	392	470	4.43	1.6×10^6
$HgSO_4$	309	564	1.51	5.44×10^5
EPA triple phosphate sample	364	447	1.31	4.72×10^5
EPA raw alumina sample	347	420	1.18	4.25×10^5
AlF_3	372	452	0.345	1.24×10^5
$Al_2(SO_4)_3$	364	430	0.32	1.15×10^5
$CuSO_4$	341	388	0.120	4.32×10^4
$CaSO_4$	369	440	0.111	4.0×10^4
Cryolite	375	458	0.109	3.92×10^4
Water (Raman)	340	384	0.063	
EPA Zn sample	349	467	0.038	1.36×10^4
EPA coal sample	365	443	0.032	1.15×10^4
$CuCl_2$	380	438	0.0103	3.7×10^3
$PbCl_2$	None			
HgO	None			
CuO	None			
Cu_2O	None			
HgS	None			
H_2SO_4	None			
$PbSO_4$	None			
PbS	None			
PbO	None			
CdO	None			
$CdSO_4$	None			
Al_2O_3	None			
$(NH_4)_2SO_4$	None			
EPA fly ash sample	None			
EPA copper sample	None			
EPA lead sample	None			
SRI fly ash (4 samples)	None			

The two mercury compounds showed slightly larger responses than the two cadmium compounds; however, all four materials had relatively weak responses and were not much larger than the stray-light response of the instrument. Although no quantitative calibrations were made between the two instruments, an estimate of the relative response would be comparable to aluminum sulfate in Table 2.

It should be noted that the shape and peak location of the excitation and fluorescence curves may shift with operation at other than these two optimal wavelengths shown above. This shift in peak location and shape of the response curve is illustrated in Fig. 4 for the EPA phosphate rock feed sample. This figure shows the change in fluorescence response curve as the excitation wavelength is shifted from 325 nm to 475 nm. Note that the amplitude of the maximum value of each fluorescent curve is different, as is the wavelength at which this maximum occurs. Note also that the width of the curve varies with the excitation wavelength and becomes narrower as the excitation wavelength becomes longer.

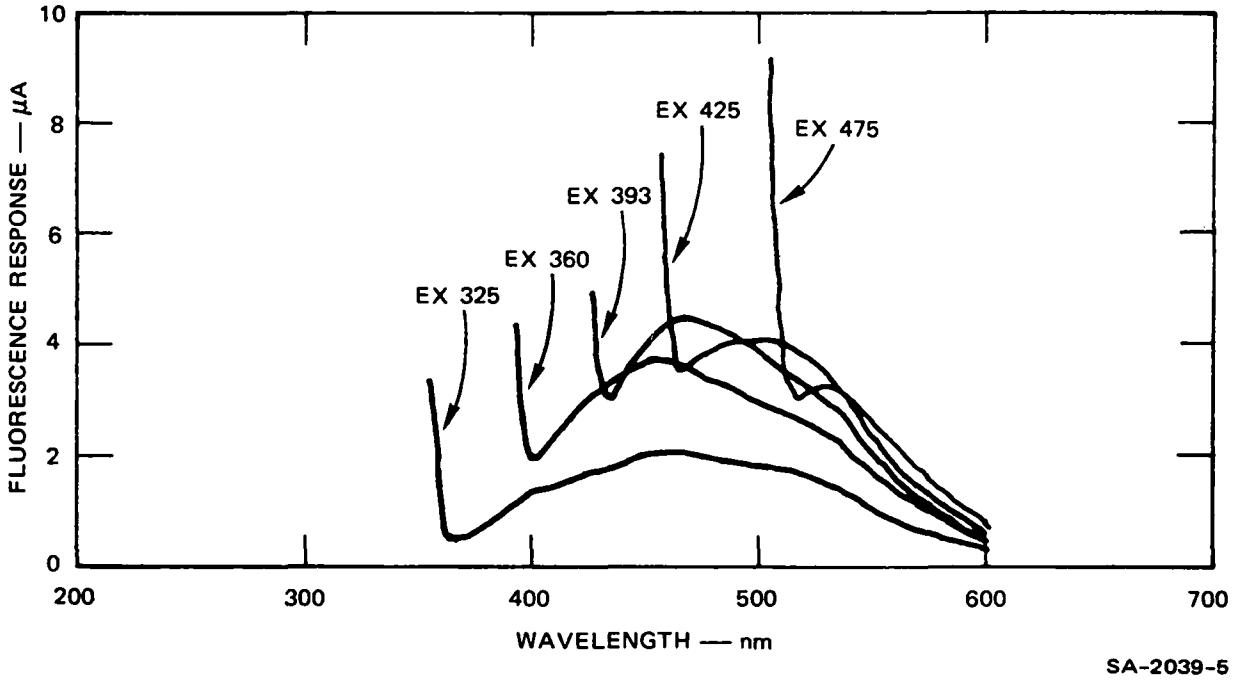

FIGURE 4 FLUORESCENCE RESPONSE SHIFT WITH VARYING EXCITATION WAVELENGTH — FOR PHOSPHATE ROCK FEED MATERIAL

Most of the materials investigated in this project have a changing response characteristic similar to that shown in Fig. 4. This changing response curve is often associated with the presence of more than one constituent in the sample. This could indeed be the case for the phosphate rock feed material; however, it is also possible for this effect to occur in single constituent materials as well. An example of this effect in a single material is shown in Fig. 5 for reagent-grade CaF_2. Some materials do not show a pronounced shift in the fluorescence response curve with varying excitation. For these materials the peak location and general shape of the fluorescence curve remains approximately the same with varying excitation wavelengths. The overall fluorescence curve moves up and down in amplitude, uniformly with varying excitation wavelengths. No material examined on this project was completely free of fluorescence curve shift. An example of a material with minimum curve-shape change is shown in Fig. 6 for the EPA triple super-phosphate storage product.

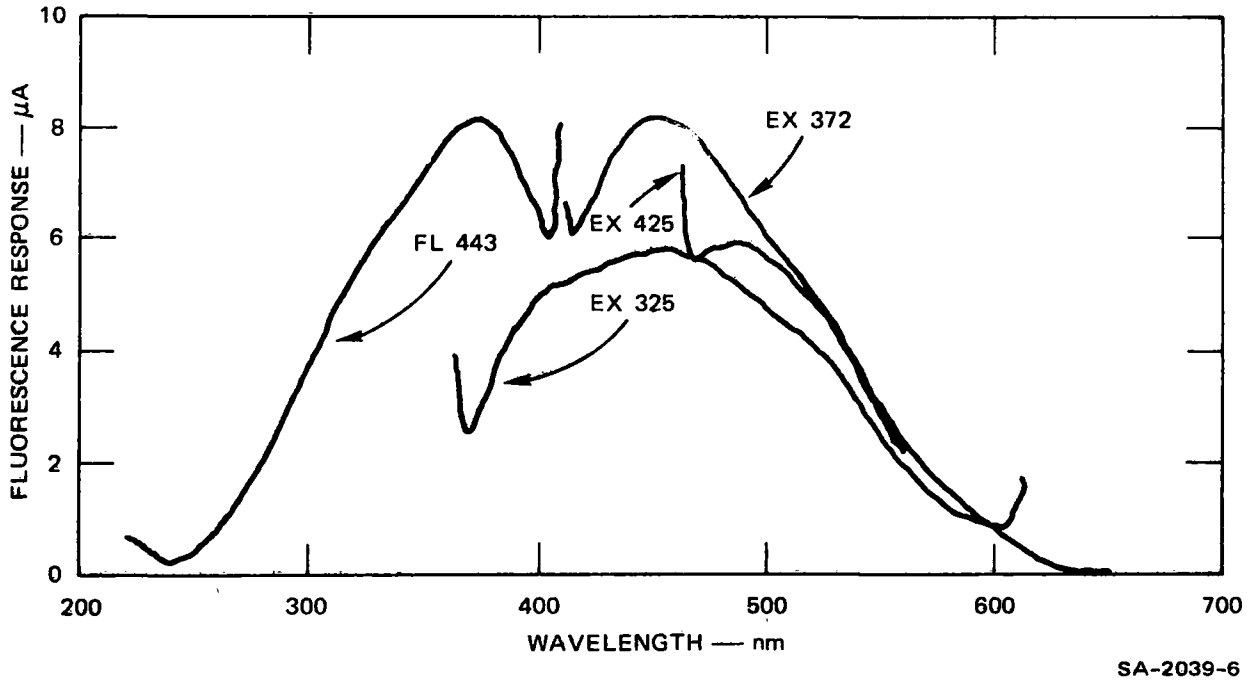

FIGURE 5 FLUORESCENCE RESPONSE SHIFT WITH A SINGLE CONSTITUENT (for CaF_2)

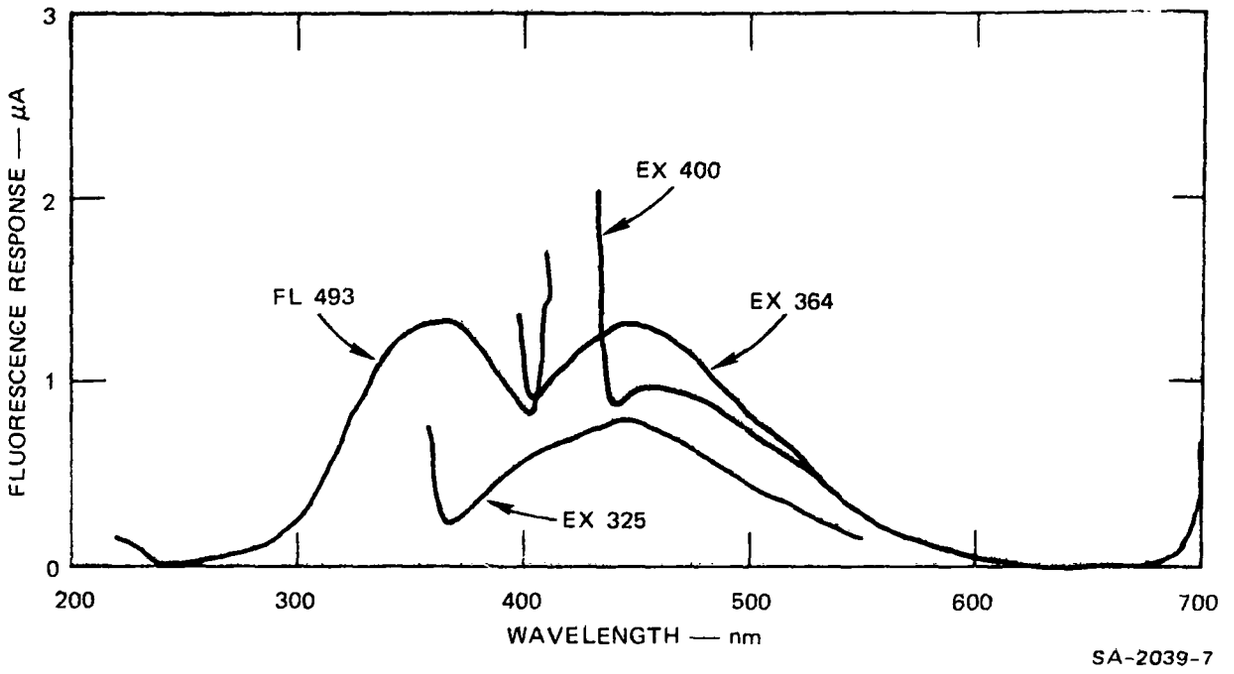

FIGURE 6 MINIMAL FLUORESCENCE RESPONSE SHIFT — FOR SUPER-PHOSPHATE STORAGE PRODUCT

This characteristic of changing emission-peak location will complicate simultaneous quantitative measurements of several materials by fluorescence techniques. Consider, for example, a monitoring system in which several detectors, each sensitive to a different wavelength, examine sequentially the fluorescence response of a mix of materials excited by different exciting wavelengths. If each individual material produces a fixed ratio of outputs in the detector array for each excitation wavelength, then that ratio matrix can be considered characteristic for that material. If, on the other hand, the ratios for each detector differ with different exciting wavelengths, then the characteristic matrix for each material is two-dimensional, thus significantly complicating the task of determining the relative composition of the unknown materials.

The fluorescence response curves for most of the materials examined in this project show rather broad, smooth curves with little fine

structure. Also, most of the peak locations in wavelength are approximately the same for the materials examined. A summary chart showing the peak location (letter E or F) and half-amplitude width (solid dots) for each of the materials as a function of wavelength is shown in Fig. 7.

It is evident from this figure that considerable response overlap exists between materials and would make the simultaneous identification of many of these materials relatively difficult. Note that CaF_2 and AlF_3 have virtually identical wavelength responses. A few materials, such as $HgSO_4$ and $CuCl_2$, are separated more widely from the others and could be distinguished on the basis of simple fluorescence measurements. It is evident from these data that the fluorescence measurement technique is not sufficiently selective to be a general chemical analysis method, but it can be useful in specific situations where the list of interfering materials is known and where the spectra are easily separable.

The measured response curves for materials with significant fluorescence are shown in Appendix A. These are uncorrected curves, taken directly from the recorder traces. The calibration curve for both the source and detector of the Baird-Atomic Spectrofluorimeter is also given in Appendix A, so that any portion of these curves could be corrected for instrument response if desired.

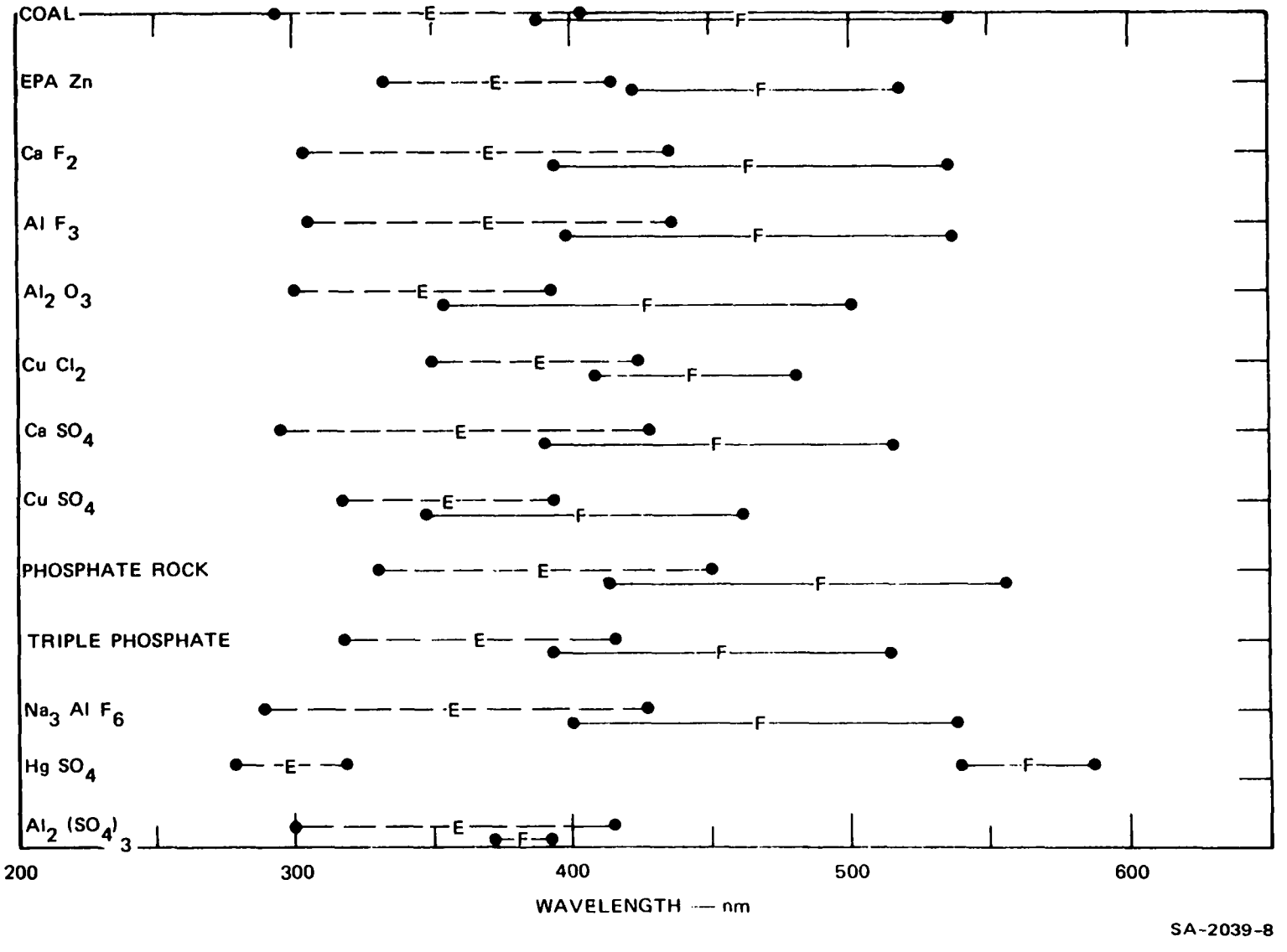

FIGURE 7 EXCITATION AND FLUORESCENCE RESPONSE WAVELENGTHS

IV RAMAN RESPONSE MEASUREMENTS

A. General

The Raman measurements were made on a Spex Ramalog Raman spectrometer. This instrument consists of a Coherent Radiation Model 52 argon-krypton laser source and a Spex Model 1401 double monochromator as the detection optical filter. The optical detector is an ITT FW130 photomultiplier that is thermoelectrically cooled to -30°C. A schematic diagram of this instrument is shown in Fig. 8. Two types of detection electronic systems are used--a dc system and a photon-counting system. The dc system monitors the photocurrent from the photomultiplier, with an adjustable electronic averaging time, and presents this information as a function of wavenumber on a strip-chart recorder. The photon-counting system digitally accumulates the photon count for a given time interval and again presents this information as a function of wavenumber on a strip-chart recorder. The photon-counting system provides better performance at extremely low light levels and is the preferred type for use with extremely weak signal levels. Both systems are adequate in sensitivity for determining Raman responses that will be usable in in-stack monitoring applications. The reason for this is that reasonably large Raman responses must be present in order to be usable with practical field instrumentation. It is evident that difficulties will be encountered in field measurements if, in the laboratory, many hours of integration are necessary to detect a material with a laboratory instrument whose optical geometry can be optimized for maximum signal on a fixed solid sample.

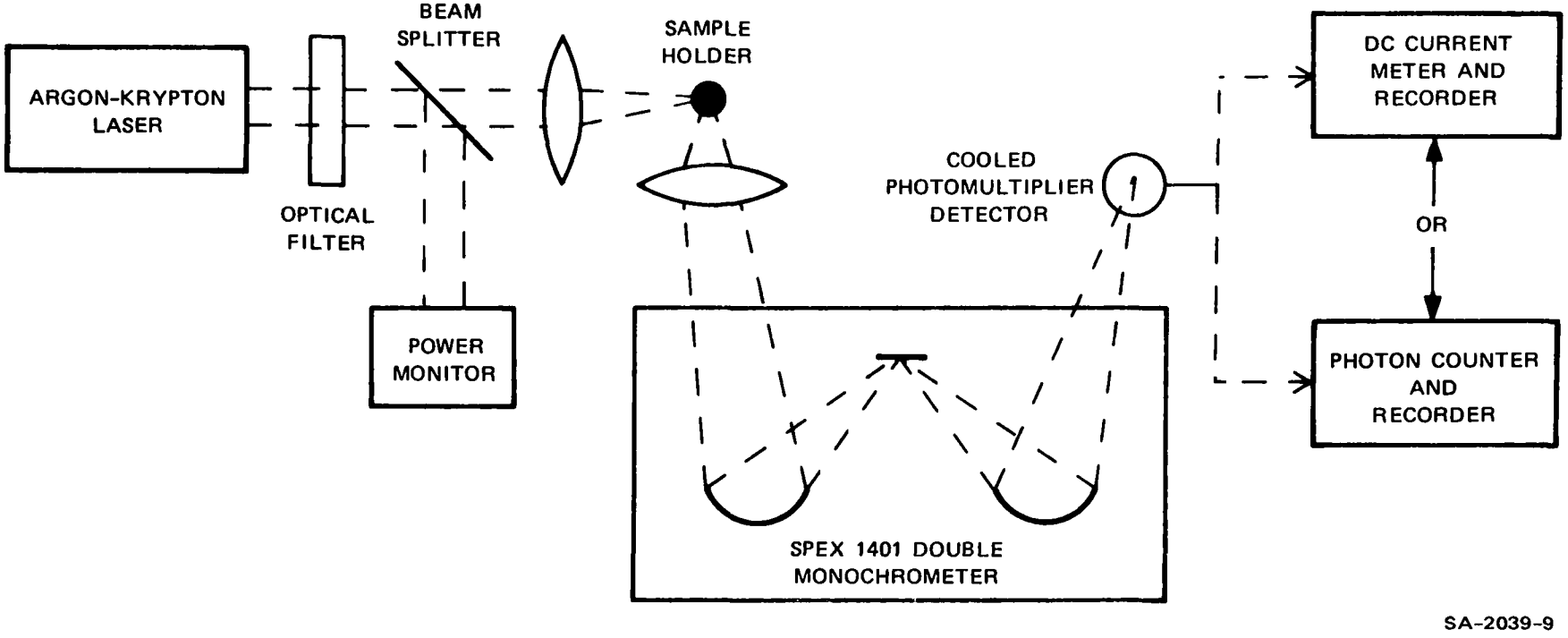

FIGURE 8 SCHEMATIC DIAGRAM OF RAMAN MEASUREMENT INSTRUMENT

The most important information needed in evaluating the feasibility of remote monitoring of various species by laser Raman spectroscopy is the intensity of the Raman scattered light, which is given by

$$I_p \propto I_o M \sigma_p^{\text{total}}$$

where I_o is the incident laser light intensity, I_p is the Raman scattered intensity, M is the amount of material present, and σ_p is the total molar Raman scattering cross section. This Raman cross section is the pertinent material property for determining the detectability of a given material and is similar to the quantum efficiency associated with the fluorescence process.

Before laser excitation was available, the stability, intensity, and other characteristics of the sources were among the major impediments to the measurements of absolute cross sections in Raman scattering, which is very weak. Since the advent of the laser, and with various improvements and refinements in analysis and detection techniques, the problem of absolute-cross-section measurements has become somewhat more tractable. However, such measurements have been made only in a small number of cases due to the considerable difficulties still present.[3-5] A great deal of thought has been given to this problem, which needs resolution before many areas of application can proceed to operational systems.

The sample properties and instrumental factors that affect the observed intensity include the following:

(1) Refractive index. This will affect:

(a) The intensity of the exciting radiation reaching the interior of the sample.

(b) The degree of convergence (relative intensities of perpendicular and parallel polarized components of exciting light as they appear to the scattering molecule).

(c) The fraction of the Raman radiation that can enter and pass through the monochromator.

(2) Molecular environment (caused by changes in sample composition).

(3) Fluorescence.

(4) Color.

(5) Intensity of the Raman source.

(6) Variations in the relative intensities of the parallel and perpendicular polarized components of the exciting radiation.

(7) Properties of the sample cell, if used, and the sampling geometry.

(8) Spectral sensitivity of the spectrophotometer.

(9) Polarization sensitivity of the spectrophotometer.

(10) Background emission. This may arise from scattering of fluorescence at the cell walls, from scattering of the continuum in the spectrum of the exciting radiation, or from stray light inside the monochromator.

(11) Instrument sensitivity (relation between the intensity of the radiation entering the monochromator and the recorder response).

The following methods are used to eliminate or correct for some of the above factors:

(1) Use of an internal standard, which eliminates the effects of variations in refractive index, as well as such instrumental factors as the intensity of the source, cell properties, and instrument sensitivity. This will not compensate for the effect of color except in gray samples.

(2) Use of a polarized laser beam, which essentially eliminates the effect of convergence and the partial polarization of the exciting light.

(3) Measurement of band intensities above a linear baseline drawn between preselected, fixed spectral positions on each side of the band, which largely corrects for background emission and

for a limited amount of sample fluorescence. (The intensity of the fluorescence normally changes slowly with the frequency with no sharp bands. However, too much fluorescence will unduly influence the signal-to-noise ratio for the Raman spectrum.)

(4) Use of a polarization scrambler placed at the entrance to the monochromator [illegible] eliminates the polarization sensitivity of the spectrometer.

(5) Periodic checks for changes in spectral sensitivity, which may be made by substituting a light source of reproducible relative spectral emissivity for the sample cell and recording the intensity over the spectral region of interest. Any changes in the observed ratios of the intensities can be used to correct the observed sample intensities.

Because of the attendant difficulties mentioned above in the measurement of Raman intensities, determination of absolute Raman cross sections is a major undertaking. For the purposes of the present feasibility study, it was deemed adequate to make relative-intensity measurements of the Raman lines for the various solid samples. The cross-section standard was a material (CdS) of known cross section.

Experimentation with several sampling techniques led to the adoption of the following sampling method. First, the chemicals were packed under pressure into the end of a 1/8-inch-diameter stainless steel rod into which a depression had been machined. The powder was given a relatively flat surface by pressing down on another flat surface. The stainless steel rod was then mounted in a holder and arranged so that the surface of the sample made an angle of approximately 45° to the vertical laser beam, which was incident from below the sample. The holder was capable of sufficient three-dimensional motion such that the laser focal spot could always be imagined centrally on the spectrometer slit. If the particle size of the sample was so coarse that sample fell out of the end of the rod when turned upside down, the sample was ground in a mortar to a finer particle size. No attempt was made to determine the particle size of the samples.

The spectra were initially recorded at a spectral slit width of 10 cm^{-1} and at a scan rate of 1000 cm^{-1} per minute. If interesting features appeared, the particular spectral ranges were reexamined at higher resolution. All the white samples were examined with 4880-Å excitation. The colored samples, including green cupric chloride, absorbed too much energy from the focused laser beam and were altered, as evidenced by discoloration at the position of the focal spot. Some of the hydrated samples appeared to lose their water of hydration at high power densities. Such samples were run with 6471-Å excitation or at reduced power (or both), as dictated by sample integrity and adequate SNR.

The ideal conditions and techniques that are desirable for Raman cross-section measurements were noted earlier. During the present investigations, several compromises had to be made, based on the available time, the large number of materials, and the expected eventual use of the data. For example, the spectral and polarization sensitivity of the spectrometer was not calibrated. Also, while every effort was made to achieve identical scattering geometries with the different samples, the effects of particle size, refractive index, color, and absorptivity were ignored. Because the effects of particle size were ignored in these measurements, no attempts were made at maintaining uniformity of particle size. All sample runs were performed after the laser power had stabilized. The laser power output, however, was monitored only occasionally, and small variations may still have occurred from run to run. Finally, because of the large variation in color, absorption, particle size, and uniformity, no attempt was made to use an internal reference standard. The net effect of all these compromises was believed not to lead to large errors in the measured results. Based on the

experience with repeated measurements of different samples and procedures, it is estimated that the results obtained are accurate to approximately ± 50% for the white samples.

B. Measurement Results and Discussion

Typical Raman response curves are shown in Figs. 9 and 10 for $(NH_4)_2SO_4$ and $CaSO_4$. Figure 9 is an example of a Raman curve with relatively low background and no fluorescence interference. A clean, strong Raman line appears at about 900 cm^{-1}, and smaller lines are shown. Figure 10 shows the effect of fluorescence interference, appearing as a broad, smooth curve over the entire chart. The Raman lines extend above this interference.

The Raman response curves are plotted as a function of wavenumber shift. A conversion to wavelength shift can be made by reference to Fig. 11, which gives wavelength shift versus wavenumber shift at several laser excitation wavelengths.

A summary of the Raman measurements is given in Table 3, listing the material, the wavenumber shift for all significant lines, and the measured signal and background levels. Also given in Table 3 is the cross section for each line, which will be discussed in a later section. For the sake of uniformity, the relative intensities in Table 3 are presented as counts per second normalized to a 10 cm^{-1} spectral slit width with 4880-Å excitation at 350 mW. This normalization removes the effects of different power levels, excitation wavelengths, and detection systems. In order to use this normalization procedure, linearity of the various devices was assumed. Also, the throughput of the system was assumed to be equal at 4880 Å and 6471 Å, and the scattered intensity was assumed to have a λ^{-4} dependence. This latter assumption is valid for the Raman intensity and the scattered background. However, it is not valid if the background was due to fluorescence or to Mie (particle)

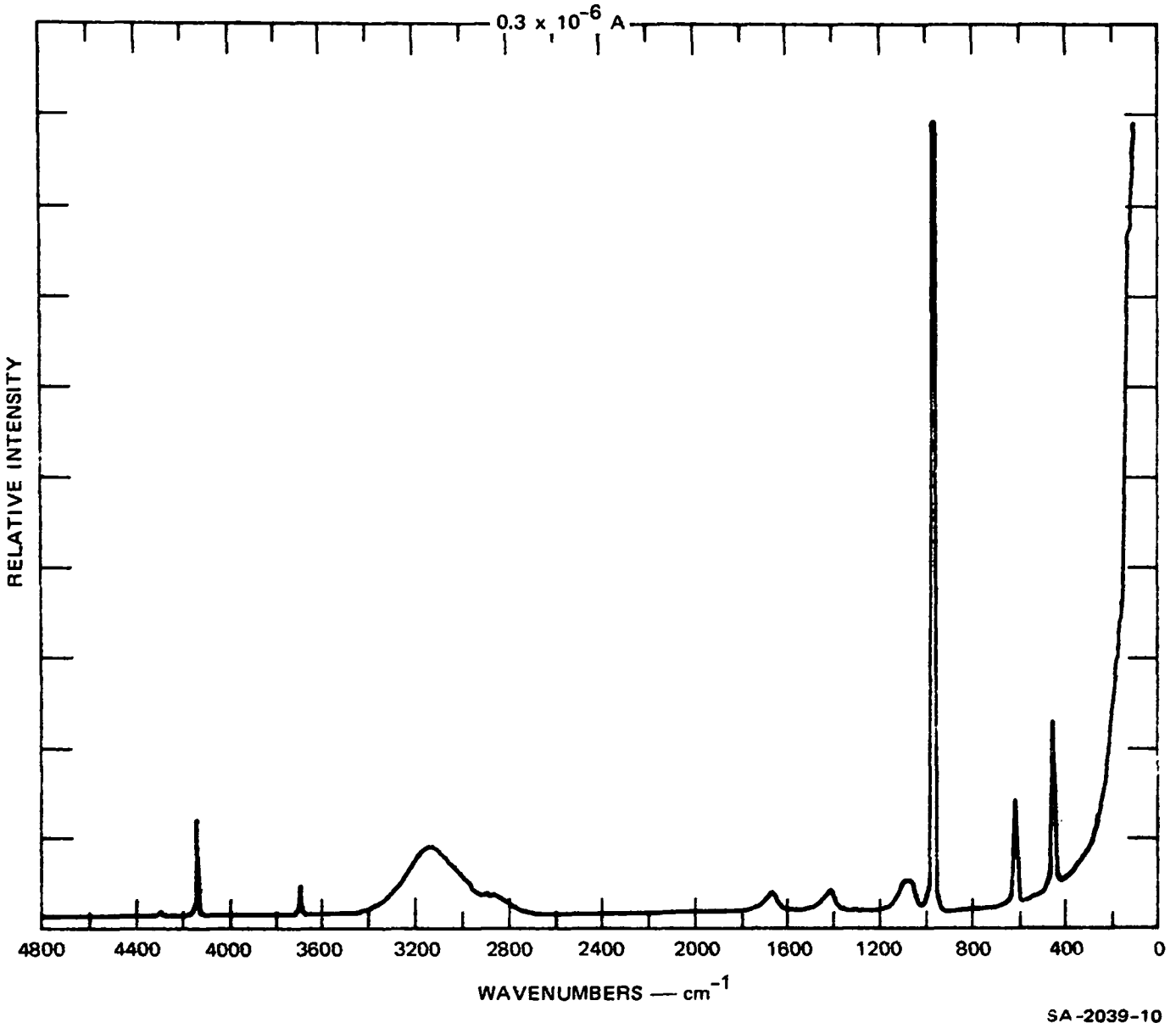

FIGURE 9 RAMAN RESPONSE CURVE FOR $(NH_4)_2SO_4$

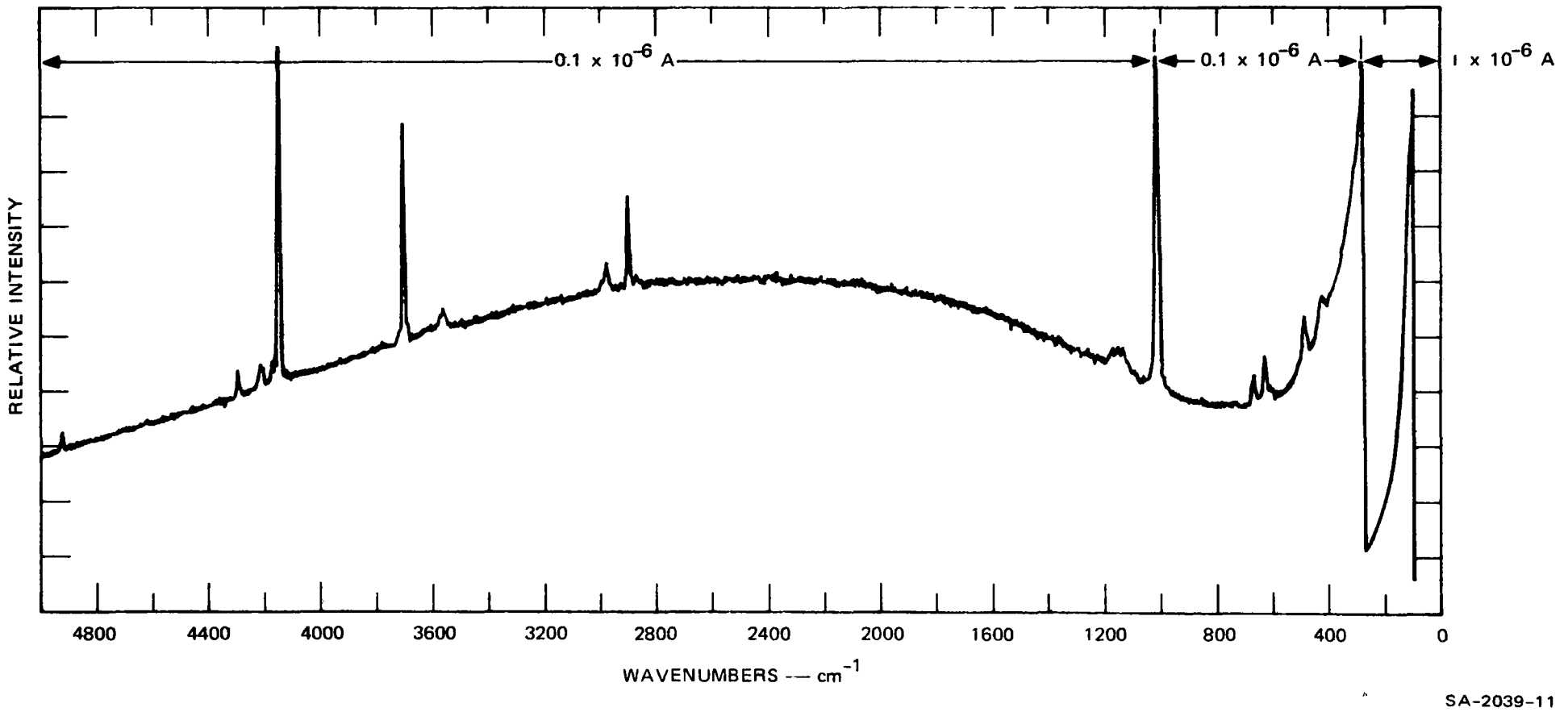

FIGURE 10 RAMAN RESPONSE CURVE FOR $CaSO_4$

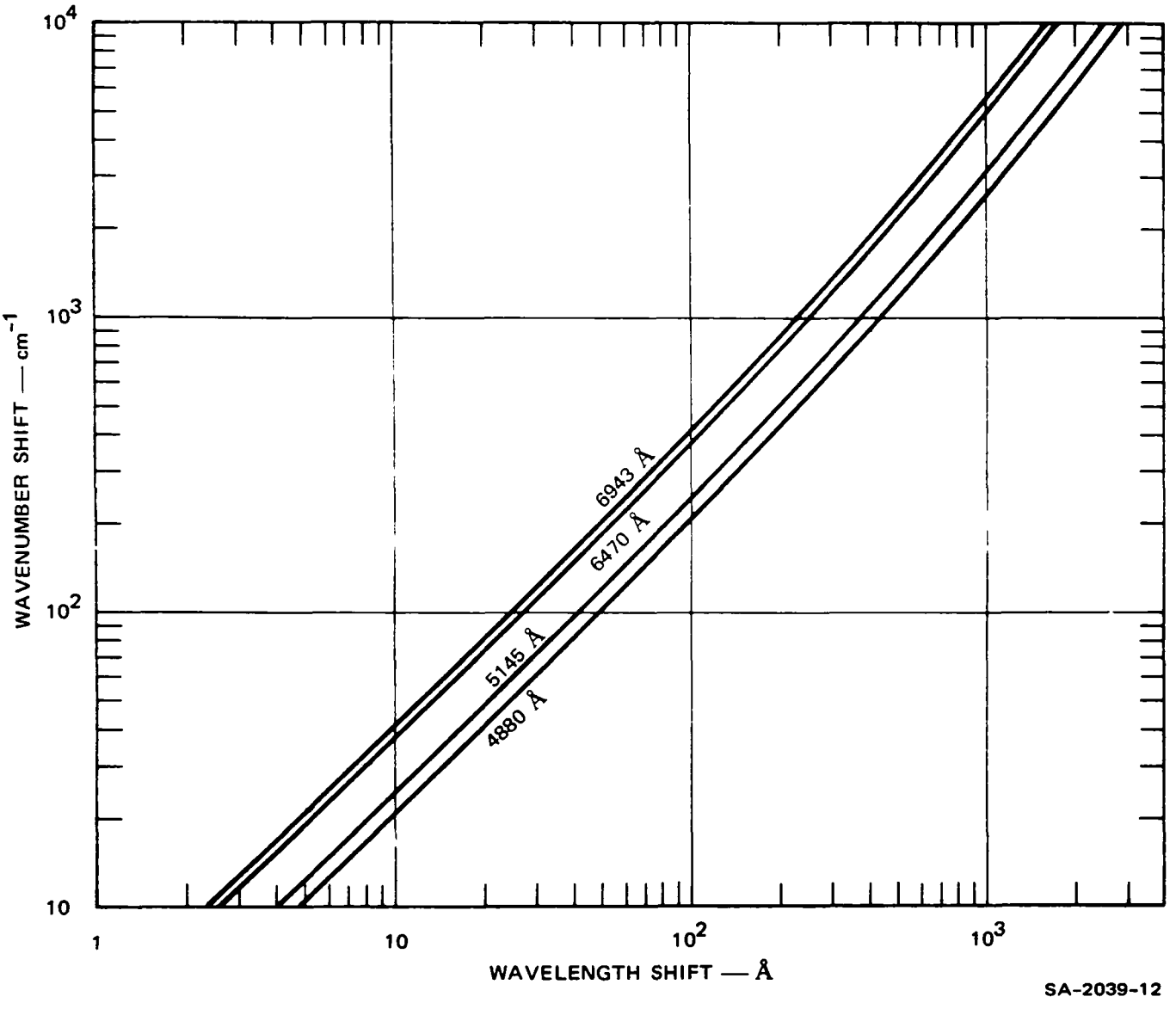

FIGURE 11 WAVENUMBER SHIFT-TO-WAVELENGTH SHIFT CONVERSION CHART

Table 3

RELATIVE RAMAN RESPONSE INTENSITIES

Material	Excitation Wavelength	Wavelength Shift	Peak Photon Count Rate	Background Photon Count Rate	Effective Raman Cross Section	Fluorescence Response	
						Maximum Response Location	Maximum Photon Count Rate
PbO	6471	60					
		69	7.8×10^6	4.3×10^6	797		
		86	1.3×10^7	4.3×10^6	1330		
		138	5.4×10^7	3.0×10^6	5520		
		279	1.4×10^7	1.7×10^6	1430		
		370	1.9×10^6	1.0×10^6	194		
$PbCl_2$	4880	60					
		86	8.4×10^5	7.9×10^6	174		
		156	1.5×10^7	4.1×10^6	3110		
$HgSO_4$	4880	93				2400	1.9×10^5
		121					
		230					
		300					
		410	5.0×10^5	1.8×10^6	100		
		495	1.5×10^7	1.5×10^6	3000		
		580, 588	2.1×10^6	1.3×10^6	420		
		660	2.8×10^6	1.3×10^6	560		
		987	8.8×10^6	1.3×10^6	1760		
		1043	9.6×10^6	1.3×10^6	1920		
		1125	1.5×10^6	1.3×10^6	300		
		1180	2.3×10^6	1.4×10^6	460		
		1342	2.5×10^5	1.5×10^6	50		
		1670	6.3×10^4	1.7×10^6	12.6		
$HgCl_2$	4880	70	1.4×10^7	5.4×10^6	3050		
		121	7.9×10^6	2.3×10^5	1720		
		312	2.4×10^7	2.1×10^5	5230		
		380	6.7×10^5	1.3×10^5	146		
RA	4880	420					
		750	4.2×10^3	6.7×10^4			
		1250	2.9×10^3	5.0×10^4			
	6471	720	1.9×10^6	5.4×10^6			
		1022	5.4×10^6	4.9×10^6			
		1052	8.1×10^6	4.9×10^6			
$PbSO_4$	4880	443	9.2×10^5	1.3×10^5	196		
		608	1.8×10^4	4.2×10^4	38.4		
		640	7.5×10^6	3.3×10^4	16		
		978	3.1×10^5	1.3×10^4	662		
		1065	1.7×10^5	1.3×10^4	36.3		
		1165	2.9×10^5	1.3×10^4	61.9		
$(NH_4)_2SO_4$	4880	450	2.3×10^5	4.6×10^4	75		
		613, 623	1.5×10^5	1.9×10^4	48.9		
		976	1.1×10^6	6.3×10^3	359		
		1090	4.6×10^4	6.3×10^3	15		
		1420	3.1×10^4	6.3×10^3	10.1		
		1650	2.5×10^4	6.3×10^3	8.15		
		3150	9.6×10^4	0 ?	31.3		
$CuCl_2$	4880	64					
		109					
		215	1.1×10^6	3.2×10^5	322		
		236, 249	3.4×10^5	2.5×10^5	99.6		
		407	1.6×10^5	1.1×10^5	46.9		
		700	4.2×10^4	4.9×10^4	12.3		

Table 3 (continued)

Material	Excitation Wavelength	Wavelength Shift	Peak Photon Count Rate	Background Photon Count Rate	Effective Raman Cross Section	Fluorescence Response	
						Maximum Response Location	Maximum Photon Count Rate
$CdCl_2$	4880	80					
		85					
		115					
		158					
		218	7.5×10^5	8.4×10^5	225		
		320	8.4×10^4	3.1×10^5	25.2		
		1585	8.4×10^3	1.2×10^4	2.52		
		3470	1.8×10^5	5.4×10^3	53.9		
$CdSO_4$	4880	160					
		185					
		255					
		280					
		315					
		415	7.1×10^4	7.9×10^4	25.7		
		450	2.5×10^4	6.7×10^4	9.06		
		497	9.6×10^4	5.4×10^4	34.8		
		603, 615	6.3×10^4	2.9×10^4	22.8		
		658, 670	1.9×10^4	2.6×10^4	6.88		
		835					
		925					
		1000	7.1×10^5	1.6×10^4	257		
		1050, 1063	9.6×10^4	1.6×10^4	34.8		
		1100, 1118	5.4×10^4	1.6×10^4	19.6		
		1168, 1173	5.9×10^4	1.6×10^4	21.4		
		1554					
		2700-3500	2.5×10^4	1.3×10^4	9.06		
HgO	6471	25					
		35					
		65					
		130					
		328	6.3×10^5	1.6×10^4	53.7		
		550	7.5×10^4	7.5×10^3	6.39		
HgS	6471	250	3.4×10^5	3.4×10^4	44.7		
		275	3.2×10^4	3.0×10^4	4.2		
		341	7.1×10^4	1.7×10^4	9.33		
$CaSO_4$	4880	425	2.1×10^4	2.1×10^5	5.32	2400	2.4×10^5
		490	3.8×10^4	1.8×10^5	9.63		
		620	3.3×10^4	1.5×10^5	8.36		
		670	2.3×10^5	1.5×10^5	5.83		
		1015	2.5×10^4	1.6×10^5	63.4		
		1150	1.7×10^4	1.8×10^5	4.31		
CdS	6471	212	1.2×10^5	2.6×10^5	15.7		
		305	7.0×10^4	1.5×10^5	9.16		
		347	6.2×10^4	1.3×10^5	8.63		
		365			8.11		
		563	1.9×10^4	6.2×10^4	2.49		
		599	5.9×10^4	5.9×10^4	7.72		

Table 3 (concluded)

Material	Excitation Wavelength	Wavelength Shift	Peak Photon Count Rate	Background Photon Count Rate	Effective Raman Cross Section	Fluorescence Response	
						Maximum Response Location	Maximum Photon Count Rate
$Al_2(SO_4)_3$	4880	480	2.5×10^4	2.0×10^4	13.8	2000	5.0×10^5
		620	1.9×10^4	1.9×10^4	10.5		
		1000-1200	3.8×10^4	4.2×10^3	20.9		
	6471	480	7.1×10^3	6.6×10^4			
		620	4.5×10^3	5.3×10^4			
		1000-1200	1.4×10^4	3.7×10^4			
Phosphate	6471					300	2.5×10^6
Rock Feed	4880	945	1.7×10^4	7.1×10^4		5000	1.2×10^5
		580	4.2×10^3	7.5×10^4			
Al_2O_3	4880	378	8.4×10^3	1.6×10^5	1.01	800	1.3×10^5
		415	1.3×10^4	1.4×10^4	1.56		
		585					
		643					
		750					
CaF_2	6471	None					
	4880	322	1.3×10^4	1.1×10^6	1.39		
Na_3AlF_6	6471	1040	7.8×10^3	3.1×10^4	2.46		
	4880	550	8.8×10^3	3.3×10^5	2.78	2200	5.0×10^5
Lead Concentrate	6471	950	3.8×10^2	4.2×10^2			
NBS Coal	4880	1350	375	9.4×10^3		2100	1.1×10^4
		1600	750	1.0×10^4			
	6471	None				1400	1.2×10^4
PbS	6471	None					
CdO	6471	None					
Cu_2O	6471	None					
CuS	6471	None					
AlF_3	6471	None				500	4.8×10^6
	4880	None				2700	6.7×10^5
CuO	6471	None					
Zinc Concentrate	6471	None					
	4880	None				>6000	5.4×10^4
Copper Concentrate	6471	None					
Super Phosphate	6471	None				400	4.0×10^5
B47 Fly Ash	6471	None				1100	5.4×10^3

scatter. The values of relative intensities are estimated to be accurate to ± 50% in the case of the white samples. In the case of the colored samples, the values are less reliable due to absorption effects.

Both the background and line intensities were determined at the position of the peaks. The background was determined by drawing a smooth line through the base of the peaks. The line intensity was then measured as the peak height above this background. It should be noted that the spectrometer slit of 10 cm^{-1} does not significantly influence the relative intensity of the background and broad Raman lines (broader than 20 cm^{-1}, say). The relative intensity of the narrower lines and the background will, however, depend on the slit width. These narrower lines are usually located at small wavenumber shifts from the exciting line and would not normally be used in field systems because of the stray-light-rejection problem. For this reason, the narrow lines have not been evaluated, although they could be, from the measured data.

It was not feasible to examine the region close to the exciting line (0 to 150 cm^{-1}) under a uniform set of conditions for all the samples, since the variation in scattered intensity in this region was very large for different samples. While several lines appear in this region, the available time and the eventual use of the data led to the decision not to examine them in detail. Scattered source light in this region was believed to be too sensitive a function of particle size. The level of the background from scattered exciting radiation within 100 cm^{-1} (or a spectral separation of 24 Å at 4880 Å) of the (unshifted) rayleigh line was felt to be too high to permit use of this region in any nondispersive system. The need for discrimination between the several substances that have lines in this narrow region is a further nontrivial problem.

The absolute values of the listed wavenumber shifts are estimated to be within ±5 cm^{-1}. The linewidths shown are believed to be accurate ±20%, without deconvolution of the instrument functions.

Some of the spectra (see Fig. 10, for example) show lines at 2900, 3700, and 4150 cm^{-1}. These have been shown to be grating ghosts and not characteristic of the scatterer. The spectral region above 2000 cm^{-1} was not evaluated for responses with 6471-Å excitation because it had too many artifacts caused by unfiltered plasma lines or grating ghosts. During the data analysis some of the very weakest lines were ignored when it was felt that their value relative to other lines for the same substance was minimal.

The measured lines are also shown in "spectral" form in Fig. 12 in order to illustrate the spectral distribution of the lines observed for the present materials. Note that there is a relatively uniform distribution of lines both in wavenumber offset and amplitude. Fig. 12 indicates amplitude in measured counts per second. Note that this count-per-second scale corresponds to the laboratory experimental measurement values and not to the in-stack monitoring-system values given in Table 2 for the fluorescence measurements. The relative magnitudes of these count rates would be correct for the in-stack monitoring system, however.

Some general remarks about the observed spectra are in order. It can be seen from Fig. 12 that the white solids were the most efficient scatterers. The colored solids either did not have a developed spectrum, or their intensities were low. It was also observed that the substances involving heavier elements had stronger lines. For example, the strongest lines in the figure are due to mercury and lead compounds. Even in the region 900 to 1200 cm^{-1} where the Raman lines are due to the sulfate

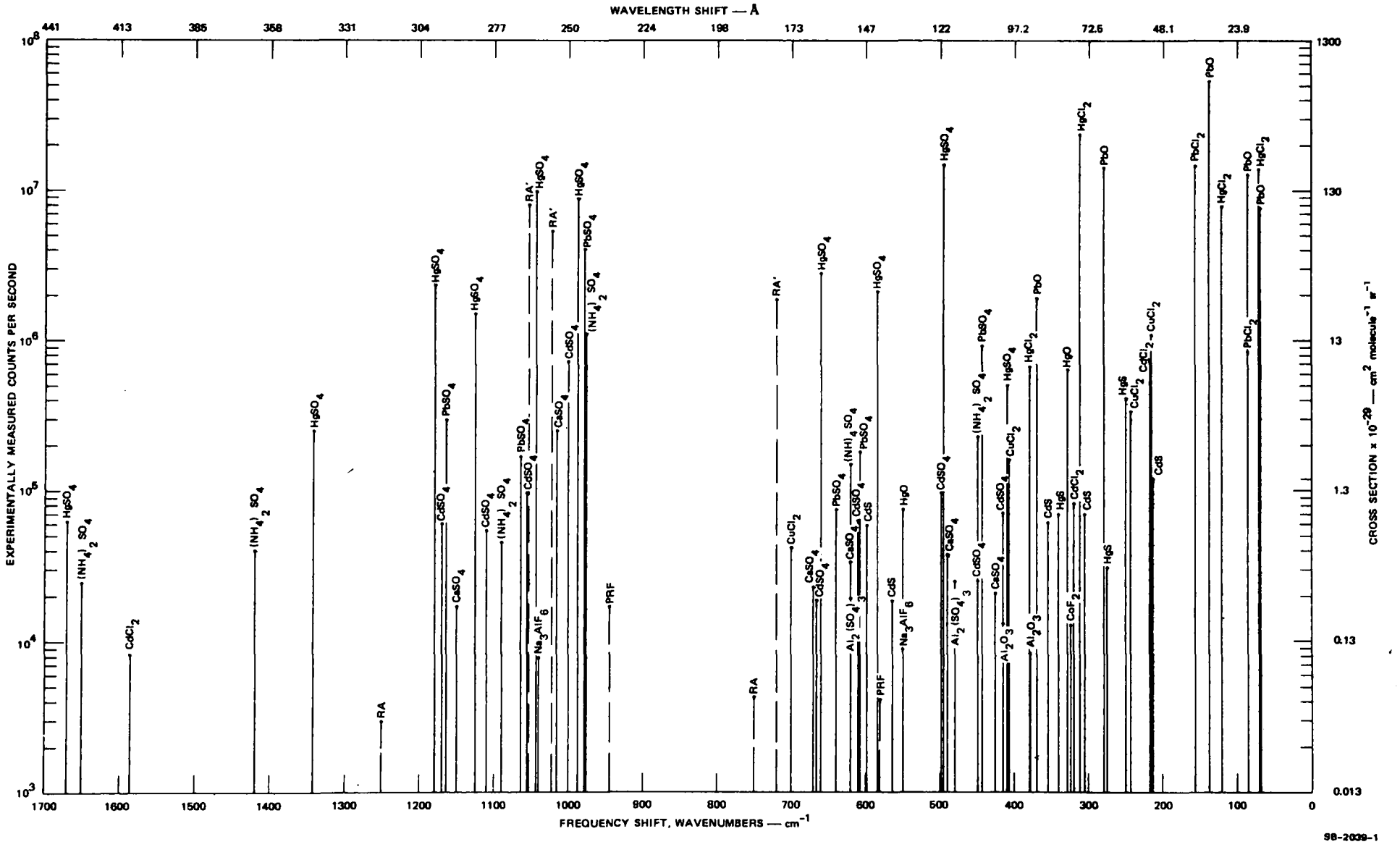

FIGURE 12 RAMAN SPECTRAL RESPONSE SUMMARY

ion, the lead and mercury sulfates have the highest count rates. The spectra of alumina and other aluminum compounds (fluorides, sulphate) were among the weakest even though they were all white.

The chosen materials included oxides, sulfides, halides, and sulfates. Among these only the sulfates have a vibrating sub-unit--the SO_4 molecular ion. On examining the spectra, it is noted that with very few exceptions, only the sulfates have Raman lines with shifts greater than 700 cm^{-1}. Note that the sulfate lines are grouped in three regions: 400 to 500 cm^{-1}, 600 to 700 cm^{-1}, and 950 to 1200 cm^{-1}. It is thus seen that even though the vibrational sub-unit SO_4 has frequencies which are, to first order, characteristic of the SO_4 unit, the actual frequencies are dependent on the specific compound in which they are present.

The point to be made most strongly is that the Raman spectral shifts or intensities cannot be accurately predicted by existing theory and are capable of wide variation. Thus, a general method for positive identification cannot depend on one specific spectral feature but must necessarily depend on several. Also, in the samples measured there are about 50 lines in the range 100 to 700 cm^{-1} (about 150 Å). This close spacing means that good resolution will be needed to discriminate between the several lines in any general identification scheme.

The spectra generated during the course of this program agree well with the published spectra that are available. The spectral shifts agree to within 5 cm^{-1}. Since relative-intensity data are usually not available, no comparisons of amplitude can be made. Further, since the published spectra are for oriented single crystals, a direct comparison with powder samples may not be completely accurate.

To convert the intensities to a cross-section value for the purposes of feasibility analysis, the published value of the cross section of

the 207 cm^{-1} line of CdS powder was used.[6] This reference is not clear about the details of the excitation frequency, the units used, and whether the cross section is for the entire line or the peak value. It is inferred from the body of the paper that the quoted Raman cross section for the 207 cm^{-1} line of CdS powder (0.7×10^{-28} cm^2 at 293°K) is the total cross section (4π sr) per molecule, measured with 6328-Å excitation. Assuming λ^{-4} dependence on wavelength and that the entire line was measured, the cross section at 4880 Å is calculated as 1.57×10^{-29} cm^2 sr^{-1} $molecule^{-1}$.

Only one value for the CdS cross section is available. In other materials a wide spread of measured cross-section values is often reported. For example, the cross-section value quoted in the same paper for the 992 cm^{-1} line of liquid benzene leads to a calculated cross-section value at 4880 Å of 4.5×10^{-29} cm^2 $molecule^{-1}$ sr^{-1}. Table 4 shows the range of values of the Benzene cross section as measured by various workers. It is seen that there is a spread of more than an order of magnitude in the values, with the value of Ref. 6 being the highest reported value. While comparable results were not available for CdS powder, it is conceivable that the techniques of Ref. 6 may have systematically given high values. Thus, the value of 1.57×10^{-29} cm^2 $molecule^{-1}$ sr^{-1} is used with reservations about its accuracy. Since the linewidth measured during this investigation (with a 10 cm^{-1} spectrometer slit) is 20 cm^{-1}, the measured peak intensity corresponds to the entire line. Thus, the measured rate of 1.2×10^5 counts per second corresponds to the above cross section with 350 mW of 4880-Å excitation.

Table 4

COMPARISON OF VARIOUS MEASUREMENTS OF THE RAMAN CROSS SECTION OF BENZENE (992 cm^{-1} LINE)

Excitation Å	Reported Cross Section (cm^2 sr^{-1} $molecule^{-1}$)	Cross Section at 4880 Å (cm^2 sr^{-1} $molecule^{-1}$)	Reference
6328	1.59×10^{-29}	4.5×10^{-29}	6
4880	3.25×10^{-29}	3.25×10^{-29}	3
4880	2.42×10^{-29}	2.42×10^{-29}	4
4880	5.48×10^{-30}	5.48×10^{-30}	7
4880	3.0×10^{-30}	3.0×10^{-30}	8
6943	4.5×10^{-31}	1.84×10^{-30}	9

A measurement-system constant, K_o, can be calculated from a knowledge of the measured count rate and the published cross section as

$$K_o = \frac{N_r M}{\rho \sigma} .$$

Using $N_r = 1.2 \times 10^5$ counts s^{-1}, $\rho = 4.82$ g cm^{-3}, $M = 144.476$, and $\sigma = 1.57 \times 10^{-29}$ cm^2 $molecule^{-1}$ sr^{-1} for CdS, we calculate $K_o = 2.29 \times 10^{35}$ counts cm molecule sr s^{-1} $molecule^{-1}$. The cross section of any other material can then be calculated as

$$\sigma = N_r M / K_o \rho .$$

It should be recalled that the measurements were made with a slit width of 10 cm^{-1}; thus the above relation gives the cross section for the entire line for lines with halfwidths smaller than 10 cm^{-1}, but for lines with larger widths it gives the cross section per 10 cm^{-1} at the peak.

The calculated cross sections for the materials evaluated on this contract are shown in Table 3. Note again that the measured count rate is more representative of the variation in signal strength with material than is the cross section.

V IN-STACK MONITORING SYSTEMS

A. General

In considering the application of optical in-stack monitoring systems, two types of monitoring functions were postulated. The first function is the assessment of the relative concentration of a number of constituents without a knowledge of the absolute concentration of any single component. Because absolute numbers are not required, this type can also be considered as a qualitative measurement. Second is the quantitative measurement of the amount of a single constituent present in the stack particle stream. Ideally, of course, one would hope that a quantitative measure of each of the constituents in the particulate stream would be measurable. The extent to which this is possible can be determined by extrapolating the results of the quantitative and qualitative approaches taken in this project.

In addition to these two types of applications discussed above, both Raman and fluorescence material interactions were considered as sensing mechanisms. As the project progressed, it seemed that there was a match between the application and the sensing mechanism. In particular, the fluorescence response seemed more appropriate for the quantitative sensing of one kind of material in the particulate stream, and the Raman response seemed more appropriate for the relative analysis of several constituents on a qualitative basis. This comes about because the fluorescence response is relatively large and can thus yield relatively good quantitative information, but the spectral characteristic of fluorescence is such that it would be difficult to separate a variety of constituents. In contrast, the Raman response shows relatively distinct spectral features for each material; however, the low level of the response would

make the collection of quantitative information rather difficult. For this reason, the systems analyzed in this section will be divided into fluorescent systems, with emphasis on quantitative measurements, and Raman systems, with primary emphasis on separation of spectral information and less emphasis on amplitude-calibration techniques.

The in-stack fluorescence monitoring system can provide a high level of performance relative to the experimental laboratory measurements because of the large fluorescence response. This means that all the materials that have observable fluorescence in the laboratory measurements can be detected by an in-stack system, although a few materials may be marginal with inexpensive monitoring systems. Thirteen materials were observed to have significant fluorescence responses, and these can be detected by the in-stack system. Twenty-one materials did not have observable fluorescence and would not be detectable by the in-stack system.

Two Raman systems have been considered. The first uses a spectrometer and is similar to the laboratory measuring instrument. The other uses an optical filter and may provide for a limited analysis capability at a lowered cost. Generally speaking, for these systems, a lower performance level would be obtained in the in-stack system than was present in the laboratory measuring instruments. Twenty-two materials had measurable Raman spectra and twelve materials did not. Of the twenty-two materials that had observable Raman spectra, approximately fifteen materials would be detectable in the in-stack system, four materials would be marginal, and three materials would not be detectable in the in-stack system, even though they had observable Raman spectra in the laboratory.

B. Fluorescence-Monitoring Systems

In order to make reasonable estimates of the in-stack detectability of the fluorescent materials measured in the laboratory, some common

signal reference level must be used to relate these laboratory amplitudes to calculated in-stack-monitoring-system signal levels. The most appropriate approach was believed to be the use of a diffuse white reflector to relate calculated and measured signal levels. The reflector chosen was a freshly-prepared, diffuse, white magnesium oxide surface. This reference material was measured on the Baird-Atomic spectrofluorimeter and served as a reference amplitude level to which material fluorescent responses could be related. The assumed unity diffuse reflection coefficient could then be used as a reference response signal level for the in-stack monitoring system as well. If the effects of scattering, absorption, obscuration, etc., are neglected for the particle stream, it is thus possible to obtain estimates of the in-stack fluorescence-monitoring system performance for each of the materials measured by the laboratory instrument.

The measured reference signal level for the diffuse white reflector is shown in Table 5. This reference measurement was made at a peak wavelength of 455 nm and after normalization resulted in a relatively large peak signal level compared to the existing fluorescent-material responses. The peak photon count for the diffuse reflector is shown in the sixth column and represents the calculated in-stack monitoring-system reference signal level (i.e., the signal level that would be observed with an in-stack monitoring system viewing a white reflector rather than a particulate stream).

Also included in Table 5 are the responses for three highly fluorescent scintillation dye materials: bis-MSB [p-bis (O-methylstyryl) benzene], POPOP [2, 2'-p-phenylenebis (5-phenyloxazole)], and PPO [2, 5 diphenyloxazole]. These highly fluorescent materials have a quantum efficiency of approximately 0.5. A crude check on this quantum efficiency, and thus on the assumed reference level, was made by calculating the normalized integrated signal level in addition to the peak signal level. The integrated signal level is a calculated value of the instrument

Table 5

FLUORESCENT-REFERENCE-MATERIAL MEASUREMENT

Material	Peak Wavelength (nm)		Normalized Peak Signal Level (μa)	Normalized Integrated Signal Level (μa)	Peak Photon Count (pnotons/s)	Integrated Photon Count (photons/s)
	Excitation	Fluorescence				
Diffuse white reflector	455	--	34,700	34,700	1.25×10^{10}	1.25×10^{10}
BIS(MSB)	402;425	480	1,340	17,900	4.83×10^{8}	6.45×10^{9}
POPOP	424	460	1,880	21,400	6.77×10^{8}	7.71×10^{9}
POP	365	395	2,411	23,900	8.69×10^{8}	8.61×10^{9}

response, assuming that all the light emitted over the entire fluorescence response curve was measured by the instrument, while the peak signal level corresponds to the optical signal measured just through the narrow bandwidth of the instrument itself. These two levels are substantially different because these dye materials were measured at the maximum resolution of 2 nm by the Baird-Atomic instrument, and the width of the fluorescent response is significantly larger than 2 nm. Note from Table 5 that the integrated signal levels for the three highly fluorescent materials represent a substantial fraction (≈ 0.5) of the integrated response for the diffuse white reflector. This check of the integrated signal level for the three highly fluorescent materials serves as an additional verification for the use of the diffuse white reflector as a fluorescence amplitude reference.

The response of the in-stack monitoring system to a diffuse white particulate material must be calculated in order to derive estimates of detectability for the measured materials in a typical in-stack monitoring system. This response can then be related to the material measurements through the white-reflector measurement. This method assumes that the relative particulate fluorescence properties are the same as the relative bulk fluorescence properties and that the relationship between the fluorescence response and the diffuse white-reflector response is identical for both powders and bulk reflecting surfaces. This assumption neglects the effects of self-absorption, Mie and other particulate scattering effects, and some geometrical optical effects.

Assume a fluorescence-monitoring system that illuminates a volume of particulate material, suspended in an airstream, with an optical signal whose wavelength is assumed to be at the peak of the desired material excitation response curve. The light from the fluorescing particulate materials is collected by a collecting lens, and, after optical filtering, is directed to an appropriate optical detector. It

is also assumed that the function of this fluorescence-monitoring system is to obtain quantitative data on a known constituent or constituents. Thus, the predominant signal-processing requirements have to do with amplitude measurements in a fixed channel (or channels) of optical filtering, with no intercomparison of multichannel amplitude information being required for constituent analysis.

The schematic diagram of this in-stack fluorescence monitoring system would be virtually identical to the schematic diagram for the laboratory fluorescence-measurement systems as shown in Fig. 1. The most significant difference in this schematic diagram would be that the common optical volume would be within the stack rather than within some sample chamber, as was the case for laboratory measurements. Other differences will exist in physical configuration and in component values; however, these differences in numerical value do not change the schematic diagram for the resulting instrument.

If we assume a common optical volume of diameter D_L and length ℓ, the number of particles illuminated in this common volume is

$$n = \frac{\pi D_L^2 \ell \nu}{4}$$

where ν is the particulate density in particles per cubic centimeter. The equivalent particle area is

$$A_p = \frac{\pi D_P^2}{4}$$

where D_P is the mean particle diameter. The fraction of light intercepted by the total particulate area in the common illuminated volume is equal to

$$\frac{\pi D_P^2}{4} \ell\nu \quad .$$

If we assume an illumination power of P watts and a collection efficiency ω, an optical efficiency η, and quantum efficiency Q, the detector count in photons per seconds is equal to

$$N_F = 0.2 \times 10^{20} \frac{\pi D_P^2}{4} P\ell\nu\omega\eta Q \quad .$$

With $\omega = 0.1/4\pi$, $\eta = 0.1$, and $Q = 0.21$, the detector count is 1.25×10^{10} photons/s. This is shown in Table 5 as the reference peak photon-count level for the diffuse white reflector. Also given in Table 5 are the peak photon counts for the three highly fluorescent dye materials. An integrated photon-count level is also shown for the fluorescent material to indicate the photon count that would be available assuming that all of the fluorescent response light could be collected and utilized by the optical detector. It is not usually feasible to use the full response width in practice because of the necessary rejection of the excitation light by the optical filter. Thus a response closer to the peak photon count would be observed in practical in-stack monitoring systems. Fortunately, the peak photon-count level is sufficiently high that it provides a useful signal level for all of the materials investigated. This peak photon-count level is given in Table 2 for the chemical materials investigated on this project. Reasonably high count rates would be obtainable for all of the fluorescent materials investigated in this project. A count rate is not given for the Raman response of water because of the significant difference in geometry for the liquid measurement. The larger common volume of the liquid samples would yield a higher response level than would be achieved with the smaller common volume that is obtained with the solid samples. The

position of the entry for water in Table 2 does, however, give an indication of the signal levels of Raman responses relative to the responses of slightly fluorescent materials.

The lower limit for response measurements is set by the dark count of the detector. The dark count for a typical photomultiplier detector (i.e., Type 1P28) is approximately 8000 counts/s. This dark count sets a minimum level on the number of photons/s that can be detected by the system. This dark count can be reduced by using a low-noise tube such as the EMI 6094S, with a dark count of 660 counts/s. If necessary, these count rates can be reduced by at least a factor of 10 by cooling and tube selection. Thus, it is possible to detect even the low-fluorescence materials with feasible systems.

C. Raman Monitoring Systems

1. General

Two types of Raman measurement instruments will be discussed for in-stack monitoring applications. The first of these is an instrument utilizing a spectrometer that scans the entire spectral region of interest. The second is a lower-cost filter-type instrument that looks only at specific wavelengths, and will be considered for more limited applications of the Raman monitoring technique.

The spectrometer-type instrument is similar to the instrument used for the laboratory measurements. The major difference, as for the fluorescence system, is in the common optical volume, which is inside the stack rather than located at the sample-holder position. A schematic diagram for such a system would be similar to that shown in Fig. 8 for the laboratory system.

2. Spectrometer-Type System

For this instrument, assume a laser beam of power P watts, diameter w cm, wavelength λ cm, and negligible divergence passes

through an aerosol containing the particles of interest. These particles are assumed to be spherical, with an average diameter d cm, and to have a number density n cm^{-3}, density ρ g cm^{-3}, molecular weight M g mole^{-1}, and Raman cross section σ cm^{2} molecule^{-1} sr^{-1}.

Assume that the Raman light is collected at 90^{o} by a lens system and analyzed by a spectrometer of f-number F, and dispersion D cm/cm^{-1}. If the needed resolution is ν cm^{-1}, then the slit width to be used is $D\nu$ cm. Let the slit height be H cm. The acceptance angle of the spectrometer is $(1/F)$. The corresponding solid angle is $\pi/(4F^{2})$. The entendue of the system is then $\pi D\nu H/(4F^{2})$, which should remain constant in the optimum optical system.

The following typical values are used in the discussions:

$P = 1$ watt	$\rho = 4.82$ g cm^{-3}
$\lambda = 0.488 \times 10^{-4}$ cm	$M = 144.46$ g mole^{-1}
$w = 0.1$ cm	$\sigma = 1.57 \times 10^{-29}$ cm^{2} molecule^{-1} sr^{-1}
$d = 1 \times 10^{-4}$ cm	$F = 6.8$
$n = 10^{6}$ cm^{-3}	$D = 4.5 \times 10^{-3}$ cm/cm^{-1}
$\eta = 0.268$	$\nu = 10$ cm^{-1}
$Q = 0.15$	$H = 1$ cm .

The mass density of the aerosol is then

$$n\pi d^{3}\rho/6 = 2.52 \times 10^{-6} \text{ g cm}^{-3} .$$

The number of particles per unit length of the laser beam is

$$n\pi w^{2}/4 = 7.85 \times 10^{3} \text{ cm}^{-1}$$

The total geometrical cross-sectional area of these particles is

$$n(\pi w^{2}/4)(\pi d^{2}/4) = 6.17 \times 10^{-5} \text{ cm}^{2} \text{ cm}^{-1} .$$

The fraction of the laser-beam cross section occupied by the particles is

$$\pi n d^2/4 = 7.85 \times 10^{-3} \text{ cm}^{-1} = 0.79\% \text{ cm}^{-1} \quad .$$

This is a small fraction of the laser beam and therefore represents only a small loss or attenuation of light in the common optical volume. The actual fraction of light scattered is determined by an effective cross section, which may be different from the geometrical cross section. The theory of scattering by small particles indicates that the scattering efficiency, q, of the particles can vary from 2 to 6 depending on the size and refractive index (i.e., 2 to 6 times the energy intercepted by the geometrical cross section of the particle is scattered). This scattered light appears as attenuation for the transmitted beam. Thus, the attenuation coefficient due to scattering is $\alpha = nq\pi d^2/4 \text{ cm}^{-1}$. The scattered radiation may still be effective in causing an observed Raman signal because of multiple scatter. This has the effect of increasing the beam diameter or decreasing the photon flux density. However, calculations of these multiple-scattering events is a difficult undertaking. Because of this difficulty and the fact that the attenuation in the particulate common optical volume is a small percentage under the assumed conditions, it will be neglected in the following treatment.

If the laser beam of length ℓ is imaged to fill the slit with a collection angle of Ωsr, then

$$w\ell\Omega = \pi D\nu H/(4F^2)$$

where $wm = D\nu$; and $H = \ell m$ where m is the magnification of the system. Thus,

$$\Omega = \frac{\pi D\nu H}{4F^2}\frac{1}{w\ell} = \frac{\pi}{4}\left(\frac{m}{F}\right)^2$$

$$= \frac{\pi}{4}\left(\frac{D\nu}{wF}\right)^2 = 3.44 \times 10^{-3} \text{ sr} \quad .$$

The photon flux density is then

$$\frac{4P}{\pi w^2}\frac{\lambda}{hc} = 3.13 \times 10^{20} \text{ photons cm}^{-2} \text{ s}^{-1} \quad .$$

The sample volume is

$$\pi w^2 \ell/4 = \frac{\pi w^2}{4}\frac{Hw}{D\nu} = 0.017 \text{ cm}^3 \quad .$$

The number of particles in the sample volume is

$$n\frac{\pi w^3}{4}\frac{H}{D\nu} = 1.74 \times 10^4 \quad .$$

Neglecting attenuation, the number of scattering molecules in the sample volume is

$$n\frac{\pi w^3}{4}\frac{H}{D\nu}\frac{\pi d^3}{6}\frac{\rho}{M}A = 1.84 \times 10^{14} \text{ molecules} \quad .$$

From this, the number of Raman scattered photons is

$$N_r = \frac{4P}{\pi w^2}\frac{\lambda}{hc}\frac{n\pi w^3 H}{4D\nu}\frac{\pi d^3}{6}\frac{\rho A\sigma}{M}$$

$$= \frac{P\lambda A}{hc}\frac{n\pi d^3}{6}\frac{\rho\sigma}{M}\frac{wH}{D\nu}$$

$$= 9.03 \times 10^5 \text{ photons s}^{-1} \text{ sr}^{-1} \quad .$$

With a spectrometer transmission of $\eta = 0.268$ and a detector quantum efficiency $Q = 0.15$, the number of counts for CdS is

$$N_r = \frac{P\lambda A}{hc}\,\frac{n\pi d^3}{6}\,\frac{\rho\sigma}{M}\,\frac{wH}{D\nu}\,\Omega\eta Q$$

$$= \frac{P\lambda A}{hc}\,\frac{n\pi d^3}{6}\,\frac{\rho\sigma}{M}\,\frac{wH}{D\nu}\,\frac{\pi}{4}\left(\frac{D\nu}{wF}\right)^2\eta Q$$

$$= \frac{\pi}{4}\,\frac{\lambda A}{hc}\,\frac{P}{w}\,\frac{\pi n d^3}{6}\,\frac{\rho\sigma}{M}\,\frac{D\nu H\eta Q}{F^2}$$

$$= 125 \text{ count } s^{-1} \quad .$$

The above equation may be rewritten as

$$N_r = 1.16 \times 10^{42}\,\frac{P}{w}\,\frac{\pi n d^3}{6}\,\frac{\rho\sigma}{M}\,\frac{D_\nu H\eta Q}{F^2}$$

$$= K_1\,\frac{P}{w}\,L\mathcal{M}S \text{ counts } s^{-1}$$

where $K_1 = 1.16 \times 10^{42}$ molecule mole^{-1} J^{-1}

$$L = \pi n d^3/6 = 5.24 \times 10^{-7}$$

$$\mathcal{M} = \rho\sigma/M = 5.24 \times 10^{-31} \text{ mole molecule}^{-1} \text{ cm}^{-1} \text{ sr}^{-1} \text{ (for CdS)}$$

$$S = D\nu H\eta Q/F^2 = 3.91 \times 10^{-5} \text{ cm}^2 \text{ sr}$$

for the chosen spectrometer system.

$\mathcal{M}$ is determined by material characteristics, S by spectrometer and detector characteristics, and L is the volume fraction of the material in the aerosol. Thus, given a particular spectrometer system, particle type, and concentration, the only parameters that can be changed to increase the number of counts are the laser power and the beam diameter.

Increases in laser power are limited by technology and expense. The beam diameter w cannot be reduced indefinitely because the beam divergence will increase and lead to a lower limit on w. More importantly, the total number of particles in the sample volume will also decrease as the cube of the beam diameter w. The decreasing sample volume is compensated for by a higher flux, and a larger collection angle Ω, both of which increase as w^2.

Up to this point, the analysis has considered only the optical effects in the common volume illuminated by the laser and viewed by the spectrometer. In particular, the attenuation in this region has been neglected. Although the attenuation in the common volume is small, the attenuation in the optical path to and from the common volume may be significant and is calculated as follows:

Assume that the laser beam travels a distance u_o through the aerosol to the common sample volume, and the Raman scattered photons travel a distance u_1 through the aerosol to reach the detector optics. Since the sample length is ℓ, it is readily shown that, if the light attenuation of the aerosol is taken into account, the above expression must be multiplied by an attenuation factor Δ given by

$$\Delta = \frac{e^{-\alpha(u_o + u_1)}}{\alpha\ell}\left[1 - e^{-\alpha\ell}\right]$$

where $\alpha = nq\pi d^2/4 \text{ cm}^{-1}$.

For a typical system, $u_o = u_1 = 30$ cm, and assuming $q = 3$, then

$$\Delta = 0.237$$

and for CdS,

$$N_r = 29.6 \text{ counts } s^{-1} .$$

The count rate is thus reduced from 125 counts/s to 29.6 counts/s; it is evident that the attenuation in the path is significant under the assumed conditions.

Implicit in the above calculation of count rate is the assumption that the particle density is constant. Actually, however, there will be fluctuations in the number of particles in a given volume, and this can appear as noise in the detected optical signal. For example, for the values used above, the sample volume contains on the average 1.74×10^4 particles. The rms fluctuation in this value is $(1.74 \times 10^4)^{1/2} = 132$ or 0.76%. If the beam diameter were reduced by a factor b under stationary conditions (particles are stationary), the percentage fluctuation will increase by $b\sqrt{b}$. However, when the aerosol is moving at a flow rate of v cm s^{-1}, the actual aerosol volume swept through the sampling volume will be $wv\ell$ cm^3 s^{-1}, if the laser beam is normal to the direction of the flow. Thus, the number of particles in the volume will be $nwv\ell$ s^{-1}. For $v = 100$ cm s^{-1}, the number of particles will be 2.2×10^7. The calculated number density will then be in error by 0.02%. Thus, for reasonable in-stack effluent velocities, noise due to this source is not expected to be a problem. Optimization of the beam diameter, however, will be dependent on the particle density and the in-stack velocity if one wishes the photon noise to limit the accuracy of measurement.

The SNR characteristics may be evaluated using the data presented in the previous section on measured Raman and background ratios. There are, however, additional sources of background in the in-stack configuration. Contained in the laser-illuminated sample volume, along with the particles of interest, are molecules of the gas and possibly other constituents that cause Raman and fluorescent scatter. Estimation of the fluorescent background intensity cannot be made other than by actual measurement. The Raman scatter from the gas molecules may be estimated as follows. At atmospheric pressure and $300^{\circ}K$, the number

density of any gas molecule is $n_a = 2.45 \times 10^{19}$ molecules cm^{-3}. The number in the sample volume is $(\pi w^2 \ell n_a/4) = 4.16 \times 10^{17}$ molecules. Thus, the number of air molecules is 2.26×10^3 larger than the number of molecules of interest and could perhaps cause a large signal that would mask the return from the desired species.

Fortunately, most gases have Raman shifts higher than 1000 cm^{-1}, which is the approximate upper limit needed for the solid materials of interest. Table 6 is a list of the vibrational Raman shifts of these gases as well as their measured cross sections relative to nitrogen. Nitrogen, the reference gas, has a cross section of $3.3 \pm 1.1 \times 10^{-31}$ cm^2 s^{-1} $molecule^{-1}$. Also, the gas cross sections are, on the average, an order of magnitude smaller than those of the solids, and will partially compensate for the larger concentration. The pure rotational Raman shifts of most of the gases occur in the region below 100 cm^{-1} and have higher cross sections. Again, this spectral region will not be useful, because of scatter from particles. Thus, except for the 519 cm^{-1} line of SO_2, no large interference from gases is expected in the range 100 to 1000 cm^{-1} where most of the lines of interest occur. However, it should be remembered that these gas molecules will contribute to rayleigh scattering and, with low particle concentrations, to the background level in the spectrometer.

Now that a relatively interference-free spectral region is assured, the detection limits for the spectrometer system can be estimated. The detection limit will be presented as an integration time to detect a given standard condition. This method was chosen to simplify the data presentation for both long- and short-integration-time systems.

One important condition on the detection process is the expected dilution of the active material by a neutral substance. In an aerosol, this dilution can be accomplished in two ways; first, the active material may be only a part of the particle composition, and, second, the

Table 6

RELATIVE RAMAN CROSS SECTIONS FOR GASES

Gas	Wavenumber Shift (cm^{-1})	Relative Cross Section
N_2	2331	1.0
O_2	1556	1.3
H_2 (sum)	4161	2.4
H_2 (Q(1))	4161	1.6
CO	2145	1.0
NO	1877	0.27
$CO_2(\nu_1)$	1388	1.4
$CO_2(2\nu_2)$	1286	0.89
$N_2O(\nu_1)$	1285	2.2
$N_2O(\nu_3)$	2224	0.51
$SO_2(\nu_1)$	1151	5.2
$SO_2(\nu_2)$	519	0.12
$H_2S(\nu_1)$	2611	6.4
$NH_3(\nu_1)$	3334	5.0
$ND_2(\nu_1)$	2420	3.0
$CH_4(\nu_1)$	2914	6.0
$C_2H_6(\nu_3)$	993	1.6
$C_6H_6(\nu_1)$	3062	7.0
$C_6H_6(\nu_2)$	992	9.1

solid-material content in the aerosol sample volume may be changed by varying the particle size, shape, or concentration. It is convenient to define a dilution factor x that includes both of these effects in a single factor.

In order to estimate the fractional dilution at which these compounds are detectable, the following assumptions are made: (1) the measured experimental values for the Raman lines and background are for the sample at theoretical density; (2) the intensity of the Raman lines and the intensity of the background are proportional to each other and the incident power; (3) the dilution of the sample is accomplished by mixing with a neutral material that does not contribute to the background. This last assumption is true only for changes in particle size or concentration. It is not possible to change the solid-material dilution ratio without changing the ratio of Raman photon counts to background photon counts. Also, the assumption is true for aerosols only if the particulate scatter is the predominant background source and the detailed Mie scatter properties are neglected.

For consistency with the measured data, assume a Raman line of width ν_r cm^{-1} with a peak count rate of N_r counts s^{-1} when this rate is measured with a 10 cm^{-1} slit. Let the background counts at the position of the line be N_b counts s^{-1} for a 10 cm^{-1} slit. Assume also that the detection system uses a bandwidth of ν_r cm^{-1}. Then the Raman counts received will be $N_r(\nu_r/10)$ counts s^{-1} and the background counts will be $N_b(\nu_r/10)$ counts s^{-1}, if $\nu_r > 10$ (otherwise, $\nu_r = 10$). The total number of counts over a counting period T will then be $(N_r + N_b)\nu_r/10$. If the dilution factor is x, then the number of counts is $(N_r + N_b)\nu_r xT/10$.

Neglecting other noise sources, except Poisson statistical noise (photon noise), the noise component is then

$$\text{Noise} = \left[(N_r + N_b)\nu_r xT/10\right]^{1/2}$$

and the ratio of the Raman signal to the noise in signal is

$$\frac{S_{Raman}}{Noise} = \frac{N_r \nu_r xT/10}{[(N_r + N_b)\nu_r xT/10]^{1/2}} = \left(\frac{N_r \nu_r xT}{Z}\right)^{1/2}$$

where

$$Z = (N_r + N_b)/N_r \quad .$$

If one desires an accuracy of a% in the result, this may be interpreted as a desired SNR of (100/a). Thus,

$$Txa^2 = 10^5 Z/N_r \nu_r \ s \quad .$$

This expression gives the time, in seconds, to obtain enough counts to attain an accuracy of a% when the material of interest is at a dilution of x relative to experimental conditions. With $\nu_r = 10\ cm^{-1}$ and N_r calculated for other materials from

$$N_r = K_1 \frac{P}{w} LS\mathcal{M}\Delta \text{ counts } s^{-1}$$

then

$$Txa^2 = 10^4 Z/K_1 (P/w) LS\mathcal{M}\Delta(x) \quad .$$

If we use the values previously assumed, we obtain a "figure of merit:"

$$Txa^2 = 4.196 \times 10^{-29}\ Z\mathcal{M}\Delta(x) \quad .$$

For CdS, $\mathcal{M} = 5.24 \times 10^{-31}$, $Z = 3.17$, $\Delta(0.1) = 0.866$, and $Txa^2 = 293$ s.

Thus, for CdS, to detect a mass loading of 10% of the standard conditions [i.e., $(n\pi d^2 \delta/6) \times 0.1 = 0.252\ \mu g\ cm^{-3}$] with an accuracy of

1%, the counting time required is T = 2930 s, or 48.9 minutes. A summary of the performance of the spectrometer instrument in terms of this "figure of merit," Txa^2, is given in Section V-C-4.

It is important to recall the premises on which these calculations are based. First, the aerosol opacity is assumed small in the common volume so that attenuation of the laser beam as well as the Raman scatter is small. The number density and velocity of the aerosol is such that the fluctuation in the number of laser-illuminated particles has a value more precise than the attempted accuracy a, relative to the sample volume and the time of measurement. Also, the Raman-to-background ratio is assumed to be the same as that measured in the powers in the experimental program. The assumed cross section for CdS is a reference value and determines all the other cross-section values. Sample-to-sample changes in the sampling geometry during the experiments with powders are neglected.

3. Filter-Type System

With the development and general availability of high-quality dichroic and interference filters, the need for expensive dispersive optics is always under scrutiny, especially when performance is expected only over a small wavelength range. The design and analysis of a system based on such interference filters is given in this section.

Before proceeding with the analysis, however, some of the characteristics of interference filters will be reviewed. Interference filters are usually made up of thin dielectric films and can be made to achieve a narrow bandpass, typically 10 to 20 Å in the visible region of the spectrum. Transmission efficiencies on the order of 0.5 in the passband and attenuation on the order of 10^{-4} in the stopband can be achieved with these filters. In general, the peak transmission decreases as the desired passband narrows, and the cost is inversely related to the width of the passband.

The passband of an interference filter is designed for normal (90°) incidence of the optical beam. At all other angles of incidence, the passband position shifts to higher frequencies as the square of the angle of incidence. The bandpass thus widens with increasing angle of incidence. The bandpass position also changes with the temperature of the filter. Typical temperature coefficients are about +0.2 $\text{Å}/^{\circ}\text{K}$. A practical problem in the fabrication of large-area filters is the uniformity of the passband over various portions of the filter.

As we have noted earlier, the desired Raman lines of solids occur within a wavenumber-shift range of 0 to 1000 cm^{-1}. With 4880-Å excitation, this range translates to roughly 250 Å. Typical Raman line widths are about 10 cm^{-1} or about 2.5 Å. A 20-Å passband therefore means a wavenumber spread of 80 cm^{-1} and may include the lines of several species. Even if an interference filter of 2.5 Å bandwidth were obtained at some expense and loss of transmission, it is a difficult undertaking to maintain the passband at a given absolute spectral position, due to the effects of temperature and angle of incidence. Thus, it should be noted that the isolation of the Raman spectral lines of a single species for general analysis purposes is not practical for present interference filters because of the limited resolution capabilities. However, if the species of interest are known and a general analysis shows that interference from closely spaced lines is not a problem, then one might consider a nondispersive technique based on interference filters for estimation of the particular species.

The off-peak rejection capability of interference filters is important because the scatter from air molecules and particles produces a very large signal at the laser wavelength that must be rejected by the filter. It will be recalled that the number of air molecules in a given sample volume is about 2000 times higher than the number of molecules of the species of interest. Rayleigh scattering cross sections

are typically 10^3 times higher than Raman cross sections, and Mie scattering cross sections can be several orders of magnitude higher than rayleigh. It is thus seen that for each Raman photon of interest, there are typically 10^6 to 10^8 other photons present, in addition to other Raman photons that are not of interest. These additional photons must be rejected if the desired Raman signal is to be detected.

A primary advantage of the spectrometer-type instrument is the large rejection of this scattered light that can be obtained with double monochromators. The interference filter, on the other hand, faces a formidable task in sorting out the Raman photons. Elaborate interferometric techniques have been used for reducing this high background of scattered laser light, but they add to the expense and complexity, and, in particular, detract from the ruggedness of the device. Recently, the narrow absorption lines of molecular iodine vapor have been used to suppress the 5145-Å line of the argon ion laser with an attenuation of 10^8, with a corresponding attenuation of only about 6 for the desired wavelengths.[10] This is one technique for attenuating the rayleign line. The following analysis assumes that such a technique is used.

The typical attenuation capability of a spectrometer of the type used in the experiment is on the order of 10^{-8} to 10^{-10} for the rayleigh wavelength, even as close as a few wavenumbers (e.g., 10 cm^{-1}) away. Thus, the background levels measured during the experiments would be realistic values to use in the following analysis, assuming that a comparable suppression of 10^{-8} to 10^{-10} is achieved for the rayleigh wavelength.

Let the filter have a bandwidth of ν cm^{-1} and transmittance at normal incidence. In order to transmit radiation from an extended source, the filter must pass light at a finite angle θ.

The transmission peak shifts spectrally as

$$\nu_m = \frac{\nu_o}{2}\left(1 + \frac{1}{\cos\theta}\right) = \nu_o + \delta$$

where

$$2\delta = (\nu_o/\cos\theta) - \nu_o \quad .$$

The effective bandwidth of the filter will be broader, being a convolution of ν and δ, and the peak transmission η_θ is also reduced. It has been shown that[11]

$$\nu_\theta^2 = \nu^2 + 16\delta^2$$

and that

$$\eta_\theta = \eta\,\frac{\nu}{4\delta}\arctan\left(\frac{4\delta}{\nu}\right) \quad .$$

If we define the angle θ such as to make the effective bandwidth of the filter $\sqrt{2}\,\nu$, then $4\delta = \nu$ and $\eta_\theta = \pi\eta/4$. If we define $R = \nu_o/\nu$, then

$$\nu = 4\delta = 2\nu_o\left(\frac{1}{\cos\theta} - 1\right)$$

$$1 - \cos\theta = \frac{1}{2R + 1} \quad .$$

The acceptance solid angle in the medium of the filter is given by

$$\omega = 2\pi(1 - \cos\theta) = \frac{2\pi}{2R + 1} \quad .$$

If the refractive index of the filter is n^*, then the acceptance angle in air will be

$$\omega = \frac{n^{*2}\,2\pi}{2R + 1} \approx n^{*2}\,\pi/R$$

since $R \approx 10^3$.

To perform a system analysis, we assume, as before, a laser beam of dimaeter w cm and a filter whose useful linear dimension is A cm. From constancy of entendue we have

$$A^2\omega = w^2\Omega$$

or

$$\Omega = \omega(A/w)^2 = (\pi/R)(n^*A/w)^2 \quad .$$

Following the earlier derivation, we calculate the number of Raman counts to be

$$N_r = \pi \frac{\lambda A}{hc} \frac{P}{w} \frac{\pi}{6} nd^3 \frac{\rho\sigma}{M} \frac{\nu_r}{10_\nu} \frac{(n^*A)^2}{R} \eta Q\Delta$$

$$= K_2 \frac{P}{w} L/\!\!/wS\Delta \quad .$$

If the optical efficiency of the imaging system is 83.3% as before, and the peak transmission of the filter at normal incidence is 80%, then $\eta = 0.523$. For a typical 20-Å filter at 5000 Å, $R = 250$ and $n^* = 1.5$. $A = 5$ cm is a practical size for filters. Assume $Q = 0.15$. From the above equation, as before, the smaller the beam size, the larger the Raman signal. The same comments regarding practicable Ω values and particle densities are in order. Assume $w = 1$ cm, and $\Omega = 0.18$ sr (or a 15-cm-diameter lens at 30 cm). For these conditions, for CdS, the number of Raman counts will be

$$N_r = 5633 \times 0.236 \text{ counts } s^{-1}$$

$$= 1335 \text{ counts } s^{-1} \quad .$$

Again, the measured signal-to-background ratio, Z, will be used to estimate detection limits for this system. Note, however, that this signal-to-background ratio was measured with a spectral width of

10^{-1} cm. If the effective filter bandwidth is $\sqrt{2}\,\nu$ cm^{-1}, the signal-to-background ratio will be different. If we assume the background per cm^{-1} is constant, then the background counts will be $\sqrt{2}\,N_b\nu/10$. If the full width of the Raman lines is less than 10 cm^{-1}, The Raman counts will stay the same even under a broader passband. If the Raman line width is greater than 10 cm^{-1}, then the Raman counts received under the wider passband will be $N_r\nu_r/10$, or $\sqrt{2}\,N_r\nu/10$, whichever is smaller. Hence, the signal-to-background parameter now becomes

$$Z' = \begin{cases} \dfrac{N_r + \sqrt{2}\,N_b\nu/10}{N_r} & \text{for } \nu_r < 10 \\[2ex] \dfrac{N_r\nu_r + \sqrt{2}\,N_b\nu}{N_r\nu_r} & \text{for } \sqrt{2}\,\nu > \nu_r > 10 \\[2ex] \dfrac{N_r + N_b}{N_r} & \text{for } \nu_r > \sqrt{2}\,\nu \end{cases}.$$

It follows that

$$\frac{S_{Raman}}{Noise} = \begin{cases} \left(\dfrac{N_r xT}{Z'}\right)^{1/2} & \text{for } \nu_r < 10 \\[2ex] \left(\dfrac{N_r\nu_r xT}{10Z'}\right)^{1/2} & \text{for } \sqrt{2}\,\nu > \nu_r > 10 \\[2ex] \left(\dfrac{N_r\sqrt{2}\,\nu xT}{10Z'}\right)^{1/2} & \text{for } \nu_r > \sqrt{2}\,\nu \end{cases}$$

and

$$Txa^2 = \begin{cases} \dfrac{10^4 Z'}{N_r} & \text{for } \nu_r < 10 \\ \dfrac{10^4 Z'}{N_r}\dfrac{10}{\nu_r} & \text{for } \sqrt{2}\,\nu > \nu_r > 10 \\ \dfrac{10^4 Z'}{N_r}\dfrac{10}{\sqrt{2}\,\nu} & \text{for } \nu_r > \sqrt{2}\,\nu \end{cases}$$

Using the appropriate values in the expression

$$N_r = K_2 \frac{P}{w} LS\mathcal{M}\Delta$$

we get

$$Txa^2 = \begin{cases} 9.3 \times 10^{-31}\,(Z'/\Delta) & \text{for } \nu_r < 10 \\ 9.3 \times 10^{-31}\,(Z'/\Delta)(10/\nu_r) & \text{for } \sqrt{2}\,\nu > \nu_r > 10 \\ 9.3 \times 10^{-31}\,(Z'/\Delta)(10/\sqrt{2}\,\nu) & \text{for } \nu_r > \sqrt{2}\,\nu \end{cases}$$

As before, the value of attenuation, Δ, depends on the aerosol concentration x. A summary of the performance levels of this filter instrument is given at the end of this section.

4. Performance Summary for Raman Systems

The normalized detection time, Ta^2, is given in Table 7 for each Raman-active material and for both Raman systems. The concentration parameter, x, of the particulate stream is relative to 10^6 particles/cm^3 and is varied from 2 to 0.001 to demonstrate a variety of typical concentrations. The attenuation of the aerosol is accounted for in these calculations and results in a maximum detectability at about 10^6 particles/cm^3. Larger concentrations produce high optical-attenuation

Table 7

RAMAN IN-STACK MONITORING INSTRUMENT PERFORMANCE SUMMARY

Material	Line	Normalized Detection Time (Ta^2)										Minimum Detectable Material Concentration (mg/m^3)
		Spectrometer Instrument					Filter Instrument					
		x = 2	x = 1	x = 0.1	x = 0.01	x = 0.001	x = 2	x = 1	x = 0.1	x = 0.01	x = 0.001	
HgO	328	139.2	66.0	181	1590	1.57×10^4	3.88	1.84	5.03	44.1	436	25.359
	550	1254	595	1630	1.43×10^4	1.41×10^5	53.8	25.5	69.9	614	6060	357.127
HgS	250	276.7	131.2	359	3150	3.11×10^4	11.9	5.63	15.4	135	1340	57.299
	275	5.2×10^3	2.45×10^3	6720	5.90×10^4	5.83×10^5	124	58.9	161	1420	1.40×10^4	683.348
	341	1.50×10^3	708	1937	1.70×10^4	1.70×10^5	50	23.7	64.8	569	5620	241.506
$CaSo_4$	425	4.48×10^4	2.12×10^4	5.81×10^4	5.11×10^5	5.04×10^6	4098	2181	5970	5.24×10^4	5.17×10^5	33,828.182
	490	1.34×10^4	6347	1.74×10^4	1.53×10^5	1.51×10^6	2842	1348	3690	3.24×10^4	3.20×10^5	20,908.019
	620	1.44×10^4	6815	1.87×10^4	1.64×10^5	1.62×10^6	1351	641	1750	1.54×10^4	1.52×10^5	9,942.166
	670	2.80×10^4	1.33×10^4	3.63×10^4	3.19×10^5	3.15×10^6	2757	1308	3580	3.14×10^4	3.10×10^5	20,287.603
	1015	561	266	728	6390	6.31×10^4	62.5	29.6	81.1	712	7030	110.434
	1150	5.85×10^4	2.76×10^4	7.57×10^4	6.65×10^5	6.55×10^6	288	137	374	3290	3.25×10^4	2,124.925
CdS	212	2.26×10^3	1.07×10^3	2929	2.57×10^4	2.54×10^5	403	191.1	523	4590	4.53×10^4	4,806.547
	305	3.84×10^3	1.82×10^3	4983	4.38×10^4	4.32×10^5						
	347	4.04×10^3	1.92×10^3	5249	4.61×10^4	4.55×10^5	33.3	15.8	43.2	380	3750	95.578
	365	4.27×10^3	2.03×10^3	5543	4.87×10^4	4.81×10^5						
	563	1.92×10^4	9.10×10^3	2.49×10^4	2.19×10^5	2.16×10^6	329	156.1	427	3750	3.70×10^4	3,926.227
	599	2.90×10^3	1.37×10^3	3762	3.30×10^4	3.26×10^5	183	86.8	237	2090	2.06×10^4	596.102
$Al_2(SO_4)_3$	480	5.15×10^3	2920	7990	7.02×10^4	6.93×10^5	62	29.3	80.3	705	6960	99.743
	620	9.0×10^3	4269	1.17×10^4	1.03×10^5	1.01×10^6	95.5	45.3	124	1090	1.07×10^4	175.435
	1000-1200	2.71×10^4	1.29×10^4	3.52×10^4	3.09×10^5	3.05×10^6	67.5	31.9	87.4	768	7580	108.657
Phosphate Rock Feed	580	3.84×10^5	1.82×10^5	4.98×10^5	4.38×10^6	4.32×10^7	2.30×10^4	1.09×10^4	2.99×10^4	2.62×10^5	2.59×10^6	79,962.4
	945	2.60×10^4	1.23×10^4	3.38×10^4	2.97×10^5	2.93×10^6	1373	651	1780	1.56×10^4	1.54×10^5	11,939.34
CaF_2	322	5.65×10^5	2.67×10^5	7.31×10^5	6.42×10^6	6.34×10^7	3.50×10^4	1.66×10^4	4.54×10^4	3.99×10^5	3.93×10^6	110,643.648
Na_3AlF_6	550	3.74×10^5	1.77×10^5	4.86×10^5	4.26×10^6	4.21×10^7	2.30×10^4	1.09×10^4	2.98×10^4	2.62×10^5	2.58×10^6	66,254.56
	1040	5.45×10^4	2.59×10^4	7.08×10^4	6.22×10^5	6.13×10^6	744	353	965	8480	8.37×10^4	5,364.188
Lead Concentrate	950	4.61×10^5	2.19×10^5	5.98×10^5	5.25×10^6	5.18×10^7	8.3×10^3	3943	1.08×10^4	9.48×10^4	9.35×10^5	
NBS Coal	1350	5.95×10^6	2.82×10^6	7.71×10^6	6.78×10^7	6.69×10^8	1.49×10^4	7037	1.93×10^4	1.69×10^5	1.67×10^6	54,204.604
	1600	1.63×10^6	7.75×10^5	2.12×10^6	1.86×10^7	1.84×10^8	6.25×10^3	2974	8140	7.15×10^4	7.06×10^5	22,908.127

Table 7 (continued)

Material	Line	Normalized Detection Time (Ta^2)										Minimum Detectable Material Concentration (mg/m^3)
		Spectrometer Instrument					Filter Instrument					
		x = 2	x = 1	x = 0.1	x = 0.01	x = 0.001	x = 2	x = 1	x = 0.1	x = 0.01	x = 0.001	
Al_2O_3	378	2.04×10^5	9.68×10^4	2.65×10^5	2.33×10^6	2.30×10^7	4.89×10^4	2.32×10^4	6.34×10^4	5.57×10^5	5.50×10^6	170,195.2
	415	1.37×10^4	6.48×10^3	1.77×10^4	1.56×10^5	1.53×10^6	1.93×10^3	911.6	2495	2.19×10^4	2.16×10^5	16,718.744
PbO	69	17.0	8.07	22.1	194	1910	1.76	0.834	2.28	20.0	198	9.856
	86	8.75	4.15	11.4	99.8	985	0.69	0.328	0.897	7.88	77.8	3.873
	138	1.67	0.793	2.17	19.1	188	0.057	0.0271	7.42×10^{-2}	0.652	6.43	0.320
	279	6.85	3.25	8.89	78.1	771	0.114	0.0542	0.148	1.30	12.8	0.637
	370	68.7	32.6	89.2	783	7730	1.99	0.941	2.57	22.6	223	11.101
$HgSO_4$	410	787	373	1020	8970	8.85×10^4	158	75.0	205	1800	1.78×10^4	695.007
	495	6.25	2.97	8.14	71.5	706	0.270	0.128	0.350	3.07	30.3	1.027
	580, 588	65.8	31.3	85.6	752	7420	7.2	3.43	9.38	82.3	813	27.563
	660	44.7	21.2	58.0	510	5030	4.23	2.01	5.49	48.2	476	16.138
	987	11.1	5.29	14.5	127	1250	0.58	0.273	0.747	6.56	64.7	2.193
	1043	10.1	4.80	13.1	115	1140	0.152	0.0722	0.198	1.74	17.1	0.58
	1125	106.4	50.5	138	1210	1.20×10^4	13.7	6.47	17.70	156	1540	52.888
	1180	59.8	28.4	77.6	682	6730	1.24	0.587	1.61	14.1	139	4.712
	1342	2394	1136	3110	2.73×10^4	2.69×10^5	233.8	111	303	2660	2.63×10^4	3,763.211
	1670	3.80×10^4	1.80×10^4	4.93×10^4	4.33×10^5	4.27×10^6	9.2×10^3	4370	1.20×10^4	1.05×10^5	1.04×10^6	148,155.236
$PbCl_2$	86	1059	502	1375	1.21×10^4	1.19×10^5	243	115	315	2760	2.73×10^4	3,525.21
	156	7.25	3.44	9.42	82.7	817	0.0473	0.0225	6.15×10^{-2}	0.54	5.33	0.163
$HgCl_2$	70	8.45	4.01	11.0	96.5	952	0.73	0.344	0.942	8.28	81.7	2.329
	121	13.98	6.63	18.1	159	1570	0.75	0.355	0.972	8.53	84.2	2.400
	312	3.60	1.70	4.66	41.0	404	0.087	0.0412	0.113	0.989	9.76	0.278
	380	152.4	72.27	198	1740	1.71×10^4	9.05	4.29	11.7	103	1020	29.361
RA	750	3.45×10^5	1.64×10^5	4.48×10^5	3.93×10^6	3.88×10^7	2.06×10^4	9763	2.67×10^4	2.35×10^5	2.32×10^6	179,053.42
	1250	5.4×10^5	2.55×10^5	6.98×10^5	6.13×10^6	6.05×10^7	3.22×10^4	1.53×10^4	4.18×10^4	3.67×10^5	3.62×10^6	112,240.8
	720	173	82.0	224	1970	1.95×10^4	1.48	0.703	1.92	16.9	167	3.063
	1022	30.2	14.3	39.2	344	3400	3.96	1.88	5.13	45.1	445	8.161
	1052	16.9	8.04	22.0	193	1910	1.84	0.870	2.38	20.9	206	3.778
$PbSO_4$	443	106	50.3	138	1210	1.19×10^4	5.35	2.54	6.95	61.0	602	19.558
	608	586	278	760	6680	6.59×10^4	38.3	18.2	49.7	437	4310	141.972
	640	1642	779	2130	1.87×10^4	1.85×10^5	151	71.6	196	1720	1.70×10^4	636.765
	978	27.7	13.1	36	316	3120	0.64	0.304	0.831	7.30	72	2.339
	1065	542	258	703	6170	6.0×10^4	3.39	1.61	4.40	38.6	381	12.378
	1165	308	146	400	3510	3.47×10^4	4.10	1.94	5.32	46.7	461	14.977

Table 7 (concluded)

Material	Line	Normalized Detection Time (Ta^2)										Minimum Detectable Material Concentration (mg/m^3)
		Spectrometer Instrument					Filter Instrument					
		x = 2	x = 1	x = 0.1	x = 0.01	x = 0.001	x = 2	x = 1	x = 0.1	x = 0.01	x = 0.001	
$(NH_4)_2SO_4$	450	446	212	579	5090	5.02×10^4	26.9	12.8	34.9	306	3020	28.381
	613, 623	643	305	834	7320	7.23×10^4	13.7	6.50	17.8	156	1540	14.469
	976	78	37.1	101	891	8.80×10^3	1.83	0.87	2.38	20.9	206	1.911
	1090	2114	1002	2740	2.41×10^4	2.38×10^5	9.6	4.55	12.5	109	1080	10.109
	1420	3319	1574	4310	3.78×10^4	3.73×10^5	24.1	11.4	31.2	274	2710	25.413
	1650	4283	2031	5560	4.88×10^4	4.82×10^5	32.5	15.4	42.1	370	3650	34.317
	3150	895	422	1160	1.02×10^4	1.00×10^5	1.75	0.828	2.26	19.9	196	1.818
$CuCl_2 2H_2O$	215	100	47.6	130	1140	1.13×10^4	7.4	3.51	9.60	84.3	832	10.376
	236, 249	437	207	566	4980	4.91×10^4	9.65	4.58	12.5	110	1090	13.718
	407	902	428	1170	1.03×10^4	1.02×10^5	48.8	23.2	63.4	557	5500	69.464
	700	4411	2092	5730	5.03×10^4	4.96×10^5	48.5	23.0	63.0	553	5460	68.966
$CdCl_2$	218	242	114.6	313.7	2755	2.72×10^4	34.6	16.4	44.3	394	3890	83.615
	320	4780	2.26×10^3	6197	5.44×10^4	5.37×10^5	339	160.9	440	3867	3.82×10^4	3,414.62
	1585	2.47×10^4	1.17×10^4	3.21×10^4	2.82×10^5	2.78×10^6	3.87×10^3	1836	5026	4.41×10^4	4.36×10^5	38,963.592
	3470	489	232.1	635	5578	5.51×10^4	2.52	1.19	3.27	28.7	283	6.006
$CdSO_4$	415	2550	1207	3300	2.90×10^4	2.86×10^5	363	172	471	4130	4.08×10^4	4,227.003
	450	1.26×10^4	5970	1.63×10^4	1.44×10^5	1.42×10^6	613	291	795	6980	6.89×10^4	7,151.5
	497	1392	660	1810	1.59×10^4	1.57×10^5	146	68.9	189	1660	1.64×10^4	464.479
	603, 615	1982	940	2570	2.26×10^4	2.23×10^5	54	25.7	70.4	618	6100	151.877
	658, 670	1.06×10^4	5055	1.38×10^4	1.22×10^5	1.20×10^5	436	207	566	4970	4.90×10^4	5,087.15
	1000	123	58.4	160	1400	1.39×10^4	3.35	1.59	4.35	38.2	377	9.265
	1050, 1063	1039	493	1350	1.18×10^4	1.17×10^5	11.6	5.51	15.1	132	1310	32.44
	1100, 1118	2053	974	2660	2.34×10^4	2.31×10^5	46.9	22.3	61.0	535	5280	131.479
	1168, 1173, 1554	1843	874	2390	2.10×10^4	2.07×10^5	40.7	19.3	52.3	464	4580	114.031
	2900-3500	5.2×10^3	2466	6750	5.93×10^4	5.85×10^5	10.2	4.83	13.2	116	1150	28.508

values that increase detection time; smaller concentrations produce lower Raman signals that also increase detection times. The accuracy, a, is in percent and the normalized detection time, Ta^2, can be interpreted directly as a time with an accuracy of 1%. At this accuracy level, the detection times vary from about 0.03 s for PbO, a clearly detectable material, to 1.66×10^4 s (4.6 hours) for CaF_2, a clearly unreasonable material to monitor.

VI LABORATORY MEASUREMENT CAPABILITIES

A. General

The Raman effect may prove useful for particulate monitoring even as a laboratory tool in which collected samples are analyzed. For example, the sulfate content of a collected sample of particulate may be determined using a laboratory Raman instrument, because of the distinctive response of the sulfate ion. In general, the performance level that could be expected from a laboratory Raman instrument is identical to the performance that was discussed in Section IV on Raman measurements. About 50% of the materials analyzed on this project had measurable Raman responses; it appears likely, then, that such a laboratory instrument could provide useful information about particulate composition.

B. Measurable Material Properties

It is potentially possible to monitor sources of the sulfates, chlorates, carbonates, nitrates, phosphates, fluorides, chlorides, oxides, and sulfides of various metals such as lead, mercury, cadmium, zinc, copper, nickel, iron, chromium, vanadium, calcium, aluminum, and beryllium. More complex substances such as ammonium compounds and various organic materials are of interest and can also yield Raman spectra.

The Raman spectra of solids may be classified, for the present purposes, into two categories. In the first, there are vibrating molecular subunits such as amonium, sulfate, phosphate, or carbonate ions, or water of hydration. In the second category, the entire solid is one vibrating unit. In the first case, the presence of different anions (i.e., calcium carbonate vs. sodium carbonate) does not perturb the Raman shifts and the

latter maintain their character, to first order, even though crystal structures and lattice spacings may change. In the second case, however, the crystal structure determines the Raman spectrum and thus there is no guarantee that if cadmium sulfide has a Raman spectrum, lead sulfide will also have one. Even if these two sulfides do have spectra, the spectra need have no relationship to each other except, of course, if they have similar crystal structures. Table 8 lists the typical Raman shifts of some molecular ions.

It will be recalled that, as a general rule, the heavier elements such as lead and mercury were observed to have higher scattering cross sections than lighter elements such as aluminum. These heavy metal compounds will thus be more easily detected by both laboratory and in-situ instruments.

C. Instrumental Considerations

For these laboratory-type measurements, the use of a conventional spectrometer, in which a slit is swept over the desired spectral region, satisfies the basic measurements requirements. However, if the time taken for completing a sweep (typically 15 to 30 minutes under favorable SNR conditions) is unacceptable, additional instrument sophistication may be necessary. The time taken to scan a spectrum depends on the acceptable SNR. In order to maintain the same SNR with a decrease in overall measurement time, it is necessary to increase the exposure time per spectral interval. Another reason for decreasing the measurement time is that changes in sample composition may occur during a scan period. Thus it is desirable to look simultaneously at as much of the entire spectrum as is possible.

There are two different techniques available for reducing the measurement time. The first technique uses an optical multichannel analyzer in which a special-purpose vidicon tube replaces the moving slit and detector. The resolution elements of the tube divide the entire spectrum

Table 8

RAMAN SHIFTS OF MOLECULAR IONS

Ion	Raman Shifts			
SO_4^{--}	981	451	1104	613
ClO_4^{-}	935	462	1102	628
PO_4^{---}	935	363	1082	515
NH_4^{+}	3033	1685	3134	1397
CO_3^{--}	1063		1415	680
NO_3^{-}	1050		1390	720
SO_3	1069	652	1330	532

into separate channels, and photon counts are accumulated simultaneously on all channels. Each resolution element is in essence a separate exit-slit/detector combination. Thus, SNR considerations are identical to those in a conventional system. The advantage of the system is a reduction of scan time by a factor of N if there are N spectral resolution elements.

In the second technique, called multiplex spectroscopy, specially coded masks (combinations of slits at different spectral positions) are successively placed at the exit plane of the spectrometer. The light passed by the masks is recombined and is incident on a single conventional phototube. Since a large number of slits (say, n) are open at any one time, the SNR is improved by a factor of n (for the case where the count rate through each slit is the same) for the same counting time. The output of the detector is now, however, coded by the position

of the slits on the masks. A decoding procedure (usually done by a computer) is necessary to develop a spectrum. The increased SNR is achieved at the expense of additional complexity in signal processing.

The advantages of these two techniques may be quantified as follows. First, assume that the dispersing instrument is the same for each technique and the resolution limitations are not due to this device. Further, the detectors are assumed to have the same characteristics in all cases. Dark-current noise is neglected and Poisson statistics are assumed (i.e., the SNR with P counts is $\sqrt{P}$).

If there are N resolution elements in the spectrum and T is the integration time needed to obtain a given SNR, S, in the weakest spectral element, then for a conventional spectrometer the time needed to generate a spectrum is NT. For the optical multichannel analyzer, the time needed to achieve an SNR of S in the channel with the lowest count rate is T. In the multiplex case where $n(< N)$ slits are open at any one time, the count rate is thus at least n times as large and an SNR of S can be achieved in a maximum period of $T/\sqrt{n}$. However, in order to cover the entire N spectral-resolution elements, we need to repeat the measurement N times. Thus the total time needed to achieve S over the entire spectrum is $NT/\sqrt{n}$.

It is thus seen that a significant advantage in either time or SNR (or compromise combinations) may be achieved with these techniques, at the expense of additional complexity in equipment. It should be noted, however, that the state of the art in these techniques is such that a scanning spectrometer has superior resolution when a large spectral band has to be examined.

The additional speed advantage of these two advanced techniques would probably only be required in a large central laboratory facility in which a large number of samples from a wide region would be processed. It does not appear that the more sophisticated techniques would be required for regional air pollution areas.

VII AEROSOL MEASUREMENTS

An attempt was made to observe the fluorescent spectra of the more highly fluorescent materials in particulate form even though this was not called for in the contract work statement. The initial measurement attempt was oriented toward detecting a fine particulate stream in air, utilizing a closed system in which the particulate stream was pumped through the spectrofluorimeter. Several particulate pumping systems were considered, and the best readily available system was tried in the laboratory. Unfortunately, contamination of the particulate air stream and clumping of the particulates was sufficiently severe to prevent meaningful measurements of this type to be made.

The second attempt intended to utilize a liquid particulate suspension medium, rather than air, to relieve the problems encountered in a flowing air system. Because of the pump-contamination difficulties encountered in the first system, it was decided to abandon flowing systems and to use relatively thick viscous liquids in order to suspend the particulate matter for a sufficient length of time to make meaningful measurements. Several of the more fluorescent materials were found to be relatively insoluble in alcohols. Several alcohols were examined for fluorescent interferences. These ranged from methyl alcohol, which would still require a pumping system to maintain suspension, to tert-butyl alcohol, which is a solid at room temperature. It was found that certain batches of glycerol were low enough in fluorescence to permit some measurements to be made, and at the same time were sufficiently viscous to permit suspension of the particulate material for the length of time required in the measurements. Even though the best available

glycerol had relatively low fluorescence, it was still sufficiently high to mask the extremely small fluorescent return from the particulate material at low concentrations. Thus it was not possible to obtain interference-free fluorescent spectra for any of the desired materials at concentration levels approximating those that may be found in stacks.

This masking effect from the glycerol fluorescence was not expected, based on the fluorescence amplitude of the pure glycerol samples. However, it was noticed that the introduction of particulate material into the glycerol enhanced the amplitude of the measured glycerol fluorescence by a substantial factor. This resulted in an increasing masking effect as the particulate concentration was increased in an attempt to overcome the glycerol fluorescence.

In both the air and glycerol suspension experiments, however, a component of the fluorescence response of the particulate matter was detected in the presence of the severe interferences mentioned above. Thus, even though these crude initial attempts did not demonstrate a clear measurement capability, both experiments indicate a strong potential for making such measurements if the interferences can be reduced or eliminated. Thus, from both the calculations and the initial experiments, it appears that additional work in this area would result in a demonstrated particulate-measurement capability.

VIII CONCLUSIONS

The results of the measurements and analysis accomplished on this project indicate that both fluorescence and Raman in-stack monitoring systems can yield useful information about the quantity and composition of a particulate stream. This conclusion is also supported by the results of a few initial measurements of the fluorescence of particulates at concentrations comparable to those expected in smoke stacks. These conclusions are, however, based on the measurements of materials that are input substances to various industrial processes. The final determination of feasibility for various industrial-process-monitoring applications will depend on the existence of significant optical interactions with the effluents of these processes. Initial measurements made on fourteen effluent samples provided by the Bay Area Air Pollution Control District indicate observable fluorescence in at least a few of the samples. Thus, the monitoring feasibility for effluent materials also appears encouraging at the present time.

Fluorescent systems are characterized by relatively large optical-response signals over broad spectral regions. These characteristics make the analysis of mixed constituents by fluorescence a difficult task, but would allow a quantitative measurement of a single or known mix of fluorescent components to be made. Thirteen of the thirty-four materials examined on this project had fluorescent responses, and all of these are expected to be observable in the in-stack particulate stream.

Raman measurements are characterized by a relatively small optical signal from the material, but this signal is concentrated in a very

narrow, specific spectral region. Raman systems are suited to measurements of the relative concentrations of a variety of constituents, and, although it may be possible to quantitatively determine the concentration of each of these, this task is made more difficult by the low response level of the Raman interaction. Twenty-two of the thirty-four materials investigated on this project have measureable Raman responses. Of the twenty-two materials with observable spectra, approximately fifteen appear detectable by an in-stack instrument, four appear marginal, and three appear unlikely to be detected by such an instrument. Quantitative detection of these materials by Raman systems is less feasible than for fluorescence systems because of the low level of the Raman response and the more critical nature of Raman monitoring instruments. Thus, the number of materials in each Raman detectability category should be viewed as a rough estimate and could vary from a low of one or two, to a high of as much as all twenty-two materials. As for fluorescence, the feasibility assessment will depend on the strength of the Raman interaction of effluent materials. No measurements of the Raman interactions of the BAAPCD samples have been made. It is expected, however, that at least a few of these effluent materials will have Raman spectra comparable to those measured in the present project, and would thus be detectable.

IX RECOMMENDATIONS

The calculations and initial experiments performed on this project indicate that both Raman and fluorescence systems are capable of detecting materials in particulate form in smoke stacks. This result was more encouraging than had been expected initially in the project, and as a result of this potential detection capability two tasks are recommended as steps toward a prototype in-stack monitoring system.

The first task would be to measure the Raman and fluorescence characteristics of the fourteen samples obtained from the BAAPCD and to assess their detection feasibility using the methods developed on this project. These samples do not represent the full range of industrial effluents for which monitoring would be useful. It is recommended that at least one effluent sample from each industrial process of potential monitoring interest be included in this measurement program.

The next task would be to show the experimental feasibility of detecting an appropriate particulate stream of an actual effluent material under laboratory conditions. This experiment would provide direct measurement information that would require fewer assumptions in determining in-stack feasibility than is the case with the present material-measurement techniques. Particularly for fluorescence monitoring, this experiment would provide results that would allow much more accurate prediction of the capabilities of an actual stack-monitoring system. With minor modifications, the laboratory instrument used in this experiment could conceivably be employed for an actual in-stack measurement.

Appendix A

MEASURED FLUORESCENT RESPONSE SPECTRA

This appendix contains the results of the measurements of materials that have significant fluorescence responses as obtained on the Baird-Atomic Spectrofluorimeter. The curves shown are taken directly from the instrument and are not corrected for variations in wavelength response. They can and should be corrected for the source and detector characteristics shown in Fig. A-1 if quantitative use is to be made of the curves in this appendix.

The procedure for correcting the measured curves is as follows. First, determine the excitation wavelength and the relative response at that wavelength as determined from Fig. A-1. Next, determine from Fig. A-1 the wavelength of the fluorescent response and its relative response. The two relative-response numbers are multiplied together and the fluorescence response amplitude in the measured curve is divided by this factor. This procedure will result in a uniform quantitative response level for all wavelengths from 220 to 700 nm. It should be noted that this procedure does not provide an absolute response level but is designed only to make the response at different wavelengths uniform, taking into account the variation in source and detector performance in the instrument.

Several features of the curves in this appendix are worth noting. First, in Fig. A-7 for $HgSO_4$, note the wide variation in wavelength between the excitation and fluorescence response curves. This was the widest separation between these curves for any material investigated on this project. In Fig. A-9, for the EPA coal sample, note the particularly wide excitation and fluorescence response curves for that material. This

is to be expected, based on the probable composition consisting of a large number of organic components. Each of these components is expected to fluoresce at a slightly different wavelength, thus yielding a broader curve than would be observed for single constituents. Figures A-11, A-12, and A-13 for EPA copper, EPA fly ash, and EPA lead, respectively, are included to show examples of materials that do not have significant fluorescence responses. In these three figures, the smooth baselines represent the scattered-light response of the instrument, and it is evident that no fluorescent responses are visible. Figure A-14 shows the response of suspended particulate AlF_3 in water. The water has been thickened in viscosity by the addition of methyl cellulose, which is slightly fluorescent, but less so than the AlF_3. The excitation and fluorescence responses shown in this curve are a composite between the low concentration of AlF_3 in particulate form and the fluorescence of the methyl cellulose. Note the decrease in amplitude between the two excitation spectra labeled Run 1 and Run 2. This decrease in amplitude was the result of particulate settling during the time required to make this measurement. The two large peaks around 375 nm are the Raman response of the water. Note that the Raman response amplitude is changed by the amount of particulate material suspended in the water. This effect was noticed for other materials as well. The level of fluorescence that is measured here is clearly lower than the Raman response for the water. Although there is some enhancement in this response due to the suspended particulate material, this response level would be typical for an aerosol measurement.

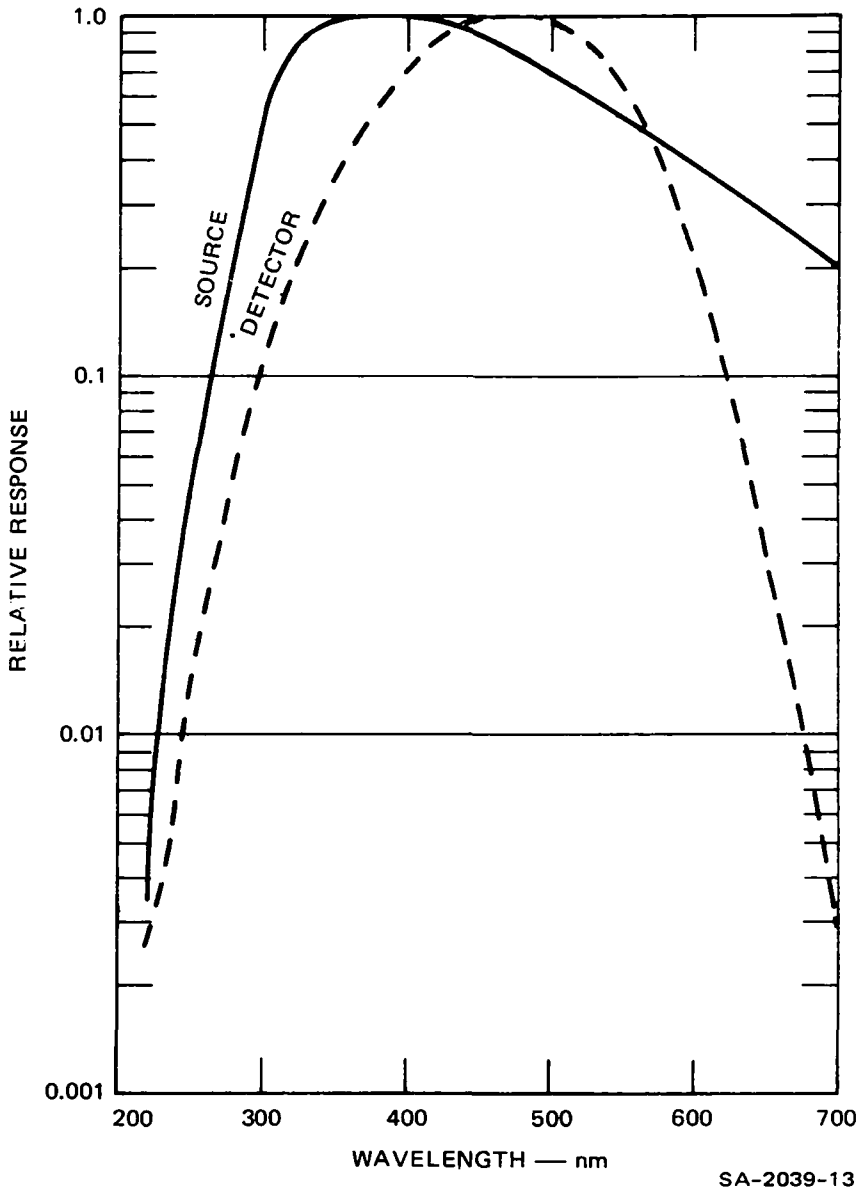

FIGURE A-1 RELATIVE RESPONSE FOR BAIRD-ATOMIC SPECTROFLUORIMETER SOURCE AND DETECTOR

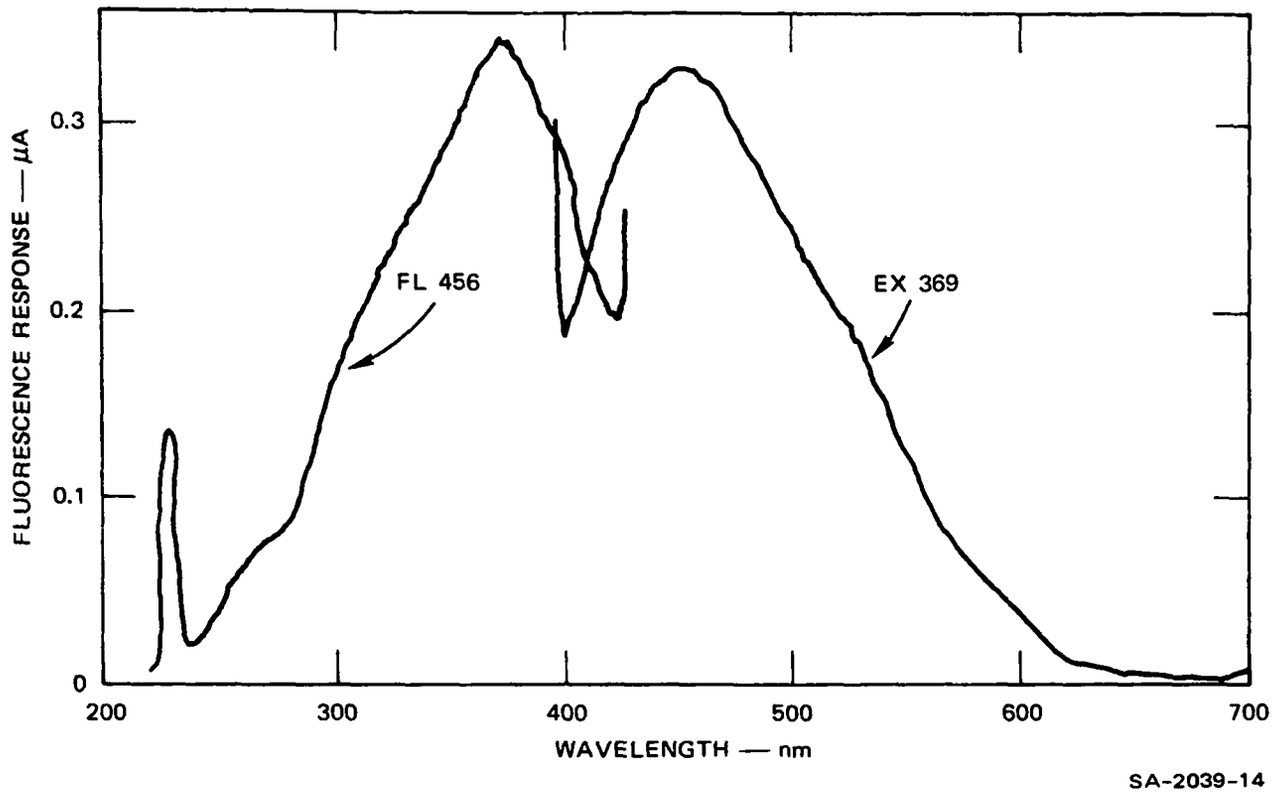

FIGURE A-2 FLUORESCENT RESPONSE OF AlF_3

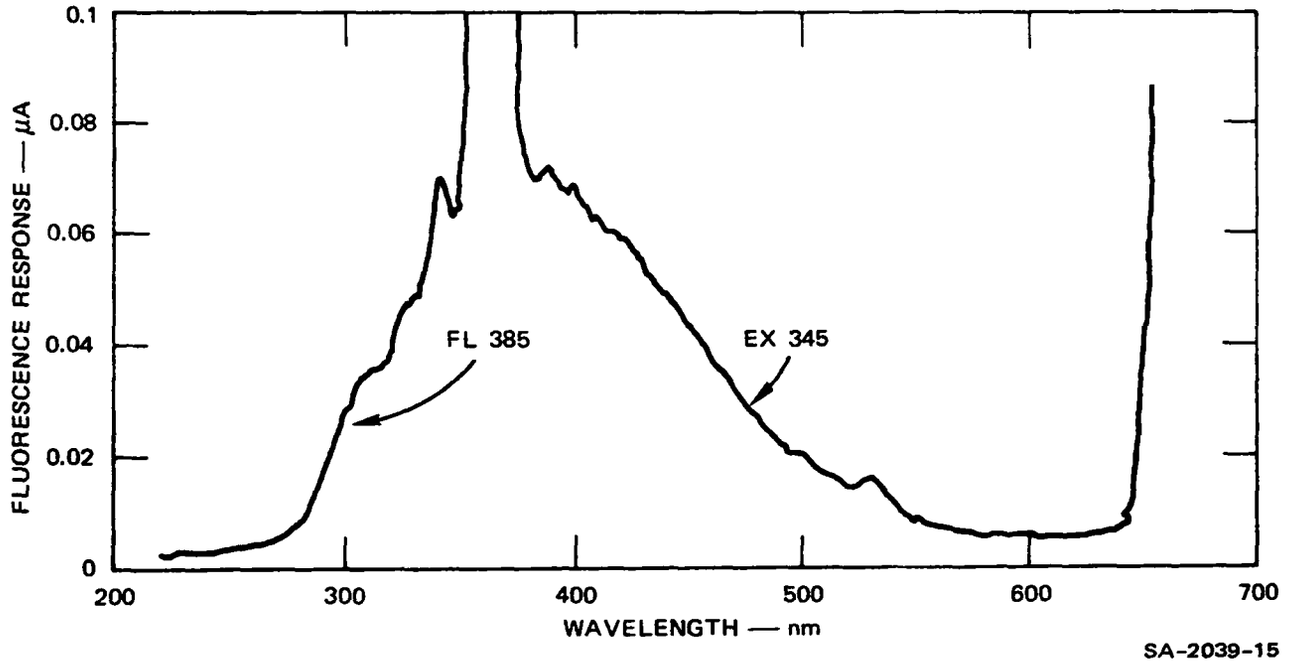

FIGURE A-3 FLUORESCENT RESPONSE OF $CuSO_4$

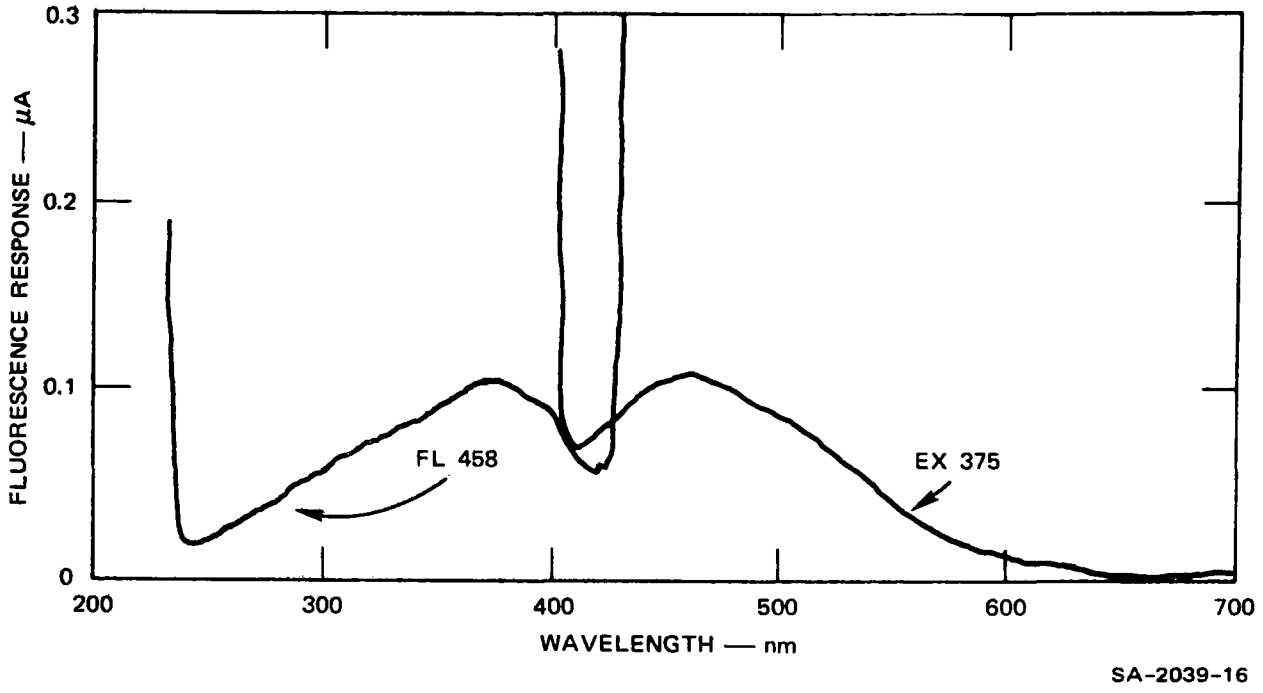

FIGURE A-4 FLUORESCENT RESPONSE OF CRYOLITE

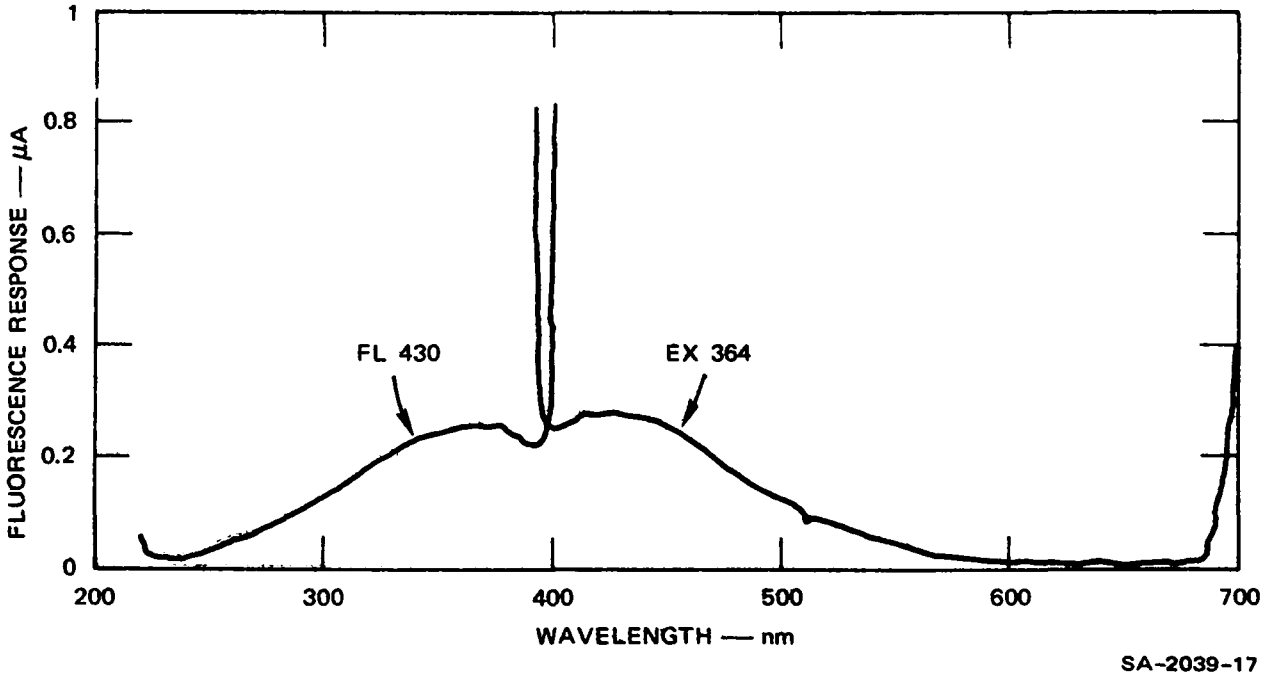

FIGURE A-5 FLUORESCENT RESPONSE OF $Al_2(SO_4)_3$

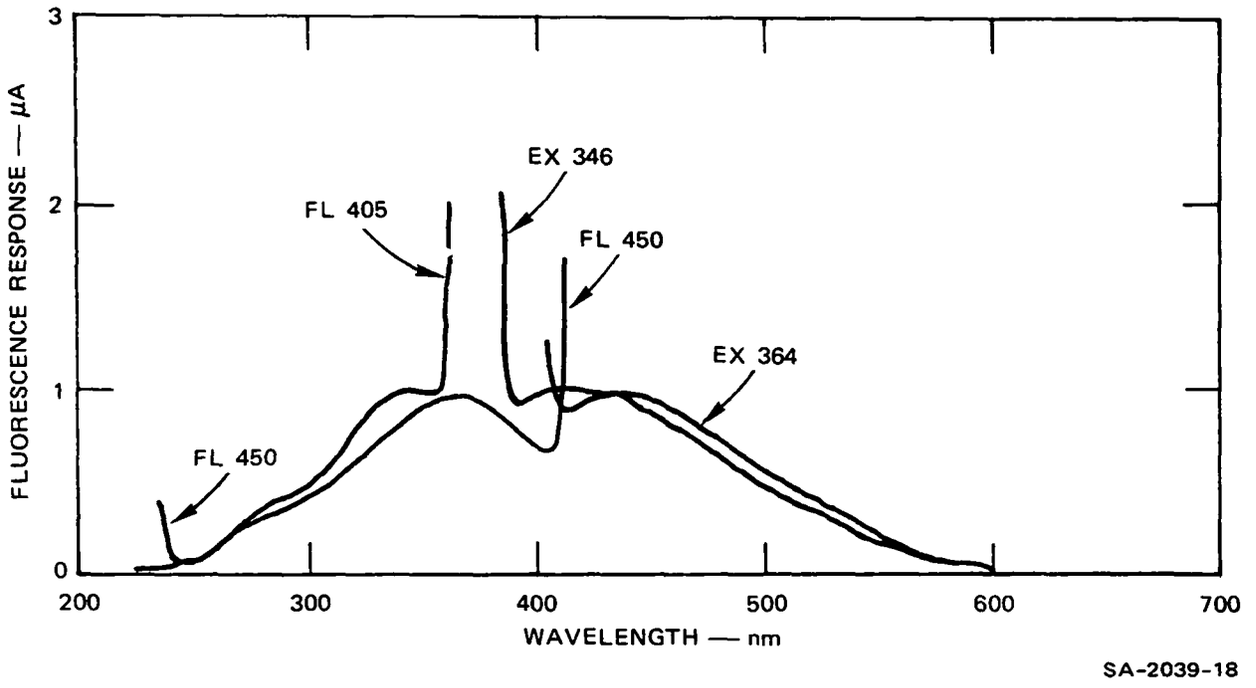

FIGURE A-6 FLUORESCENT RESPONSE OF EPA RAW ALUMINA

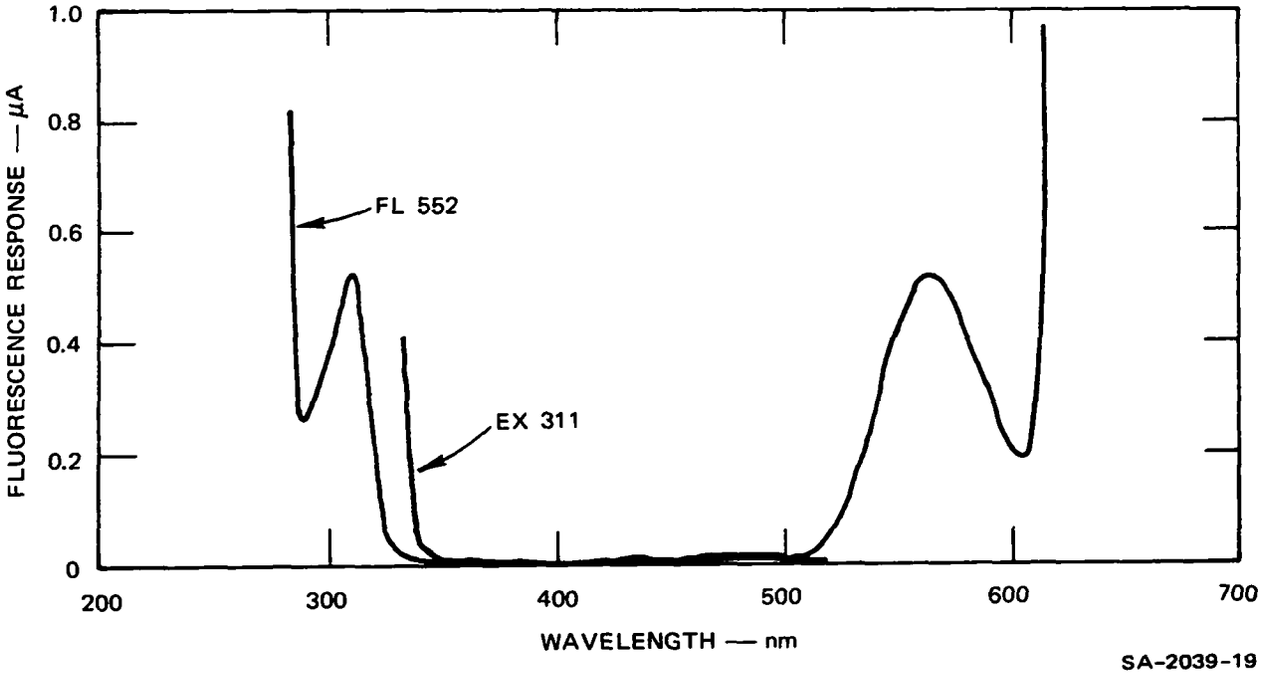

FIGURE A-7 FLUORESCENT RESPONSE OF $HgSO_4$

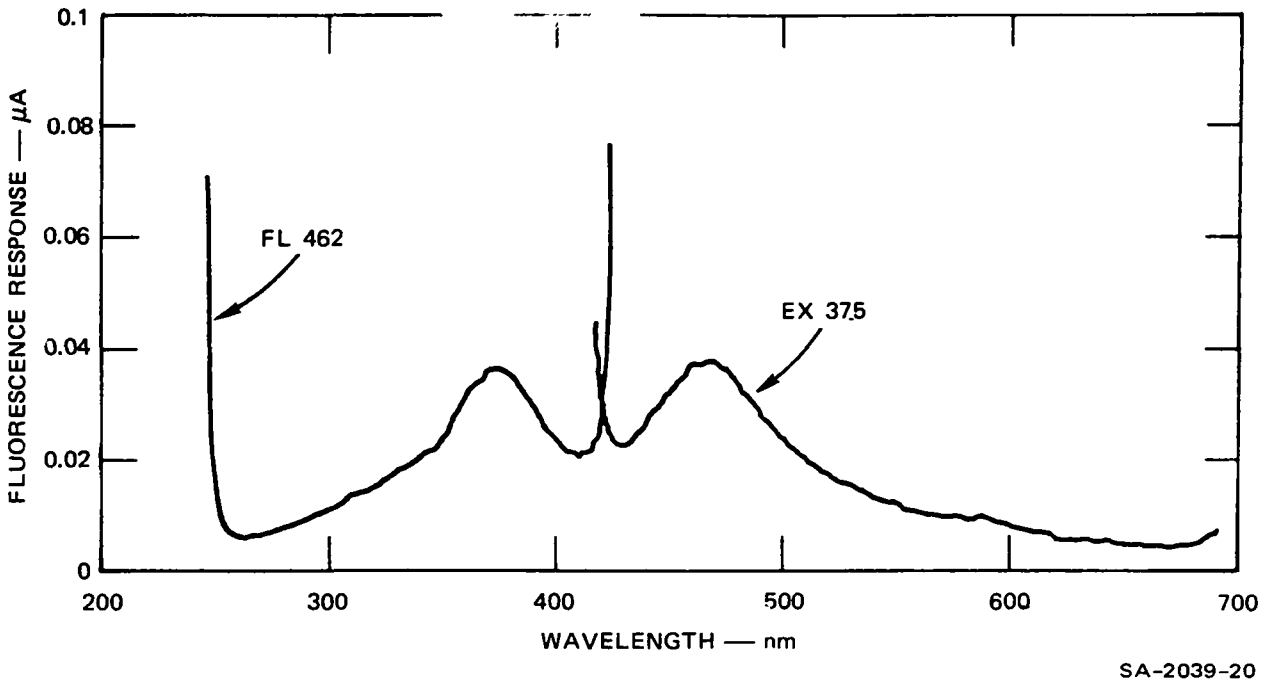

FIGURE A-8 FLUORESCENT RESPONSE OF EPA ZINC SMELTER FEED MATERIAL

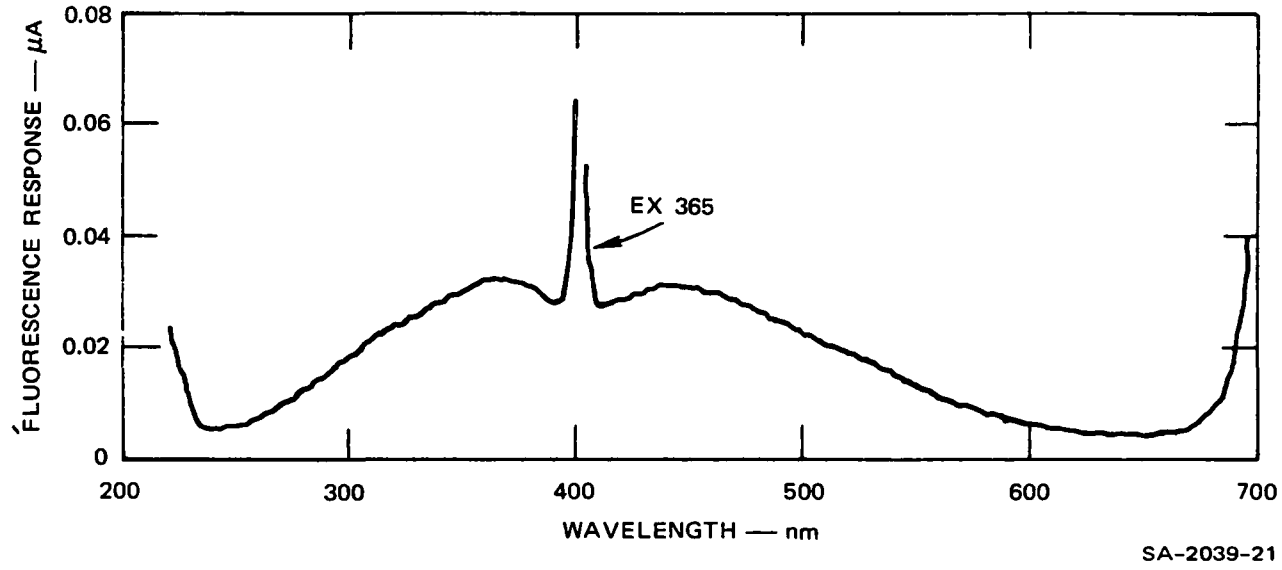

FIGURE A-9 FLUORESCENT RESPONSE OF EPA COAL — SOURCE, NBS

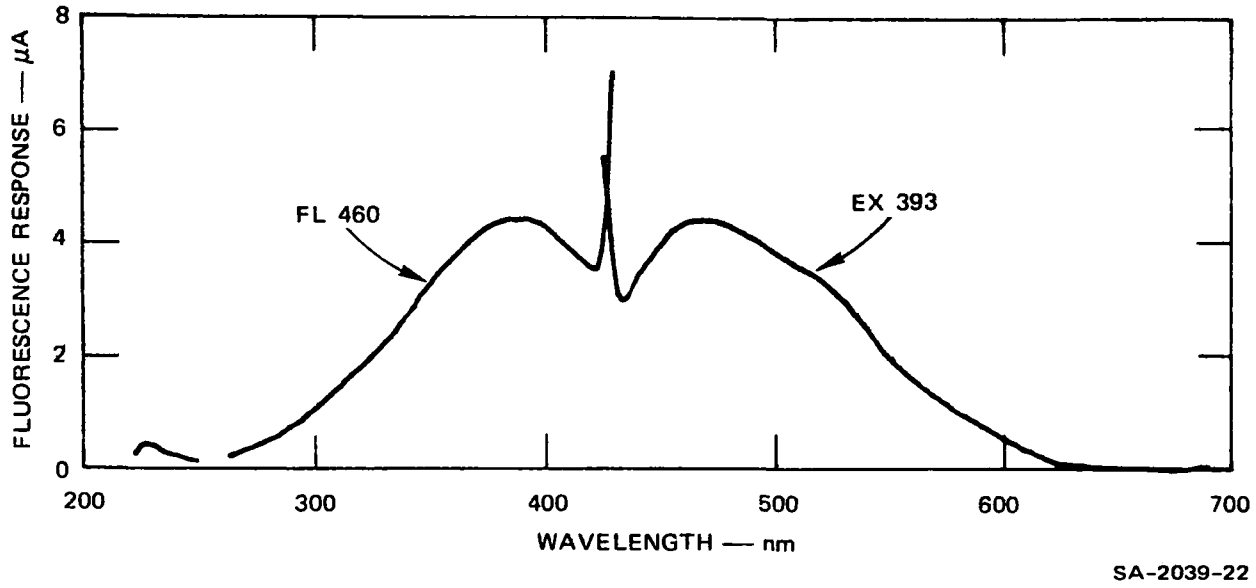

FIGURE A-10 FLUORESCENT RESPONSE OF EPA PHOSPHATE ROCK FEED MATERIAL

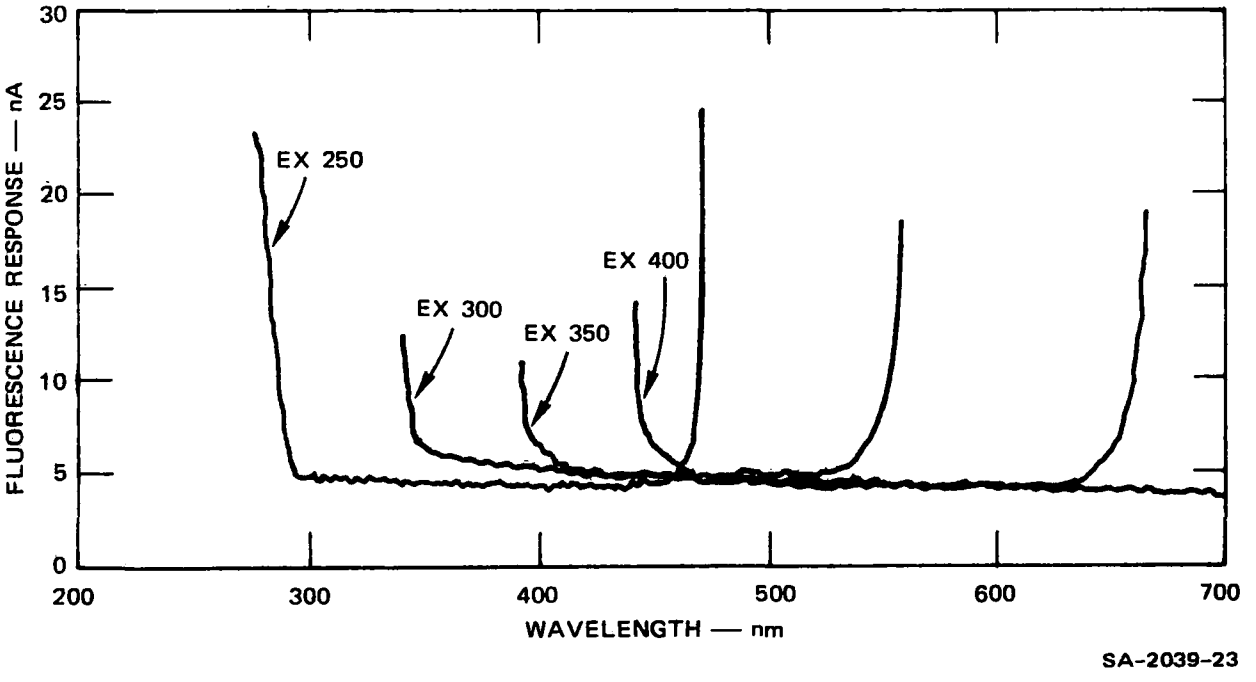

FIGURE A-11 FLUORESCENT RESPONSE OF EPA COPPER SMELTER FEED MATERIAL

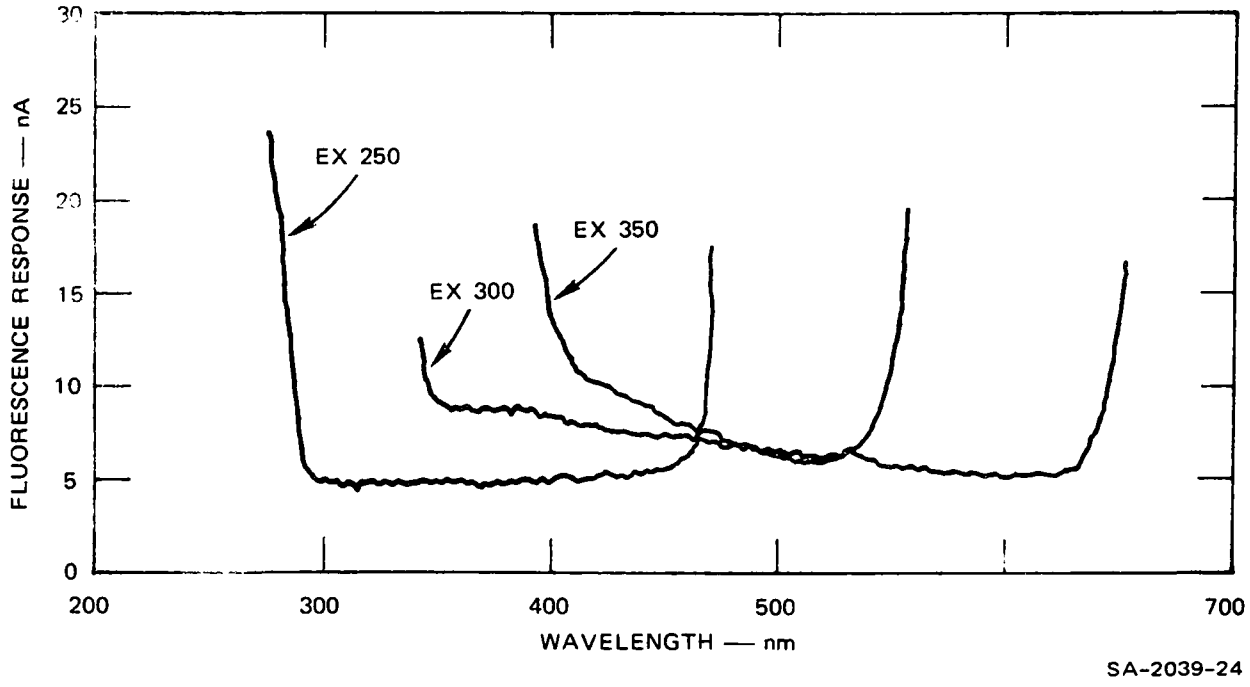

FIGURE A-12 FLUORESCENT RESPONSE OF EPA FLY ASH

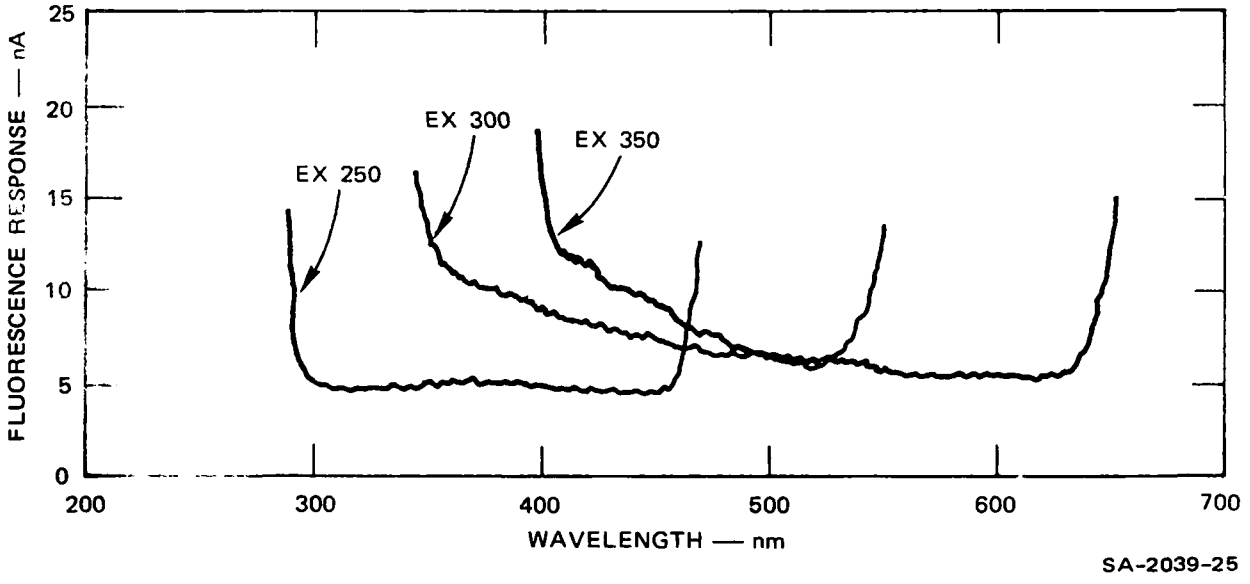

FIGURE A-13 FLUORESCENT RESPONSE OF EPA LEAD SMELTER FEED MATERIAL

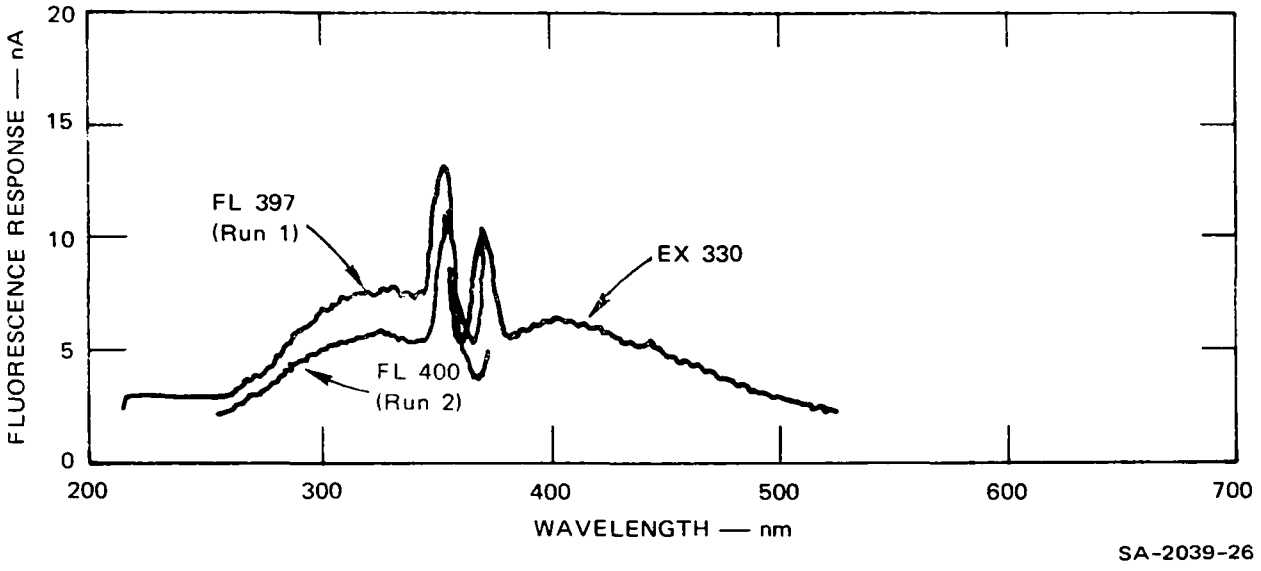

FIGURE A-14 FLUORESCENT RESPONSE OF PARTICULATE AlF_3 IN WATER

Appendix B

MEASURED RAMAN SPECTRA

This appendix contains the measured spectra of the materials investigated on this project. The curves are reproduced from the actual instrument traces.

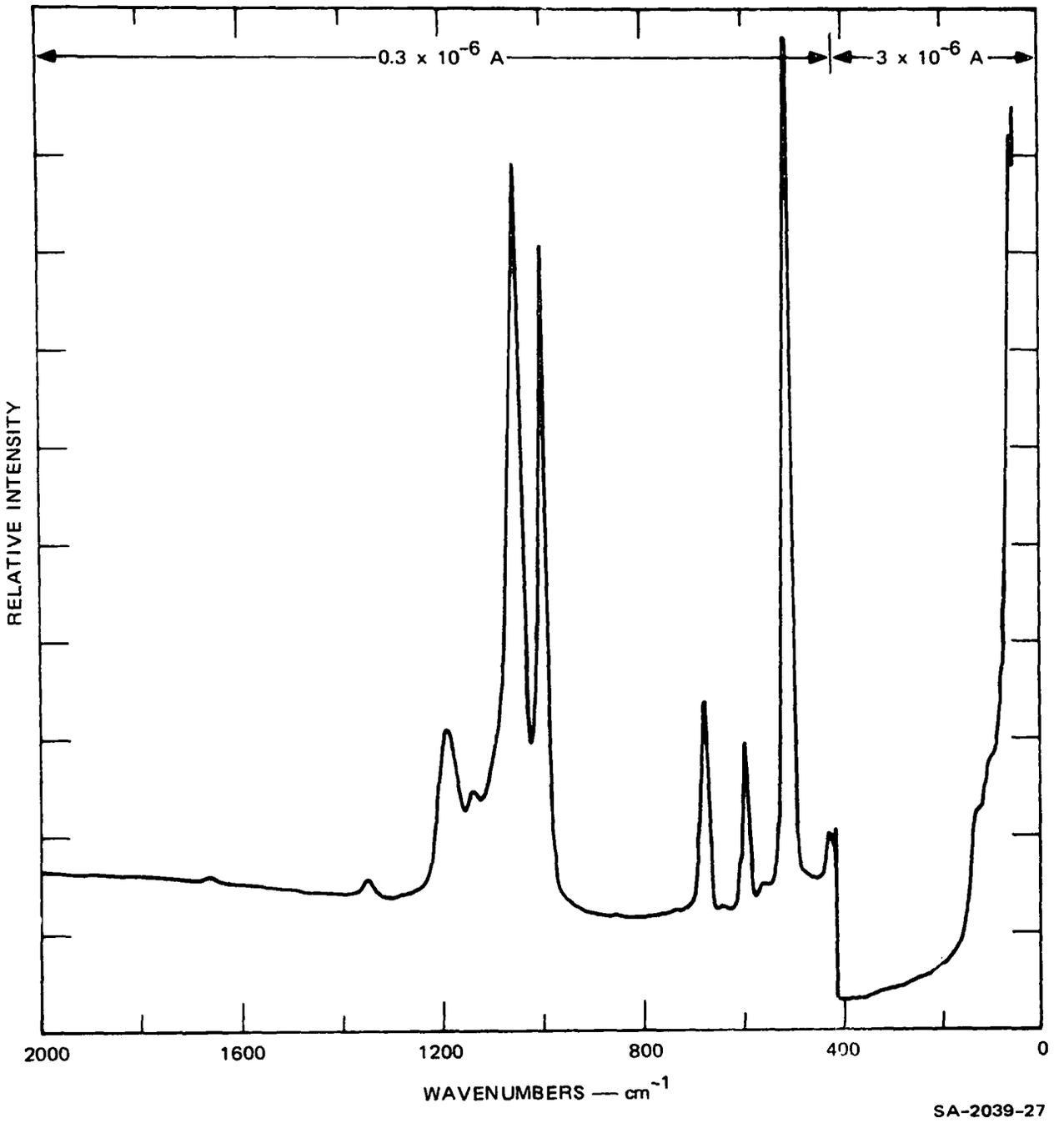

FIGURE B-1 RAMAN RESPONSE OF $HgSO_4$

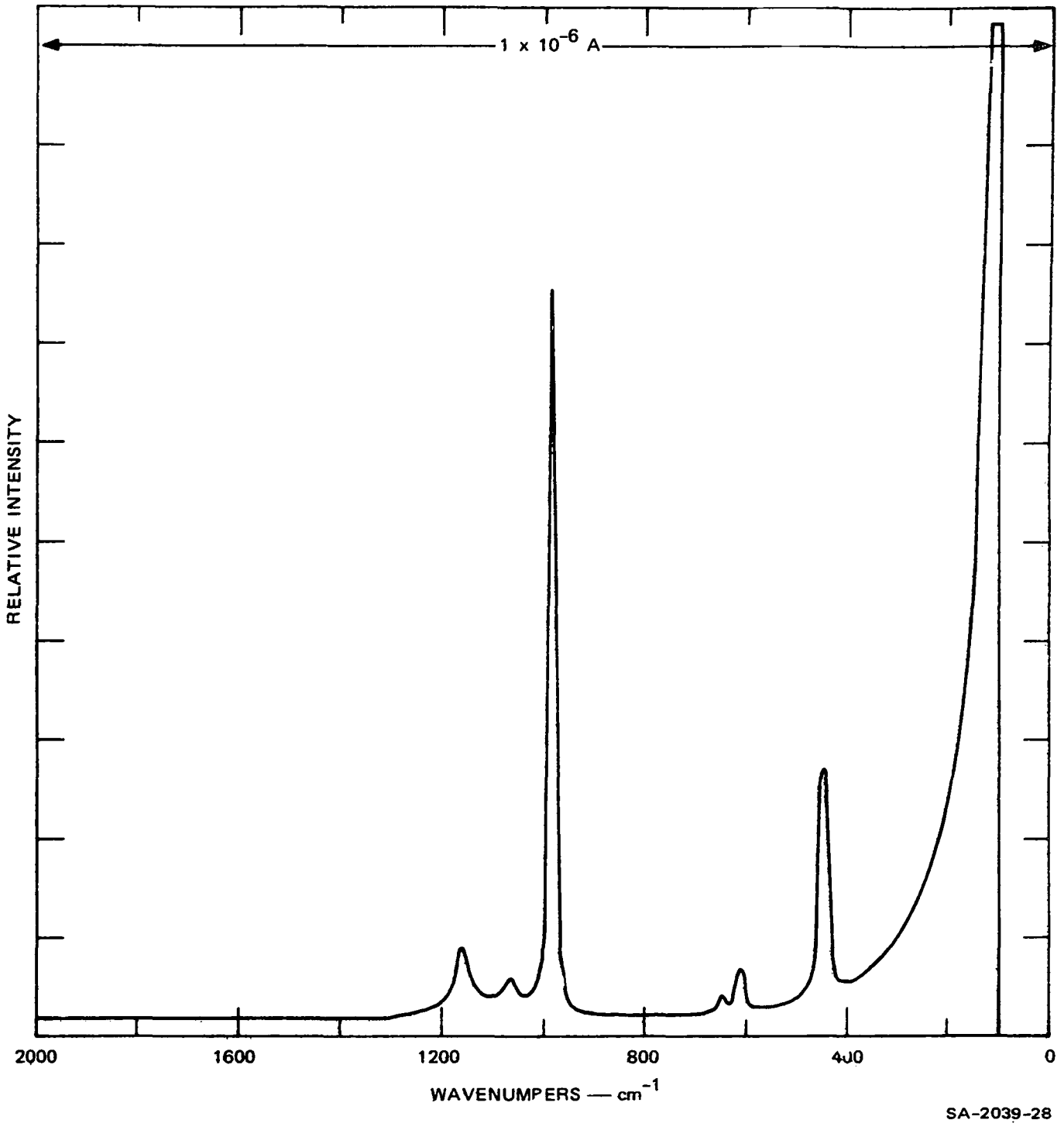

FIGURE B-2 RAMAN RESPONSE OF $PbSO_4$

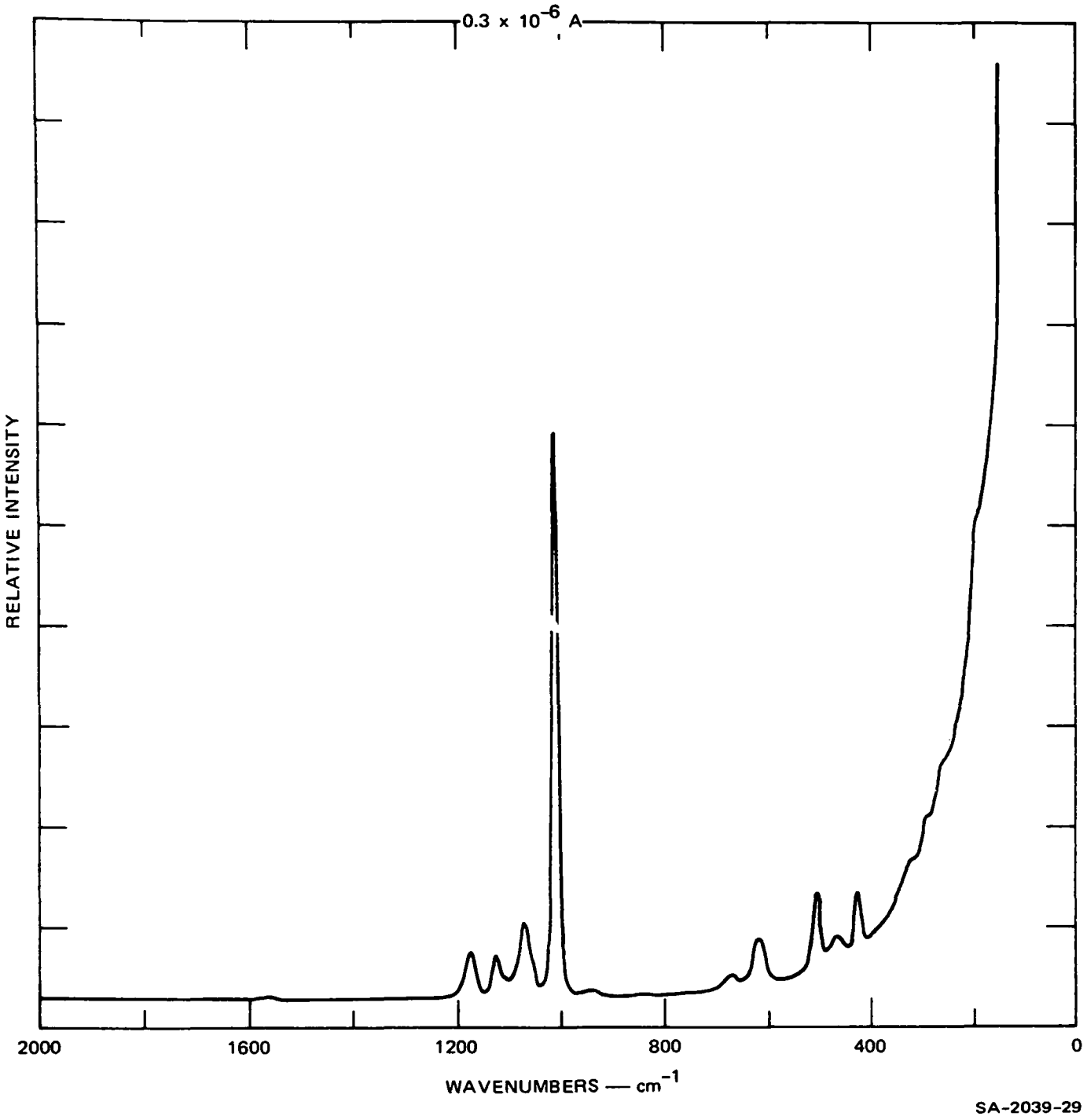

FIGURE B-3 RAMAN RESPONSE OF $CdSO_4$

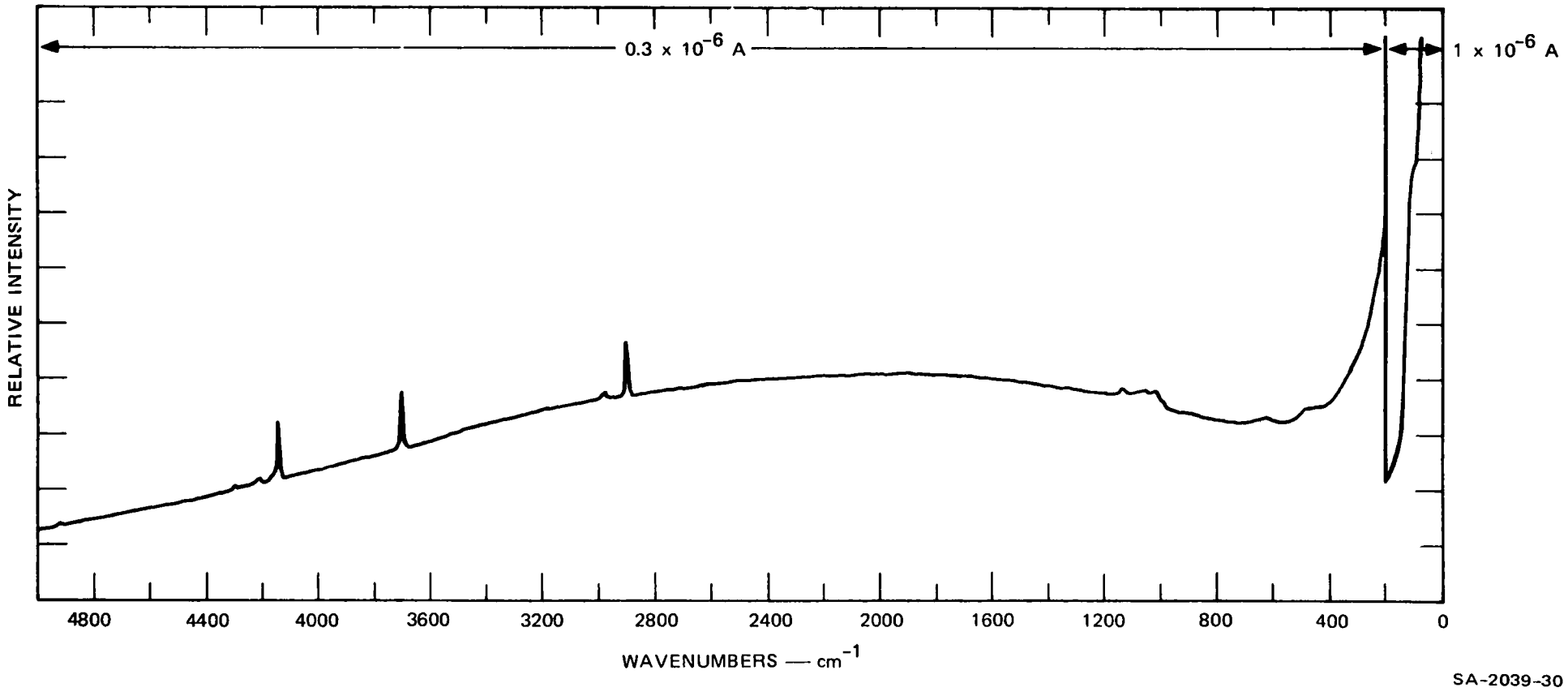

FIGURE B-4 RAMAN RESPONSE OF $Al_2(SO_4)_3$

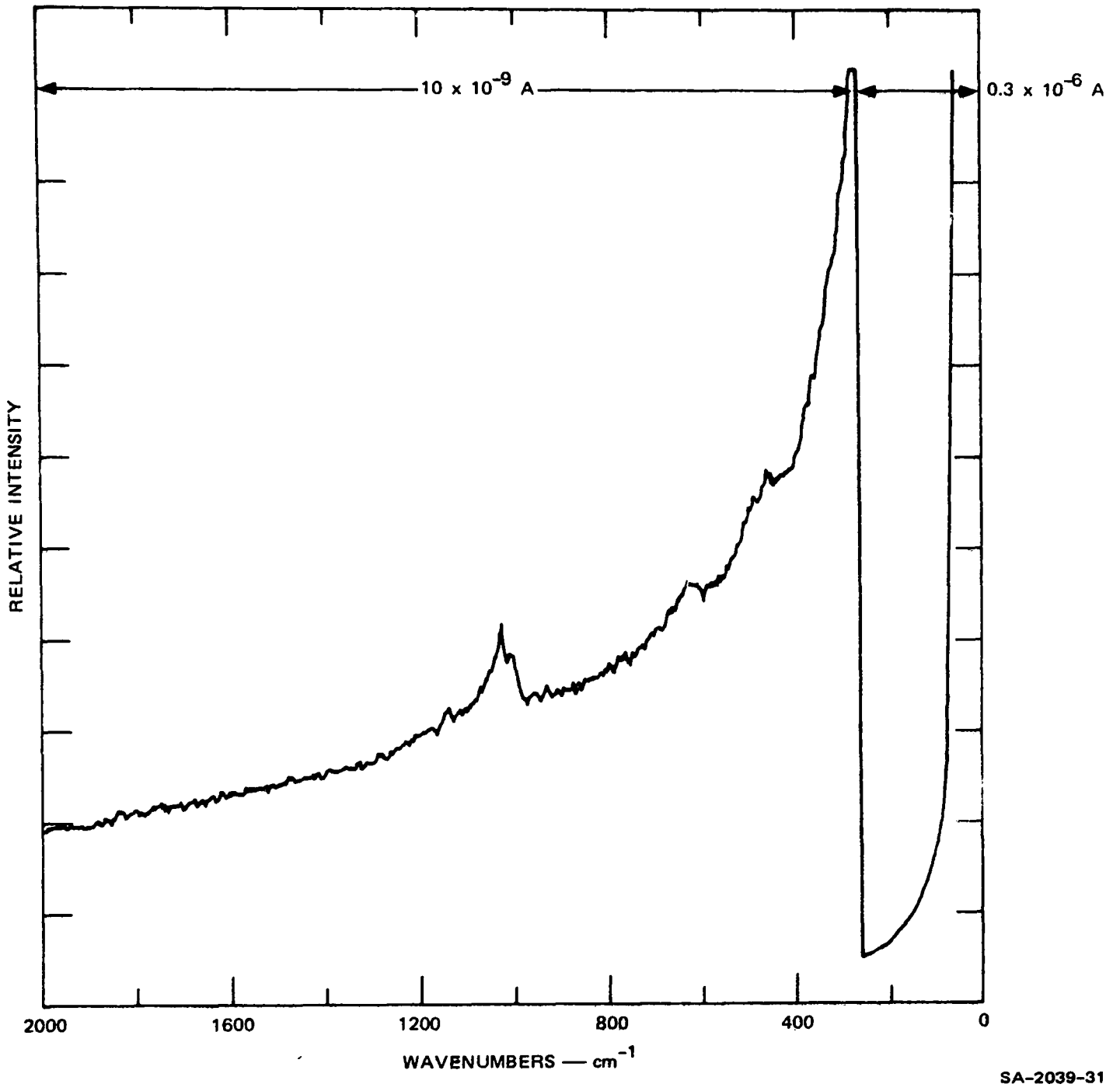

FIGURE B-5 RAMAN RESPONSE OF $Al_2(SO_4)_3$ (6471 Å)

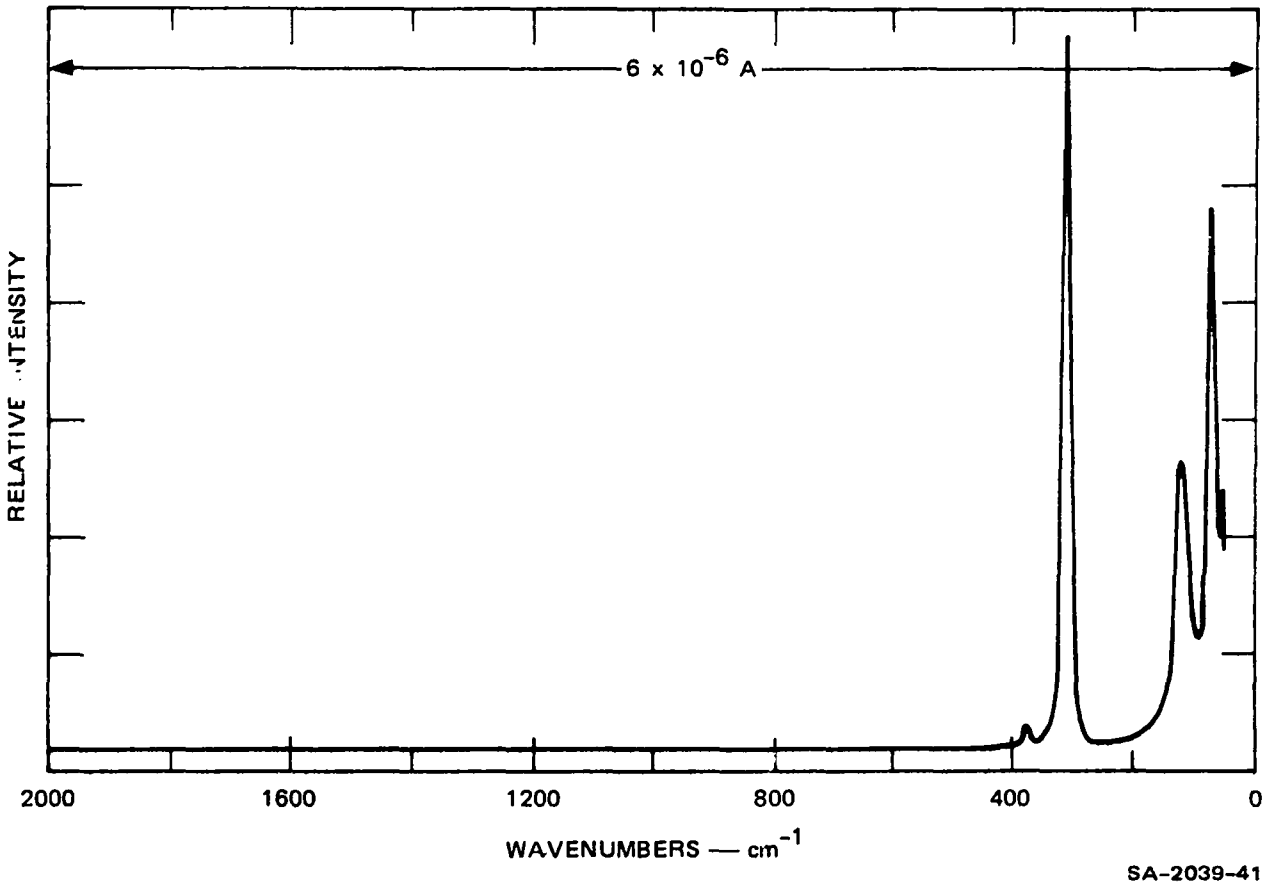

FIGURE B-6 RAMAN RESPONSE OF $HgCl_2$

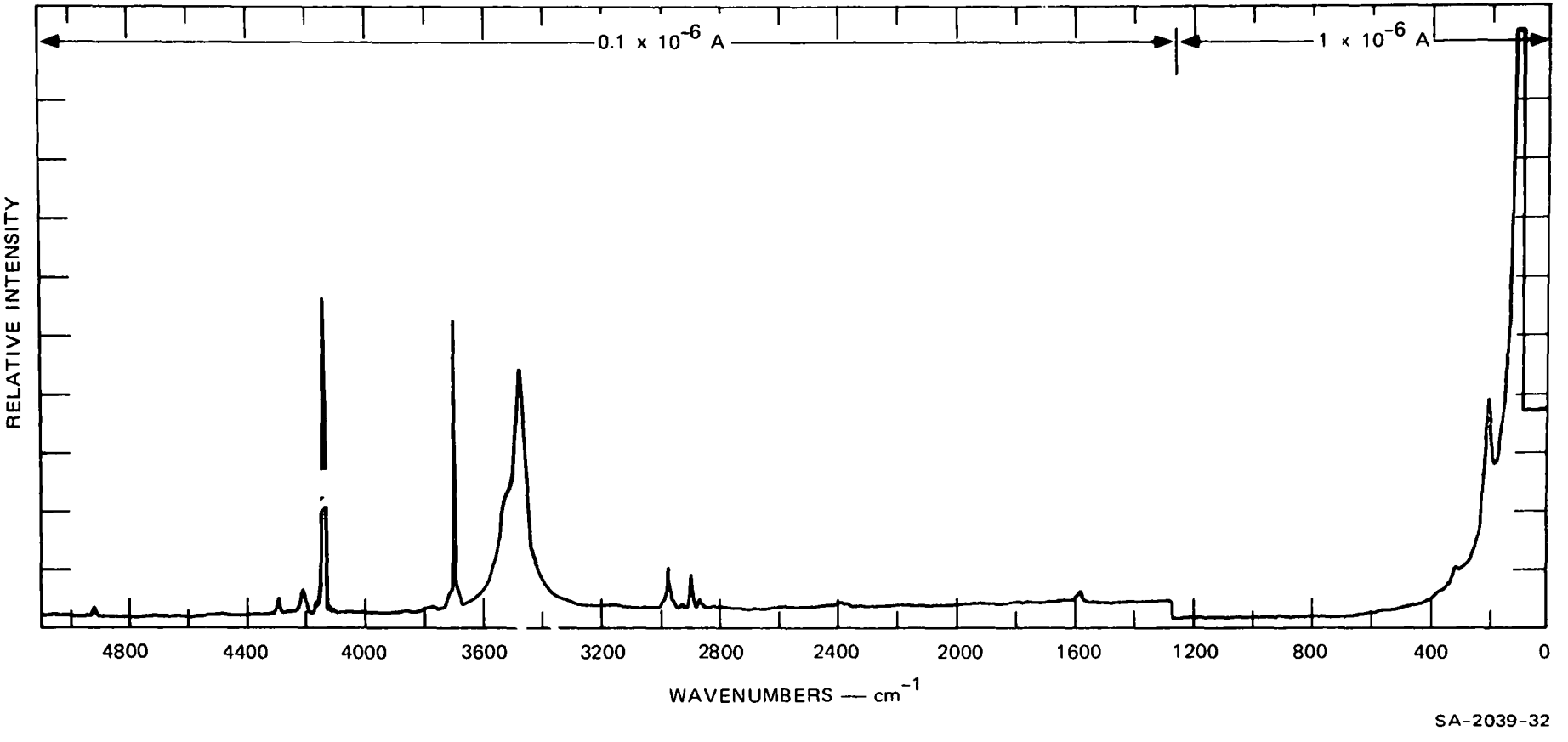

FIGURE B-7 RAMAN RESPONSE OF $CdCl_2$

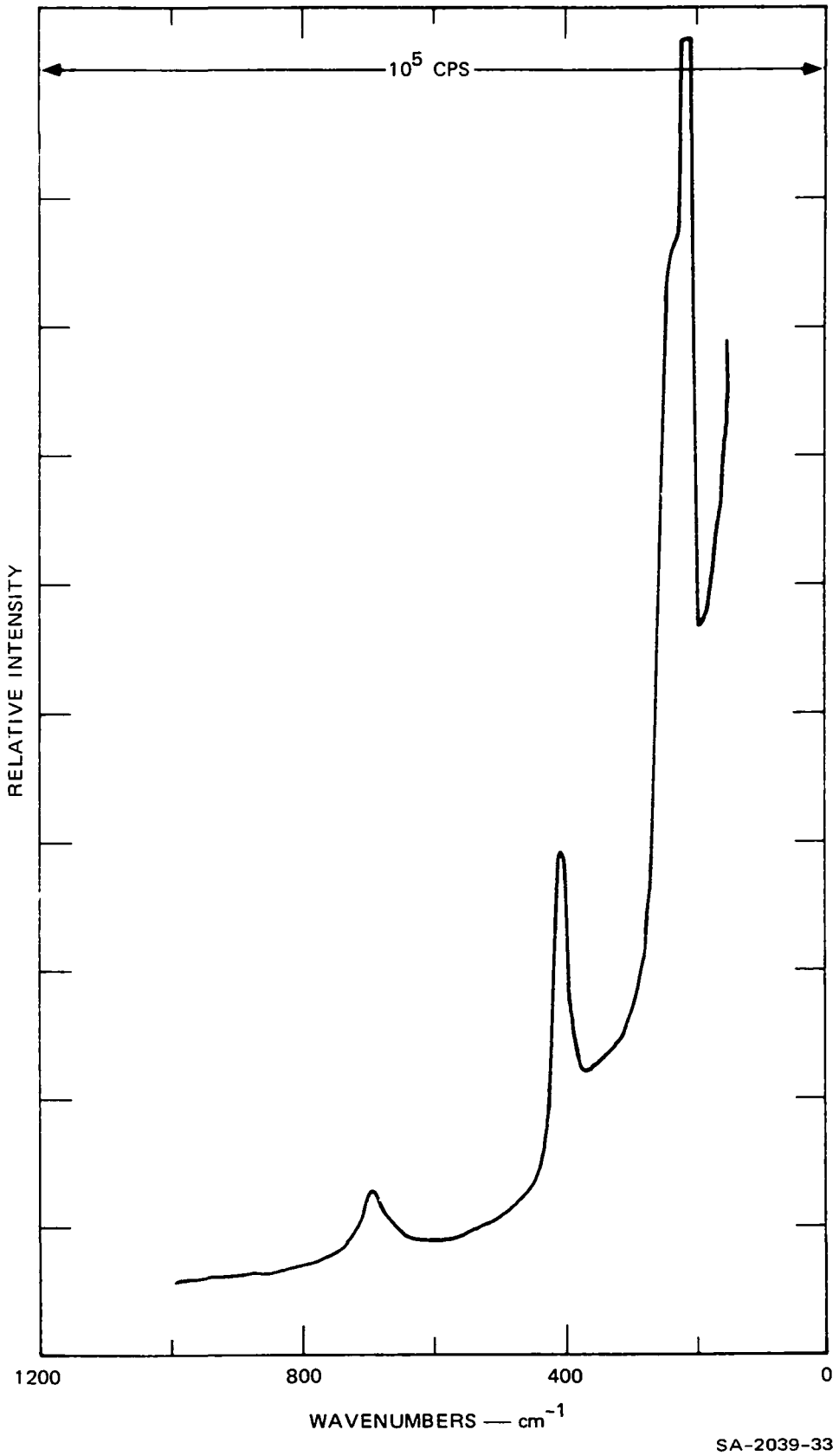

FIGURE B-8 RAMAN RESPONSE OF $CuCl_2$

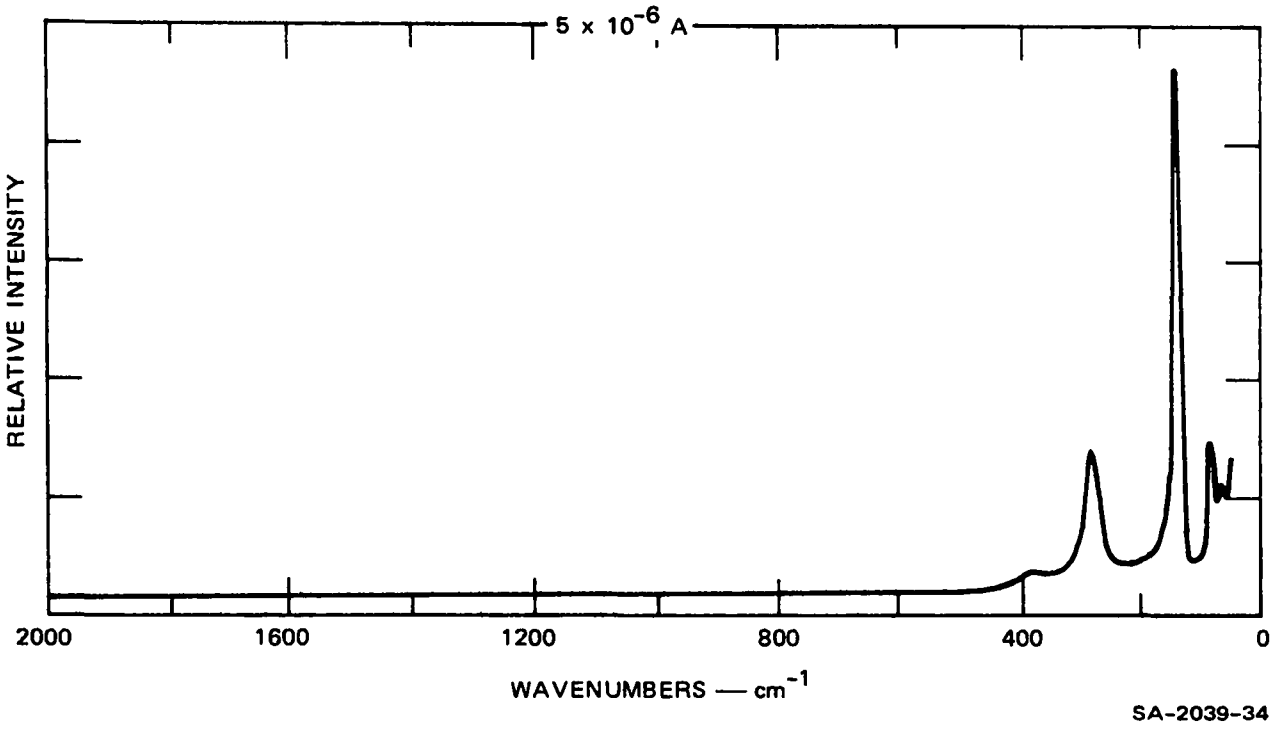

FIGURE B-9 RAMAN RESPONSE OF PbO

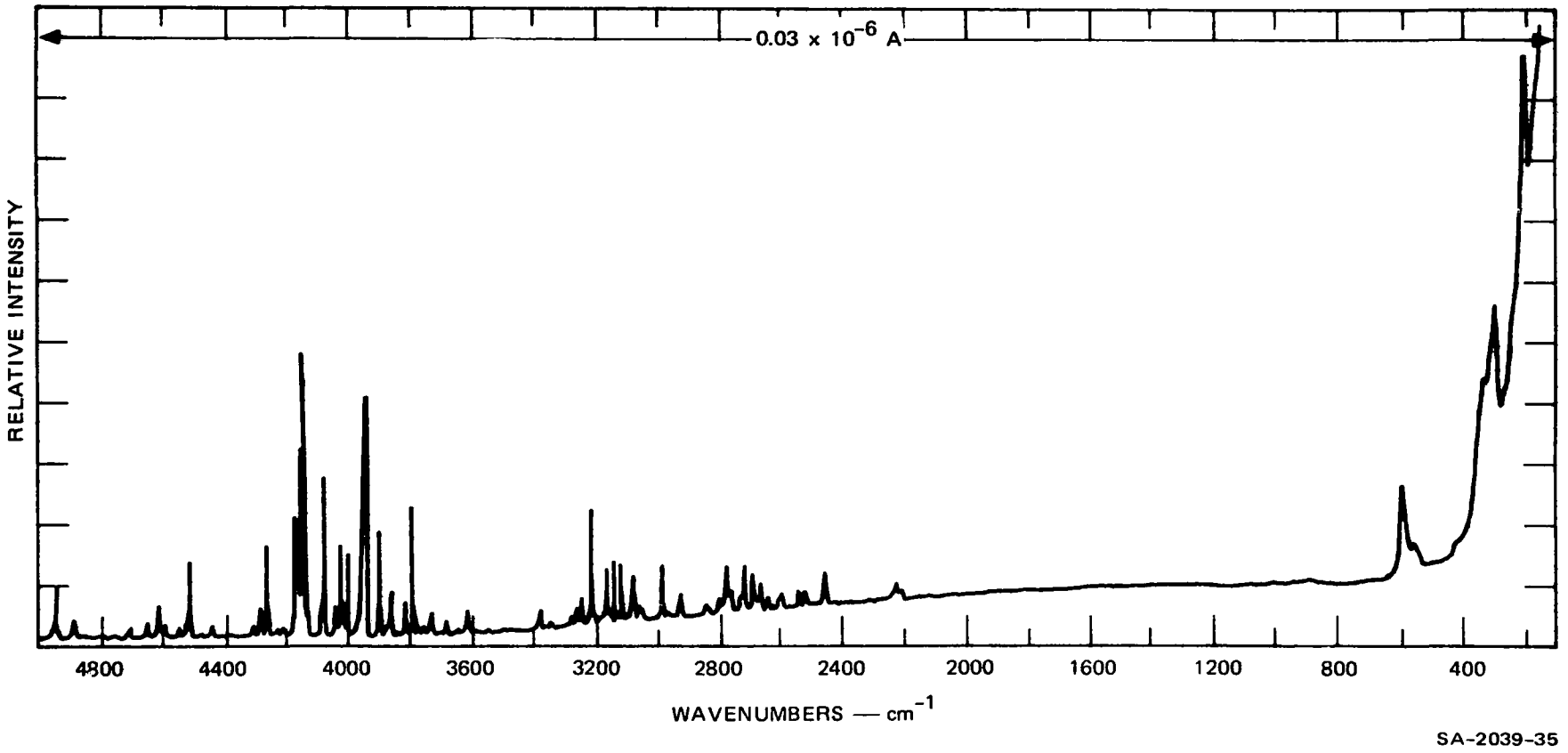

FIGURE B-10 RAMAN RESPONSE OF CdS

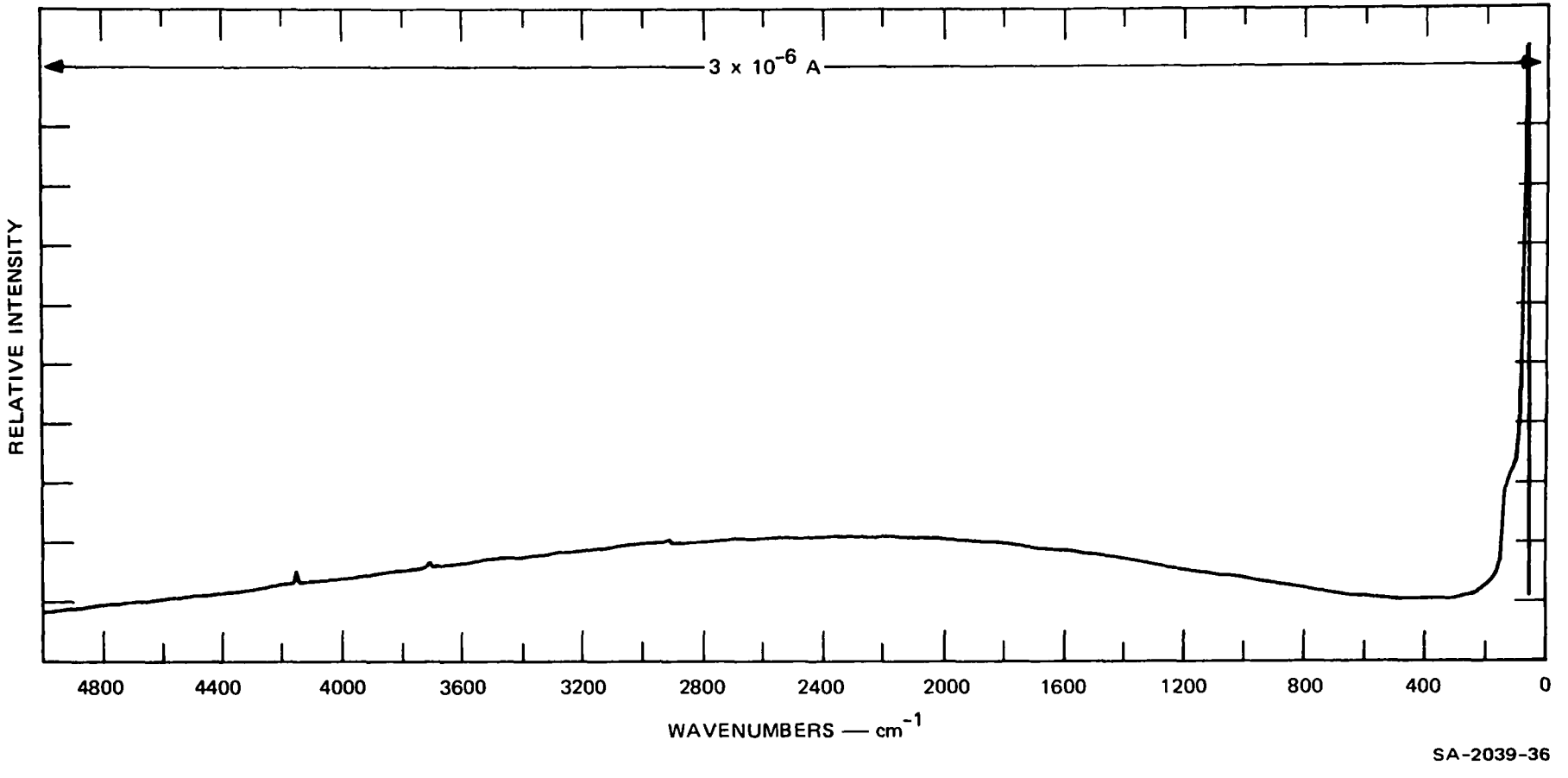

FIGURE B-11 RAMAN RESPONSE OF CaF_2

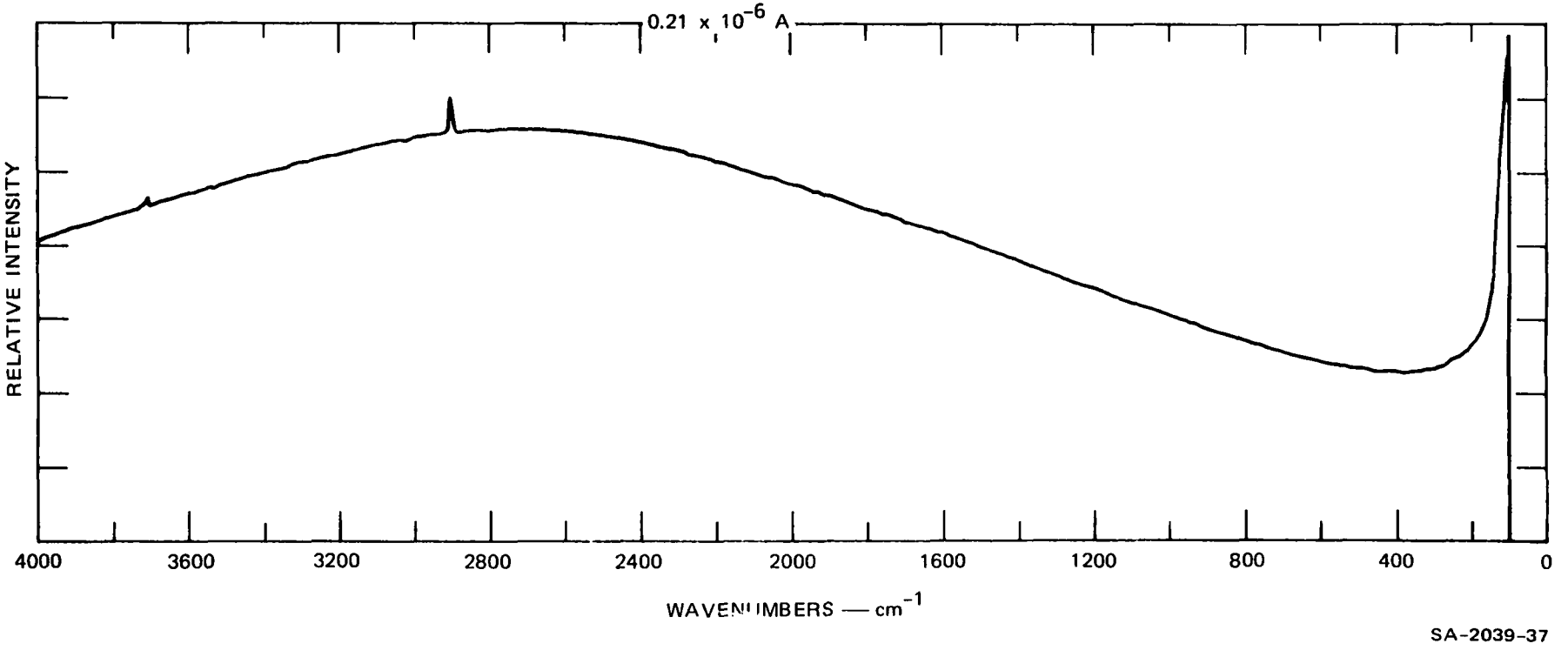

FIGURE B-12 RAMAN RESPONSE OF AlF_3

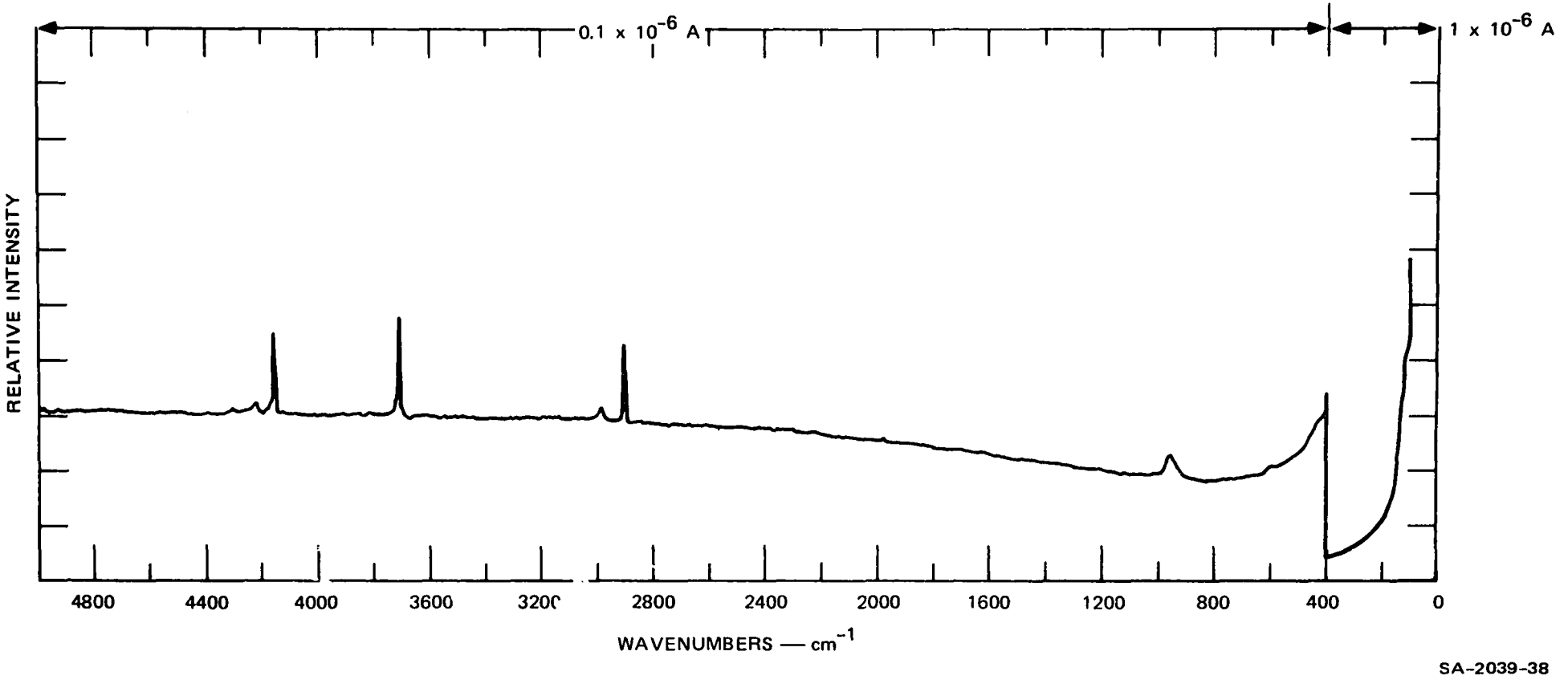

FIGURE B-13 RAMAN RESPONSE OF EPA PHOSPHATE ROCK FEED MATERIAL

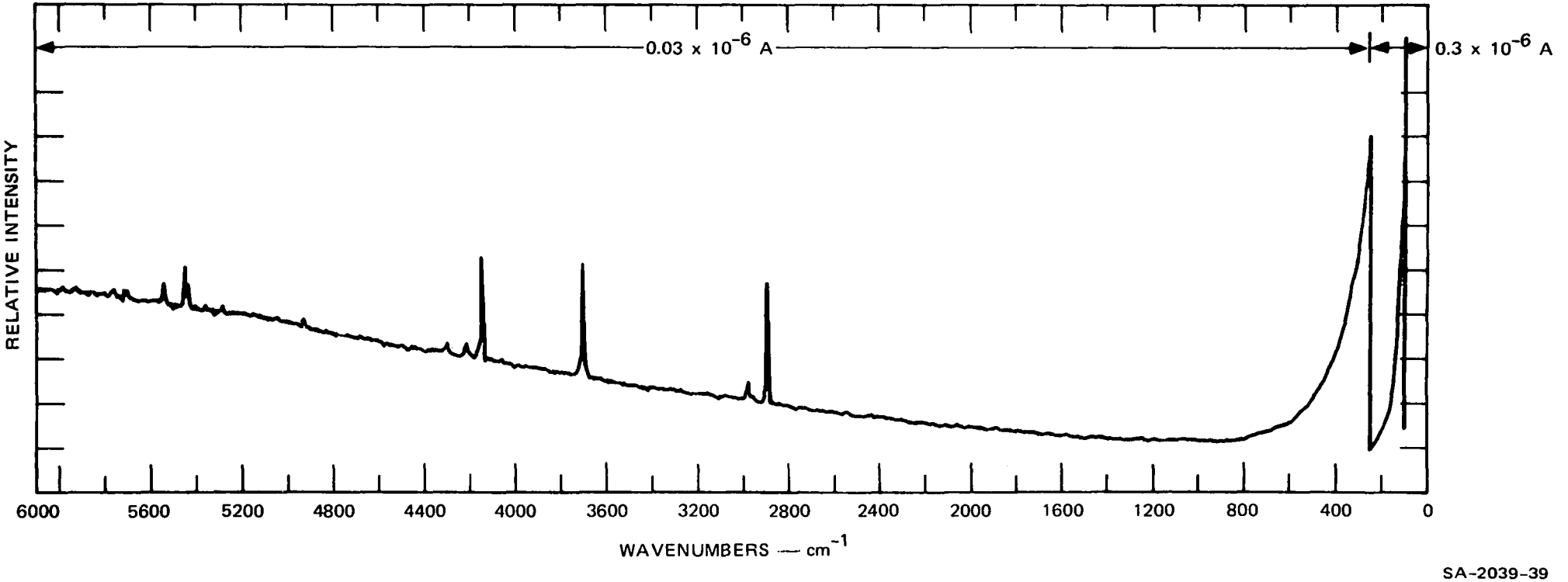

FIGURE B-14 RAMAN RESPONSE OF EPA ZINC SMELTER FEED MATERIAL

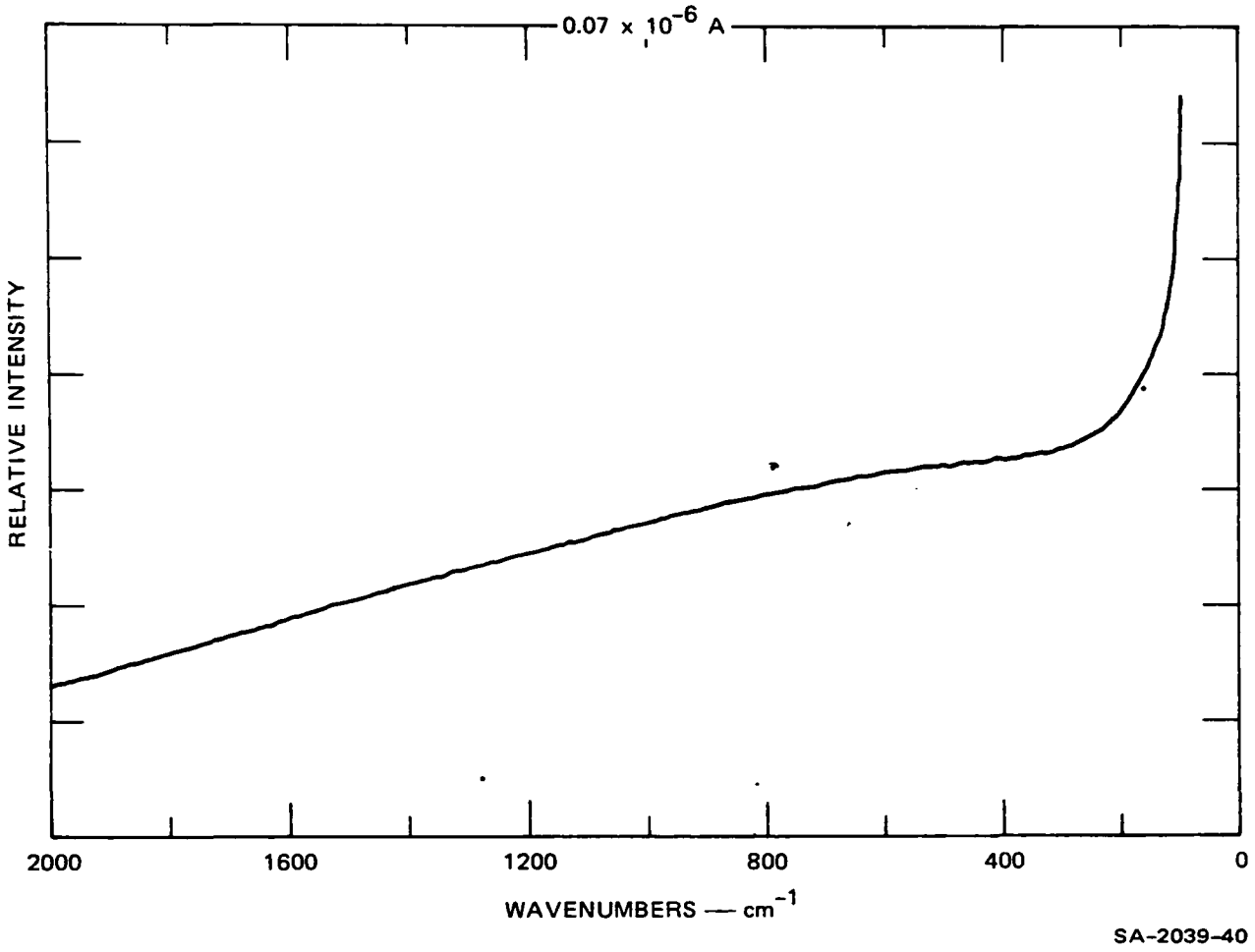

FIGURE B-15 RAMAN RESPONSE OF EPA TRIPLE SUPER-PHOSPHATE STORAGE PRODUCT (6471 Å)

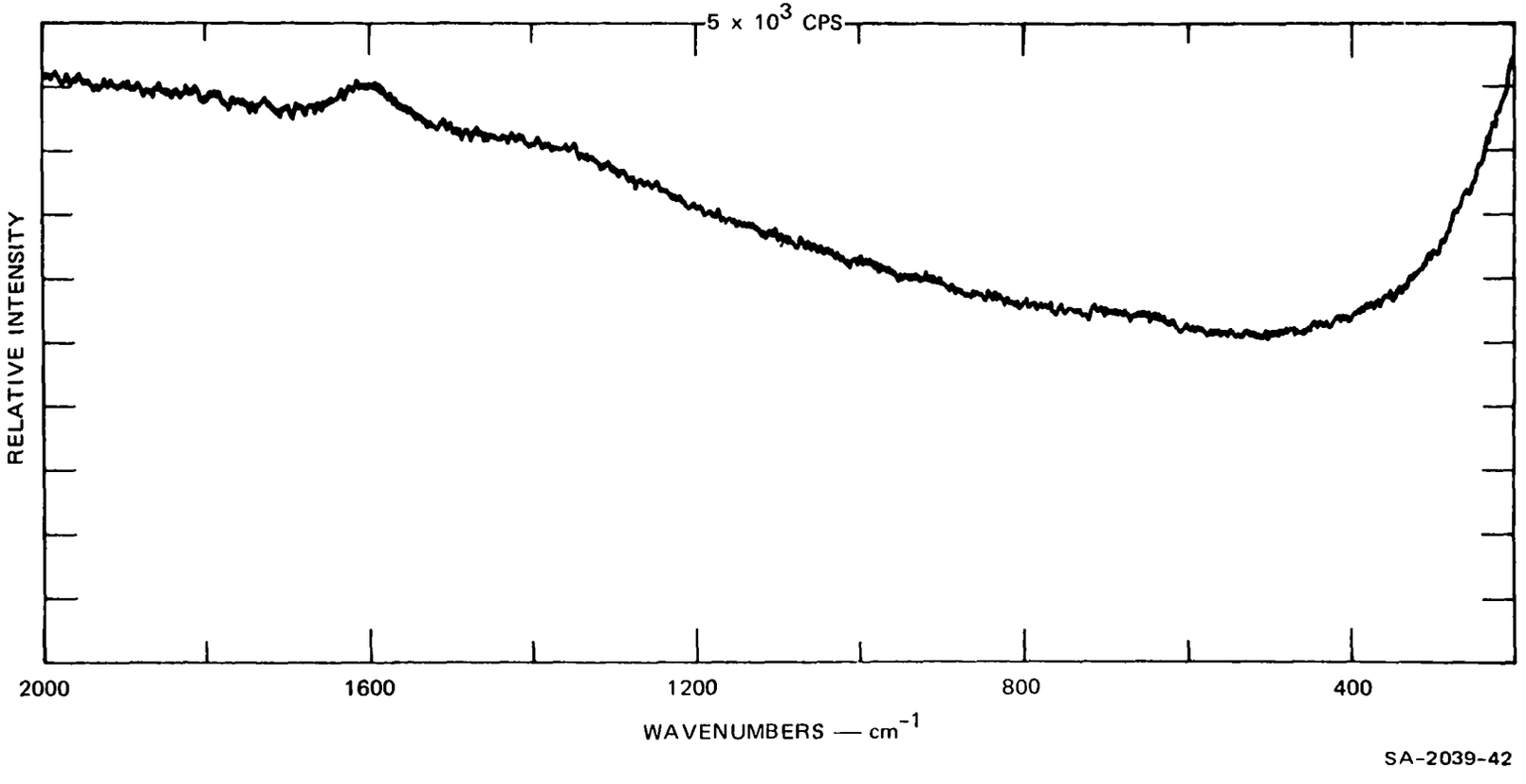

FIGURE B-16 RAMAN RESPONSE OF EPA COAL -- SOURCE, NBS (6471 Å)

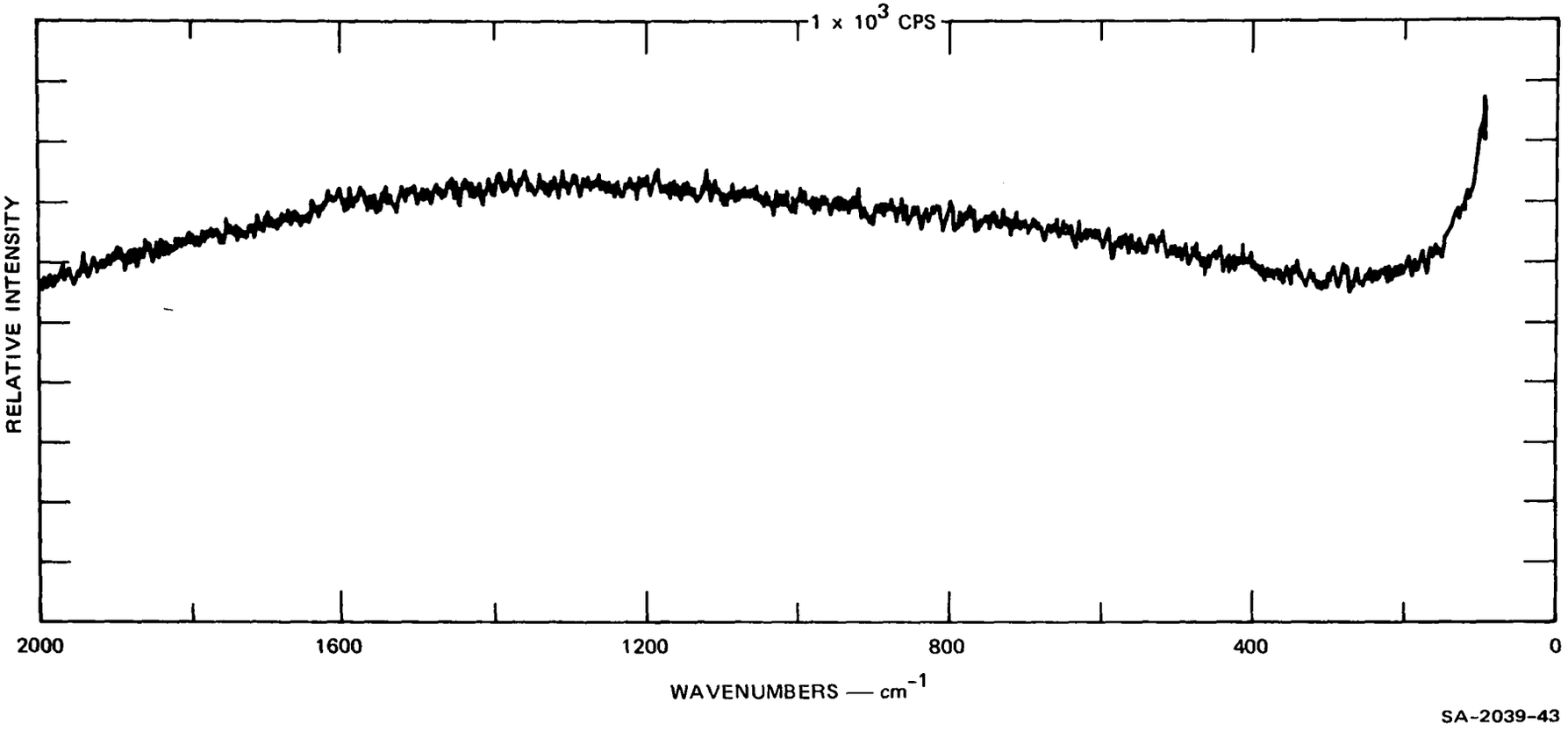

FIGURE B-17 RAMAN RESPONSE OF EPA COAL — SOURCE, NBS

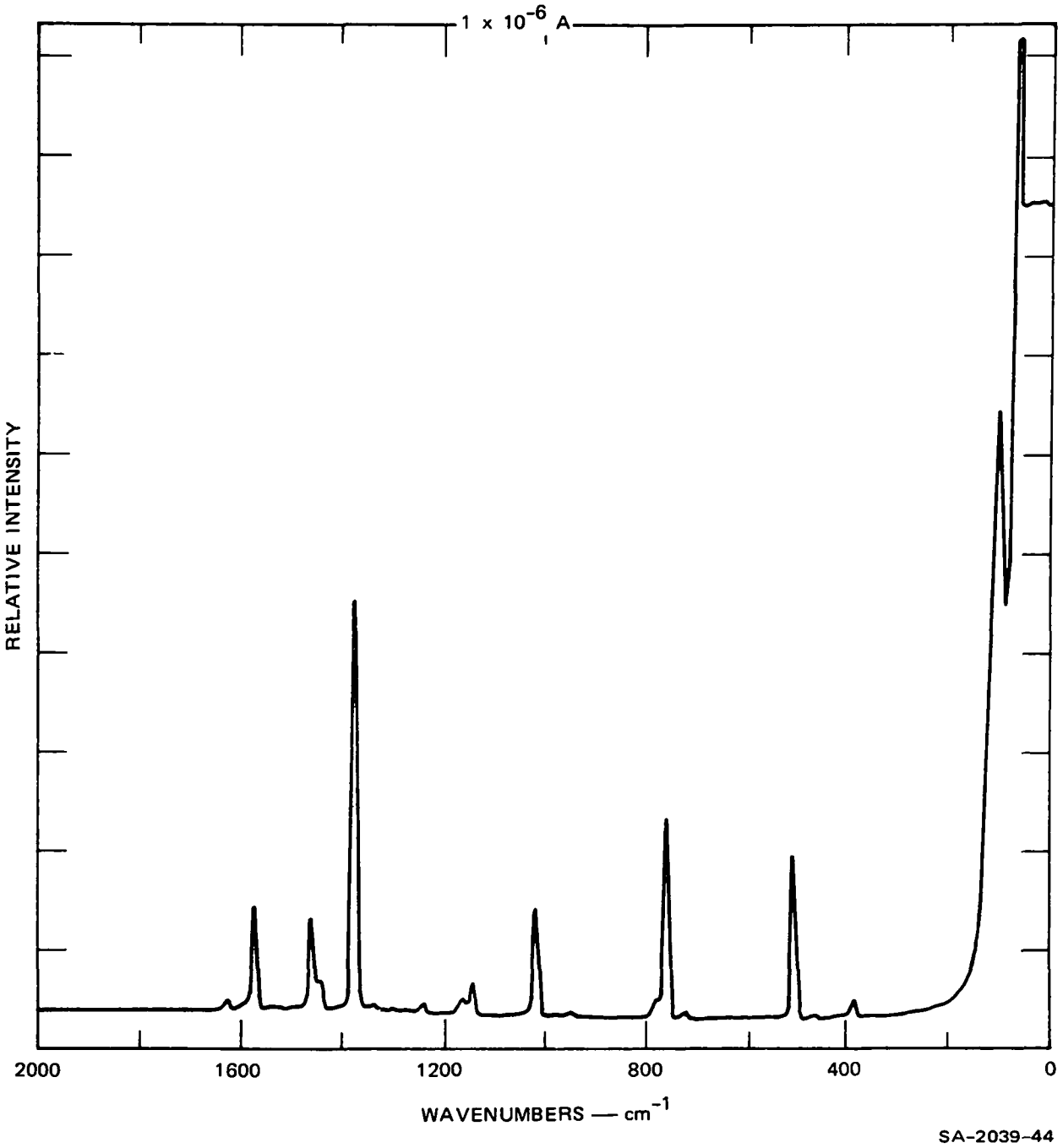

FIGURE B-18 RAMAN RESPONSE OF NAPTHALENE

REFERENCES

1. W. H. Melhuish, J. Opt. Soc. Am., Vol. 54, p. 183 (1964).

2. E. H. Gilmore et al., J. Chem. Phys., Vol. 20, p. 829 (1952).

3. Y. Kato et al., J. Opt. Soc. Am., Vol. 61, p. 347 (1971).

4. J. G. Skinner et al., J. Opt. Soc. Am., Vol. 58, p. 113 (1968).

5. F. J. McClung et al., J. Opt. Soc. Am., Vol. 54, p. 641 (1964).

6. V. S. Gorelik et al., in Light Scattering Spectra of Solids, G. B. Wright, ed. (Springer-Verlag, New York, N. Y., 1969).

7. W. F. Murphy et al., Appl. Spectrosc., Vol. 23, p. 211 (1969).

8. W. R. Fenner et al., J. Opt. Soc. Am., Vol. 63, p. 73 (1973).

9. B. P. Stoicheff, "Stimulated Raman Emission and Absorption Spectroscopy," Semi Annual Report No. 7, Department of Physics, University of Toronto, Toronto, Canada (December 1968).

10. G. E. Devlin et al., Appl. Phys. Letters, Vol. 19, p. 138 (1971).

11. C. R. Pidgeon et al., J. Opt. Soc. Am., Vol. 54, p. 1459 (1964).

BIBLIOGRAPHIC DATA SHEET	1. Report No. EPA-R2-73-219	2.	3. Recipient's Accession No.
4. Title and Subtitle Feasibility Study of In-Situ Source Monitoring of Particulate Composition by Raman or Fluorescence Scatter			5. Report Date June 1973 (D/A and D/I) 6.
7. Author(s) M. L. Wright and K. S. Krishnan			8. Performing Organization Rept. No.
9. Performing Organization Name and Address Stanford Research Institute Menlo Park, California 94025			10. Project/Task/Work Unit No. SRI Project 2039 11. Contract/Grant No. 68-02-0594
12. Sponsoring Organization Name and Address Environmental Protection Agency Research Triangle Park North Carolina 27711			13. Type of Report & Period Covered FINAL June 72 thru Apr 73 14.

15. Supplementary Notes

16. Abstracts

The purpose of this project was to assess the feasibility of in-stack monitoring of an air-suspended particulate stream by fluorescence or Raman optical interactions. The study explored the feasibility of two approaches: quantitatively monitoring a prescribed constituent, and monitoring the relative concentrations of several constituents simultaneously. Fluorescence-monitoring systems were found suitable for the second.

The method of approach was to assess the magnitude of the Raman and fluorescence interaction, and then calculate the detectability of that material for a typical in-stack system. Thirty-four materials were investigated on the project; thirteen materials had significant fluorescent responses and twenty-two materials had measurable
(continued on reverse side)

17. Key Words and Document Analysis. 17a. Descriptors

Source monitoring
Particulate
Raman
Fluorescence
Stack monitoring
Monitoring systems
Aerosols
Spectra

17b. Identifiers/Open-Ended Terms

17c. COSATI Field/Group

18. Availability Statement	19. Security Class (This Report) UNCLASSIFIED	21. No. of Pages 228
	20. Security Class (This Page UNCLASSIFIED	22. Price

FORM NTIS-35 (REV. 3-72) USCOMM-DC 14952-P72

(Abstract-concluded)
Raman responses. When these responses were used to calculate in-stack detectability, all thirteen materials could be detected by fluorescence systems (although few could be uniquely identified), and fifteen of the twenty-two Raman-active materials could be detected by a Raman system.

The use of a laboratory Raman instrument to analyze conventionally sampled particulates was considered. The primary advantage of this instrument appears to be the capability for measuring ions--for example, sulfate.

Finally, a few crude experiments were made to detect the fluorescent response of a particulate material suspended in a liquid (rather than air). These measurements showed substantial interference from fluorescence by the liquid medium; nevertheless, a component of the particulate fluorescence was detectable. This experimental result partially verifies the calculated feasibility of detection by fluorescence.

It is concluded that both fluorescence and Raman in-stack monitoring systems can yield useful information about the quantity and composition of a particulate stream. Recommendations are made for additional efforts toward achieving an operational in-stack monitoring system.

☆ G. P. O. 1973 — 747-786 / 313, REGION NO. 4